العنوان:	STRESSES AT THE JUNCTION OF TWO NORMALLY INTERSECTING CIRCULAR CYLINDERS
المؤلف الرئيسي:	Khathlan, Abd Alrahman Abd Allah
مؤلفين آخرين:	Steele, Charles(Super)
التاريخ الميلادي:	1986
موقع:	ستانفورد
الصفحات:	1 - 156
رقم MD:	614792
نوع المحتوى:	رسائل جامعية
اللغة:	English
الدرجة العلمية:	رسالة دكتوراه
الجامعة:	Stanford University
الكلية:	College of Engineering
الدولة:	الولايات المتحدة الأمريكية
قواعد المعلومات:	Dissertations
مواضيع:	الهندسة المدنية، التصميمات الهندسية، الحاسب الآلي
رابط:	https://search.mandumah.com/Record/614792

Chapter 1

Introduction

The cylindrical shell is a common structural component in nuclear, hydroelectric, and fossil fuel power plants, in offshore oil platforms, and in many other applications which require pipes and pressure vessels. It is frequently necessary to join one cylindrical shell to another, or to have openings and areas of reinforcement on the surface of the shell, which usually produce localized areas of high stress concentration (see Fig. 1.1). Due to the importance of such structures, there is a great need for a reliable, efficient analysis procedure in order to reduce the probabilities of failure. Despite that, reliable studies of the elastic stresses at the junction of two cylinders have been rare, even for the idealized problem of two cylinders with no fillet or reinforcement. Those methods that are available do not completely cover the wide range of geometrical parameters or the variety of loading configurations that exist in actual structures. Analytical solutions have generally been difficult to obtain because of the complicated geometry. Unlike perpendicular cylinder-to-sphere junctions, this problem does not possess rotational symmetry.

The Pressure Vessel Research Committee of the Welding Research Council and other organizations with interest in pressure vessels have embarked on an extensive experimental and analytical investigation program of the cylindrical shell intersection problem. Most of the theoretical work is related to idealized cylinder-to-cylinder junctions (see Fig. 1.2). In this case, the vessel (intersected cylinder)

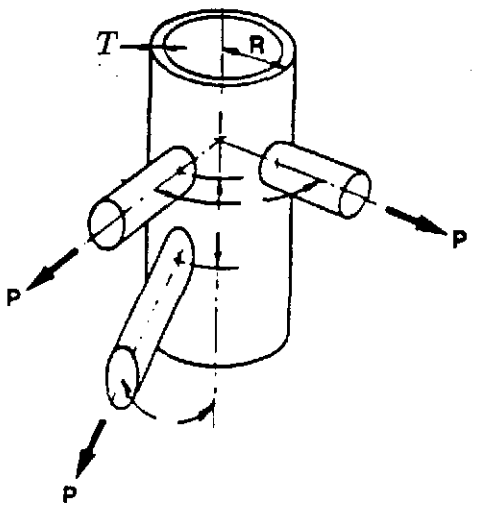

Figure 1.1

A cluster of pipes intersecting a larger pipe from different directions. This is a very common structural component in pressure vessels and offshore structures.

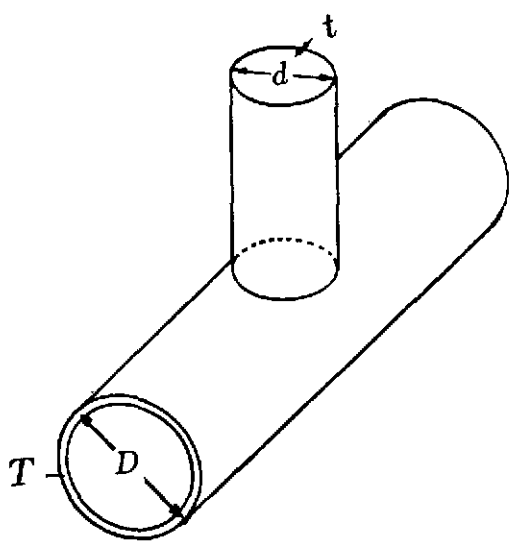

Figure 1.2

Idealized cylinder-to-cylinder junction frequently used in analytical investigations.

has a diameter D, and the nozzle (intersecting cylinder) has a diameter d. Unfortunately, the majority of the analytical solutions for this problem have been confined to cases where the nozzle is considered small relative to the vessel ($d/D \leq 0.5$). As a result, there is a demand for an analytical approach that is useful for handling cases with $d/D > 0.5$. The development of such a solution is the objective of this study.

§1.1 Literature Review

The early stages of research on the cylindrical shell intersection problem have been confined to cases in which the ratio of the diameter of the intersecting cylinder to the diameter of the intersected cylinder (d/D) is small. The reason is that for small values of d/D, it is possible to make certain approximations for the geometry of the intersection curve. In addition, because in the cases of small d/D the opening is located in a zone of the cylinder which is almost flat, referred to as the "shallow region", the use of *shallow shell theory* is justified.

1.1.1 Small Openings and Rigid Inclusions

One of the first to investigate this problem was Lufe (1947). He studied the stress field near a circular opening in a cylinder subject to uniform axial tension or internal pressure. Using perturbation techniques, Lufe expressed solutions in the form of power series in terms of a dimensionless hole size parameter that relates the size of the opening to the radius and thickness of the cylinder. The solution is valid for very small values of the hole size parameter. Following the same procedure, Van Dyke (1965) solved the same problem using an infinite series of Hankel functions of the first kind as a general solution. His approach was designed to be valid for slightly larger hole sizes. Boundary conditions at the opening were satisfied by using a collocation method, which led to a truncation of the series. In addition to the previous two loadings, his work also included the solution for torsion of the cylinder.

Solution for a rigid inclusion in a circular cylinder is important because it serves as a limiting case for a very thick nozzle intersecting a cylinder. Van Dyke (1967) solved the problem using an approach similar to his earlier work for the opening. Influence coefficients were used to satisfy the boundary conditions at the inclusion boundary. Bonde and Rao (1978) studied the problem of a pressurized cylinder with a rigid inclusion. Their solution was also in the form of Hankel functions. Unlike Van Dyke's solution which was written in terms of the displacements of the midsurface, Bonde and Rao used strain and curvature change measures to satisfy boundary conditions. Membrane and bending stresses were plotted versus the hole size parameter. The results exhibit an asymptotic behavior which is in contradiction to that obtained by Van Dyke.

Using an approximate estimate of the stresses in the vessel due to external loads applied to the nozzle, Wichman, et al. (1965) developed design curves for the Welding Research Council *Bulletin 107*. Their work is based on the analytical solution of Bijlaard (1955). He replaced the external loads by pressure distributions applied to rectangular patches on the cylinder face. A double Fourier series expansion was used to compute stresses at specific points in the vessel due to the applied loads. Although this approach is rather crude, and sometimes produces inaccurate results, it was one of the most commonly used design procedures because of its simplicity.

Wong, et al. (1985) used the same double Fourier series solution developed by Bijlaard to expand the range of problems that can be handled. Their work is supposed to be valid for large nozzles, interaction between neighboring nozzles, and rectangular nozzles. Instead of applying the surface pressure to a single rectangular area, the surface inside the intersection curve is divided into several rectangular and triangular elements. As the number of elements was increased, the solution converged to Bijlaard's solution.

1.1.2 Small-Nozzle Problems

Several investigators studied the problem of a small nozzle intersecting the main cylinder. Reidelbach (1961) attempted to solve the problem by providing a Fourier series expansion for the solution of the approximate Donnell thin shell equations. The harmonics of the Fourier series solution for the opening were assumed to be uncoupled. This assumption is essentially equivalent to the treatment of the intersected cylinder as a flat plate. Van Campen (1969) developed a triangular ring element to solve for stresses at nozzle-to-flat plate intersections. His solution was intended to serve as an approximation for cylinder-to-cylinder intersections with a diameter ratio $d/D \leq 1/4$.

Lekkerkerker (1965) used the assumption that the edge of the nozzle is flat to solve for stresses in problems with small diameter ratios. Instead of using Donnell's equations, the more accurate Flugge's equations for a flat-ended cylinder were used to evaluate influence coefficients for the nozzle edge. Similarly, influence coefficients for the opening in the vessel were developed using a combination of exponential and Bessel function solutions of the *shallow shell* equations.

During the same period, Eringen and Suhubi (1965) worked out a mathematical formulation for the problem of a cylinder-to-cylinder junction ($d/D \leq 0.3$) subjected to internal pressure. In their subsequent work (1969), numerical results for several models with a wide range of geometrical parameters were published.

Riley (1965) performed an experiment on a very thin model with diameter ratio of 0.5 subjected to internal pressure, radial load, in-plane and out-of-plane moments applied to the nozzle. Distribution of elastic stresses around the junction for all the loading cases were provided. Pan and Beckett (1970) used the same geometry to test their numerical approach to the solution using a collocation technique and the *Least Squares method.* Their solution was not stable numerically and was very sensitive to the position of the collocation points on the intersection curve. Reasonable agreement with the experimental results was obtained only by restricting all the

collocation points to exist in the shallow region of the intersection curve.

Steele and Steele (1983) developed a versatile computer code (FAST2) for the analysis of spherical and cylindrical intersections. The limitation on the solution is that the diameter ratio is less than one half. Eleven different loading configurations applied to the nozzle or the vessel can be handled, with the capability to include the effect of pad reinforcement on either shell. By approximating the opening in the vessel to be a circle, and the edge of the nozzle to be flat, Bessel function solutions of the shallow shell equations were computed Solution for singularities in shells obtained by Flugge and Conrad (1958), and Sanders and Simmonds (1970) were utilized to represent the effect of the external loads. Asymptotic corrections to the total solution were added to satisfy the boundary conditions at the supports.

In addition, Steele and Steele (1983) used FAST2 to develop an extensive set of design tables that include the peak stresses in the vessel due to four different loadings. The tables include results for several values of the nozzle radius-to-thickness ratio, and the ratio of vessel thickness to nozzle thickness. These tables were the basis for the development of WRC *Bulletin No. 297* by Mershon, et al. (1984). A detailed comparative study between FAST2 and experimental results was later performed by Steele and Steele (1985). They reported excellent agreement with strain gauge measurements obtained by a research group in Oak Ridge National Laboratory.

1.1.3 Large Openings in Cylinders

In the case of large openings in cylindrical vessels, simple analytical solutions are difficult to obtain. One of the reasons is that as the diameter ratio d/D exceeds 0.5, the approximations mentioned previously for the small openings are no longer valid. The opening in the vessel can not be accurately approximated by a circle. It is also inaccurate to assume that the lower edge of the nozzle is flat. The actual space curve describing the intersection between the two cylinders must be considered.

Another reason is the fact that for large d/D ratios, the opening in the vessel will extend outside the shallow region of the cylinder. As a result, the use of *shallow shell theory* for the solution of either cylinder is not valid. Another set of equations for the circular cylinder that are more accurate than Donnell's equations must be used for both cylinders.

Due to the complexity of the problem, the literature dealing with large openings in cylindrical shells is scarce. Most of the successful investigations have been experimental. Gwaltney, et al. (1976) performed several experiments on a carefully manufactured steel model of two intersecting cylinders with equal diameters. Using strain gauge measurements, stresses in both shells due to thirteen different loadings were given. An analytical study of the same model using a thin shell finite element program was also done. Relatively good over-all agreement between the experimental and analytical results was observed.

Using photoelastic measurements, Taylor and Lind (1966) computed stress concentration factors due to internal pressure in several models, some of which had large nozzles. Most of the models could be classified as thick shells. The results given were limited to the two principal axes of the geometry.

In general, the few investigations involving analytical solutions of the problem did not include numerical results. Bijlaard, et al. (1967) attempted to solve the equations for the special case of two equal diameter cylinders. In their solution, Flügge's equations were used for both cylinders. A set of complicated boundary conditions in terms of forces and displacements at the boundary of each cylinder were derived. No numerical results obtained through this approach were published.

§1.2 Development of FAST3

It is clear from the previous sections that there is a lack of an efficient method with a good theoretical basis for the computation of stresses at the junction of two circular cylinders. The program FAST3, the development of which is the primary

objective of this research effort, is designed to fulfill this need with strong emphasis on problems in which the nozzle is considered large relative to the size of the vessel ($d/D \geq 0.5$).

The FAST3 program was developed with an emphasis on understanding the behavior of shells and incorporating this knowledge in the solution procedure. This minimizes the amount of decision made by the user, which leads to short user preparation times. This is in contrast to the relatively large amount of time that is generally needed for establishing an efficient, useful mesh for use in finite element programs. The objective is to reduce the user preparation time to a few minutes.

The solution is obtained by dividing the state of stress in the structure into two parts. The first part is the particular solution, which is the nominal state of stress due to the applied loads in the two shells separated from each other. The other is the complementary solution, which is the solution to the residual problem obtained by subtracting the nominal solution from the total solution. This part of the solution is used to satisfy the continuity conditions at the junction between the two cylinders. Both solutions will be expanded as functions of the circumferential angle of the nozzle, in the form of a finite Fourier series. The *Fast Fourier Transform* (FFT) method is used to efficiently evaluate the Fourier coefficients of the solution. The use of symmetry to investigate only one quarter of the problem is an additional technique for reducing the numerical computations.

The next few chapters give a detailed description of the methods used to compute both solutions. In Chapter 2, the main assumptions and the geometrical description of the problem are given. Limitations on the theory in terms of material behavior, dimensions and boundary conditions are stated. The chapter also explains the notation used to describe the different loading configurations that will be used in the analysis. The second part of this chapter deals with the definition of the intersection curve between the two cylinders. A convenient coordinate system utilizing the circumferential angle of the nozzle projected on the developed surface of the vessel is used. Two sets of orthonormal vectors are also introduced to define

the direction of the stress resultants acting on the boundary of both shells. The chapter ends with a discussion of the symmetry and anti-symmetry requirements of the solution for the different loading cases.

The solution of the equations for a thin circular cylinder is discussed in Chapter 3. A brief historical review of the different types of solutions for a semi-infinite cylinder proposed by several authors is given. Out of these thin shell theories, Sanders' equations were selected due to their simplicity, consistency, and accuracy. By utilizing stress-strain relations, strain-displacement relations, and the static-geometric analogy, it is possible to derive simple formulas for the stresses and strains in the cylinder. These formulas are useful for the computation of solutions anywhere in the cylinder due to the application of an arbitrary distribution of edge forces or displacements. A brief discussion of the compatibility and equilibrium requirements of the solutions is given at the end of the chapter.

Chapter 4 is a description of the *cut method*, which is used for the computation of the particular solution and the contribution of the low harmonics to the complementary solution for the vessel. At midspan, a circumferential cut in the surface of the vessel is used to prescribe certain discontinuities in forces and displacements. These discontinuities have to satisfy the equilibrium requirements in the case of forces, and the compatibility requirements in the case of deformations. By using the edge solution for a cylinder, described in Chapter 3, one can evaluate the needed forces and displacements at mesh points around the intersection curve.

The first part of Chapter 5 is a description of the evaluation of the particular solution for the vessel which represents the effect of the application of the external loads. For loading cases of internal pressure and axial force on the vessel, the *membrane solution* for the circular cylinder is used. For other loading cases that involve external loads applied to the nozzle, the *cut method* is used to compute the particular solution. This is achieved by applying some cut distributions of forces that produce the same resultants as the applied loads. The chapter also gives a description of the procedure used for the evaluation of the low harmonics

of the complementary solution. Because of the complexity of the shell behavior near the junction, the evaluation of "stiffness" coefficients for the boundary is very complicated, but the *cut method* is expected to be a useful technique for generating such coefficients. However, its use is limited to the low harmonics of the solution, which necessitates the use of another method for handling the high harmonics.

An asymptotic solution of the *shallow shell* equations is used to complement *cut method*, and is detailed in Chapter 6. This solution is useful for handling rapidly varying functions around the opening, for which the cut solution is useless. A general exponential solution that decays rapidly away from the boundary is used to derive the *eikonal equation* of the problem. Roots of the eikonal equation are computed for each harmonic and are used to compute forces and displacements at the boundary. This provides a set of stiffness coefficients for the higher harmonics.

The particular and complementary solutions for the nozzle are discussed in Chapter 7. Simple membrane solutions for cylinders, evaluated at the boundary of the nozzle, are used to compute the effect of the external loads. Another version of the *cut method* is used to compute the stiffness coefficients for the edge of the nozzle. Periodic distributions of forces and displacements are prescribed to a flat-ended cylinder. These distributions are used to compute the solution at the actual boundary of the nozzle. Finally, by adding the nozzle solution to the vessel solution and with the use of the continuity conditions between the two shells, one can reduce the problem to a single set of equations. The solution of these equations yields the stresses at the junction of the cylinders due to the applied load.

A general discussion of FAST3, its characteristics and features is given in Chapter 8. The limitations on the validity of FAST3 results are stated in terms of the size of the nozzle. This is followed by a discussion of the special solutions for the two limiting cases of a rigid inclusion or an opening in a cylinder. The effect of the vessel length on the results is also investigated for the different loading configurations. After that, a comparative study between FAST3 and other approaches is given. Results obtained using analytical, experimental, and finite element approaches are

compared to numerical results from FAST3 to verify its validity. Then, FAST3 is used to investigate the stresses in a large number of cylinder-to-cylinder models ($d/D \geq 0.5$) subjected to five different loading configurations. The results are tabulated in Appendix A and will serve as a supplement for the existing design tables available in WRC-297 for small diameter ratios ($d/D \leq 0.5$).

Finally, Chapter 9 includes some brief conclusions and recommendations for future work.

العنوان:	STRESSES AT THE JUNCTION OF TWO NORMALLY INTERSECTING CIRCULAR CYLINDERS
المؤلف الرئيسي:	Khathlan, Abd Alrahman Abd Allah
مؤلفين آخرين:	Steele, Charles(Super)
التاريخ الميلادي:	1986
موقع:	ستانفورد
الصفحات:	1 - 156
رقم MD:	614792
نوع المحتوى:	رسائل جامعية
اللغة:	English
الدرجة العلمية:	رسالة دكتوراه
الجامعة:	Stanford University
الكلية:	College of Engineering
الدولة:	الولايات المتحدة الأمريكية
قواعد المعلومات:	Dissertations
مواضيع:	الهندسة المدنية، التصميمات الهندسية، الحاسب الآلي
رابط:	https://search.mandumah.com/Record/614792

Chapter 2

Problem Description

The structure under consideration consists of two intersecting thin circular cylindrical shells. For the vessel R, T, E, and ν denote the mean radius, thickness, Young's modulus of elasticity, and Poisson's ratio. The same quantities for the nozzle are represented by r_0, t, E_n, and ν.

The first part of this chapter is a brief description of the assumptions used in the analysis. It also includes the limitations on the validity of the analysis. The following part is a detailed study of the geometry of the intersection curve between the two intersecting cylinders. The circumferential angle of the nozzle is replaced by a new angle that will be used, in addition to the radius, as the main local coordinate for the junction. Local radii of curvature, as well as other important geometrical parameters, can be expressed in terms of this angle. The final part of the chapter discusses the different symmetry cases that are associated with the different loading configurations. A symmetry index is devised to refer to the four different symmetry cases that will be encountered in this study.

§2.1 Limitations and Assumptions

The following limitations and assumptions are used in order to define the problem to be analyzed:

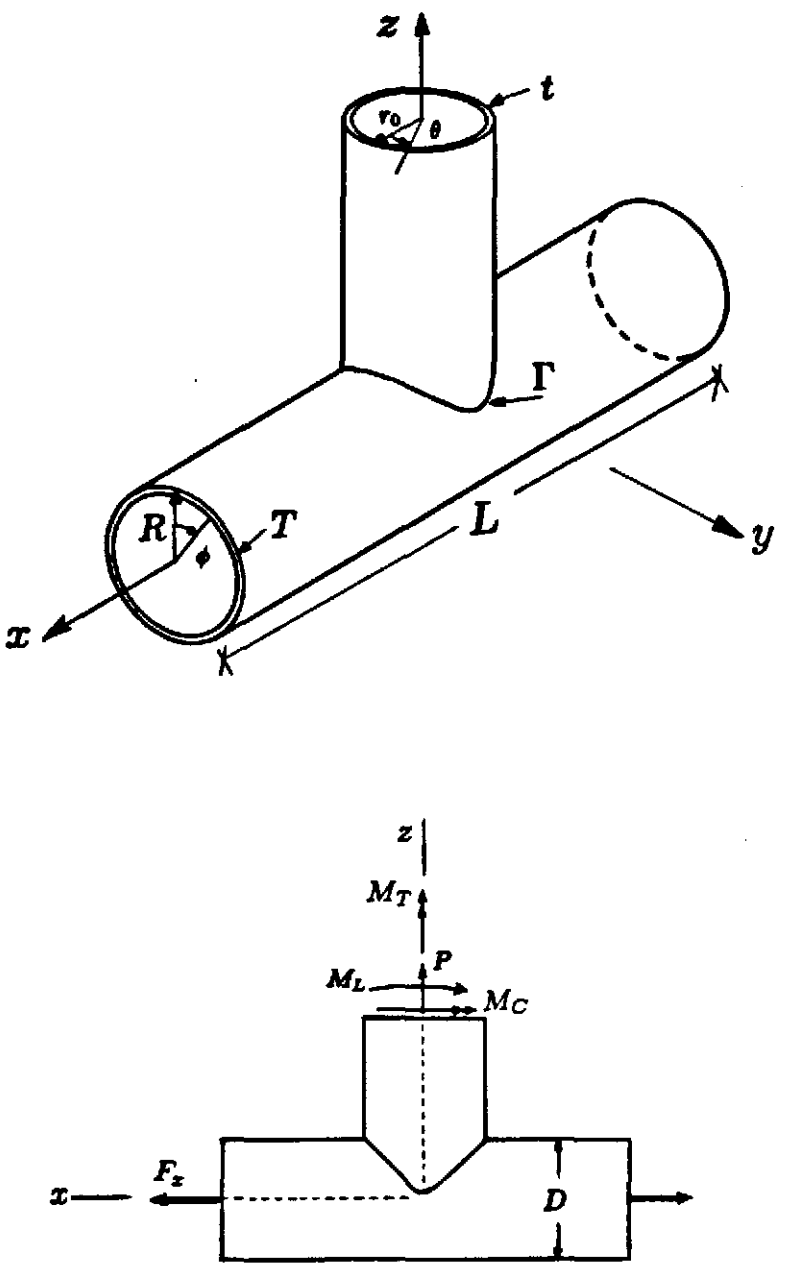

Figure 2.1

a) Coordinate axes and dimensions of the cylinder-to-cylinder idealized model, b) External loads applied to the two cylinders.

1) Both cylinders have closed circular cross sections and are considered *thin*. This translates into the requirement that

$$\frac{R}{T}\ ,\ \frac{r_0}{t}\ \geq 10 \tag{2.1.1}$$

2) The nozzle intersects the vessel perpendicularly at the vessel midspan.

3) The length L of the vessel is assumed to be large enough to cause uncoupling between the junction of the cylinders and the vessel ends. Using the definition of the decay distance for a cylinder given by Flügge (1960), this reduces to the requirement that

$$L \gg \sqrt{RT} \tag{2.1.2}$$

This should be considered as a necessary condition. Because of the slowly varying, self-equilibrating solutions the sufficient condition on length is more involved, depending on the specific loading and on the details of end constraint.

4) The nozzle is assumed to be long enough such that external loads on the nozzle can be replaced by statically equivalent membrane stresses away from the free edge.

5) The junction of the two cylinders is assumed to be ideal. No reinforcement or fillet weld is located at the junction on either shell.

6) The two ends of the vessel are unreinforced and placed on top of saddle supports. These supports cause no restraint on the cylinder face against bending or stretching. As a result, the boundary conditions are that all the normal stresses in the vessel vanish at the supports.

7) The upper edge of the nozzle is free to displace in all directions. This edge will be used for the application of the external mechanical loads to the structure.

8) In the special case of internal pressure loading, the three ends of the structure are assumed to be covered with bulk heads in order to contain the pressure.

9) The material is assumed to be homogeneous, isotropic, and linearly elastic. The two cylinders may be made of different materials.

10) All the applied loads are assumed to be well below the buckling loads of the structure.

§2.2 Loading Configurations

A structure consisting of two intersecting cylinders can be loaded by a wide variety of external loads. However, certain specific load types are considered important because of their common occurrence in real structures, or because of associated high stress concentration factors. Mechanical loads applied to the nozzle are examples of such loads. Table 2.1 gives a list of the loading cases selected for use in this study, with the definition of the loading parameter *Iload*.

Iload	Description	Notation
0	internal pressure in both cylinders	p_0
1	external axial load on the nozzle	P
2	external longitudinal moment on the nozzle	M_L
3	external transverse moment on the nozzle	M_C
4	external twisting moment on the nozzle	M_T
5	external axial load on the vessel	F_x

Table 2.1
Description of the different loading configurations and the corresponding notation.

§2.3 Geometry of the Intersection Curve

In this section, the geometry of the intersection curve between the two intersecting cylinders is investigated. First, the exact intersection curve, which is valid for all values of d/D, is computed. This is followed by a discussion of the approximations that can be made for small values of d/D.

2.3.1 The Exact Intersection Curve

The geometry of the model is illustrated in Figure 2.1. The origin of the coordinate axes x-y-z is located at the intersection point of the axes of the two cylinders. The angle ϕ is the circumferential angle for the vessel, measured from the top, clockwise. The angle θ is the circumferential angle for the nozzle measured from the x-axis, counter-clockwise.

By introducing the unit vectors $\vec{\mathbf{e}}_\mathbf{x}$, $\vec{\mathbf{e}}_\mathbf{y}$, and $\vec{\mathbf{e}}_\mathbf{z}$, the midsurface of the vessel can be described uniquely by using the position vector

$$\vec{\rho_1} = x\,\vec{\mathbf{e}}_\mathbf{x} + R\sin\phi\,\vec{\mathbf{e}}_\mathbf{y} + R\cos\phi\,\vec{\mathbf{e}}_\mathbf{z} \tag{2.3.1}$$

Similarly, the position vector for the nozzle midsurface is

$$\vec{\rho}_2 = r_0\cos\theta\,\vec{\mathbf{e}}_\mathbf{x} + r_0\sin\theta\,\vec{\mathbf{e}}_\mathbf{y} + z\,\vec{\mathbf{e}}_\mathbf{z} \tag{2.3.2}$$

All points on the intersection curve Γ are common to both position vectors. Thus, along Γ the following equation is to be satisfied

$$x\,\vec{\mathbf{e}}_\mathbf{x} + R\sin\phi\,\vec{\mathbf{e}}_\mathbf{y} + R\cos\phi\,\vec{\mathbf{e}}_\mathbf{z} = r_0\cos\theta\,\vec{\mathbf{e}}_\mathbf{x} + r_0\sin\theta\,\vec{\mathbf{e}}_\mathbf{y} + z\,\vec{\mathbf{e}}_\mathbf{z} \tag{2.3.3}$$

Equating the coefficients of $\vec{\mathbf{e}}_\mathbf{x}$ yields

$$x = r_0 \cos\theta \tag{2.3.4}$$

In a similar manner,

$$R\sin\phi = r_0 \sin\theta \tag{2.3.5}$$

$$R\cos\phi = z$$

which yields

$$\phi = \arcsin\left(\frac{r_0}{R}\sin\theta\right) \tag{2.3.6}$$

By examining the previous equations, it can be observed that the coordinates of any point on the intersection curve can be uniquely defined using the angle θ and the dimensions of the cylinders. However, it was found that the circumferential angle γ is a better choice for the independent variable. The angle γ is the projection of the angle θ on the cylindrical surface of the vessel. By examining Figure (2.2), it can be shown that

$$\tan\gamma = \frac{-dx}{R\,d\phi} = -\frac{1}{R}\frac{dx}{d\theta}\frac{d\theta}{d\phi} \tag{2.3.7}$$

Using (2.3.4) and (2.3.6)

$$\frac{dx}{d\theta} = -r_0 \sin\theta \tag{2.3.8}$$

$$\frac{d\varphi}{d\theta} = \frac{r_0\cos\theta}{R\cos\phi}$$

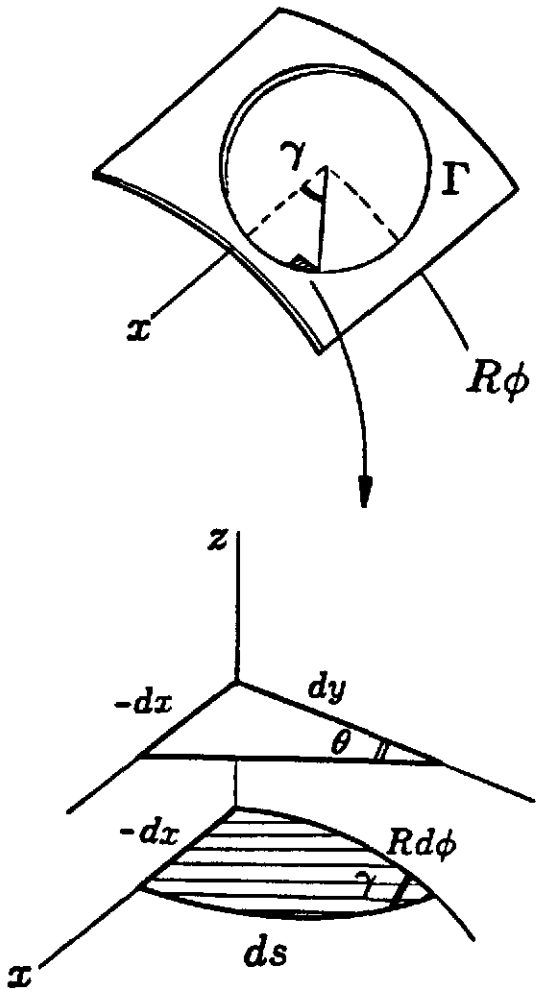

Figure 2.2

A small opening in the surface of the vessel illustrating the difference between the circumferential angles θ and γ.

By substituting in (2.3.7)

$$\tan\gamma \;=\; \tan\theta\cos\phi \tag{2.3.9}$$

It is observed that if the diameter of the nozzle is very small relative to the vessel ($\cos\phi \approx 1$), the angle γ becomes the same as θ. However, for large d/D ratios, there is a substantial difference between the two angles.

The incremental arc length can be computed using (see Figure 2.2)

$$(\overline{ds})^2 = (\overline{dx})^2 + (\overline{Rd\phi})^2 \tag{2.3.10}$$

Dividing by $(\overline{d\theta})^2$ and using (2.3.8,a-b) produces

$$\begin{aligned}\left(\frac{ds}{d\theta}\right)^2 &= r_0^2\sin^2\theta + r_0^2\frac{\cos^2\theta}{cos^2\phi} \\ &= r_0^2\frac{\sin^2\theta}{\sin^2\gamma}\end{aligned} \tag{2.3.11}$$

As a result, the arc length can be defined as

$$ds = r_s d\theta \tag{2.3.12}$$

where

$$r_s = r_0\frac{\sin\theta}{\sin\gamma} \tag{2.3.13}$$

The arc length can also be measured by using the geodesic radius of curvature r_g and the angle γ

$$ds = r_g \, d\gamma \tag{2.3.14}$$

where

$$r_g = r_0 \frac{\sin\theta \cos^2\theta \cos\phi}{\sin\gamma \cos^2\gamma} \left[\frac{1}{\cos^2\phi - \sin^2\phi \cos^2\theta} \right] \tag{2.3.15}$$

which has the special values

$$r_g = \begin{cases} r_0 & \text{if } \theta = 0 \\ r_0\sqrt{1-(r_0/R)^2} & \text{if } \theta = \pi/2 \end{cases} \tag{2.3.16}$$

The geodesic curvature of the opening in the vessel can be computed by evaluating the inverse of the radius of the geodesic curvature.

For cases where the diameter ratio is very small, which resemble a cylinder intersecting a flat plate, the following approximations can be made

$$\gamma \approx \theta \quad , \quad \phi \approx 0 \tag{2.3.17}$$

Using these approximations, it can be shown that both r_s and r_g reduce to the radius of the nozzle r_0. The deviation of the geodesic radius of curvature r_g from the value of the nozzle radius in the case of large diameter ratios is illustrated in Figure 2.3.

For the nozzle, the angle α represents the angle between the intersection curve and the horizontal plane (see Figure 2.4). It can be shown that

$$\tan\alpha = \frac{-dz}{r_0 \, d\theta} \tag{2.3.18}$$

Differentiating (2.3.6) and substituting produces

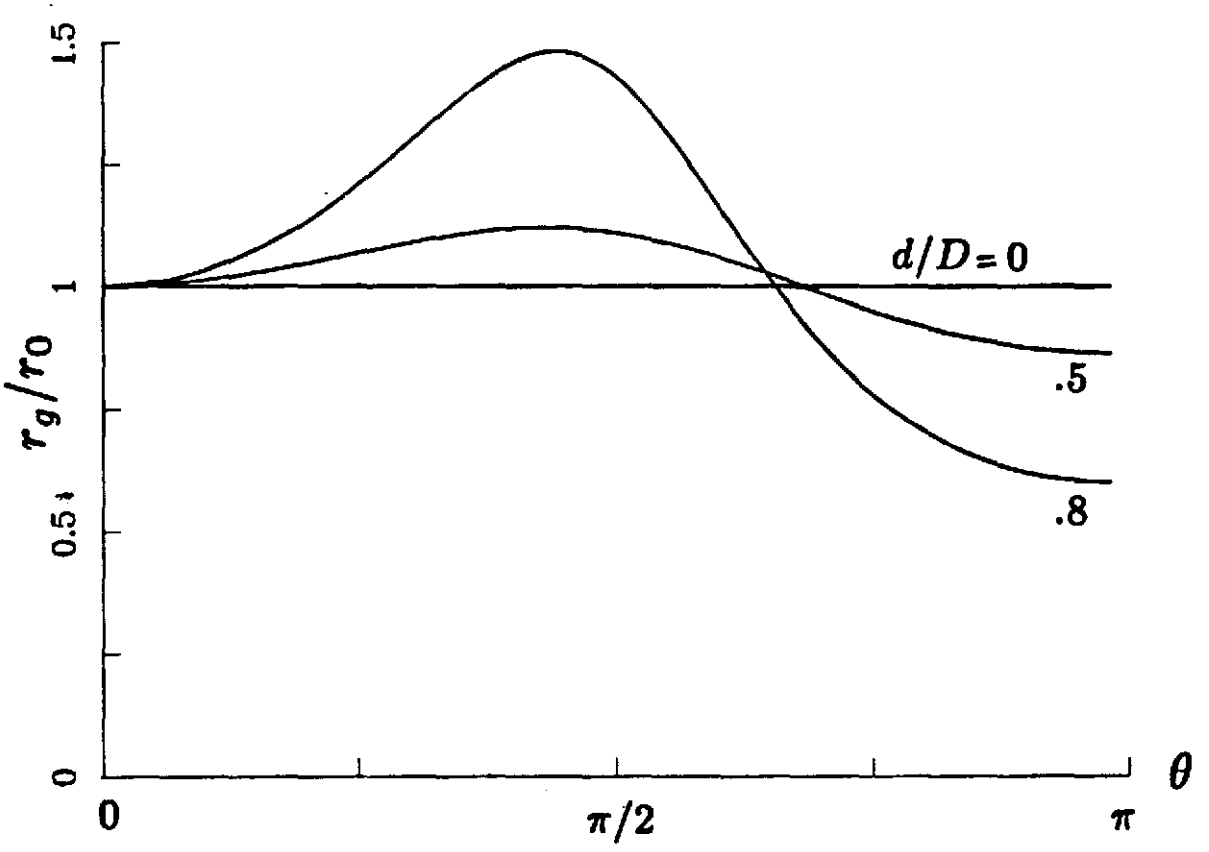

Figure 2.3

Variation of the normalized radius of geodesic curvature (r_g/r_0) for an opening in a circular cylinder with changes in the diameter ratio (d/D= 0.0, 0.5, and 0.8).

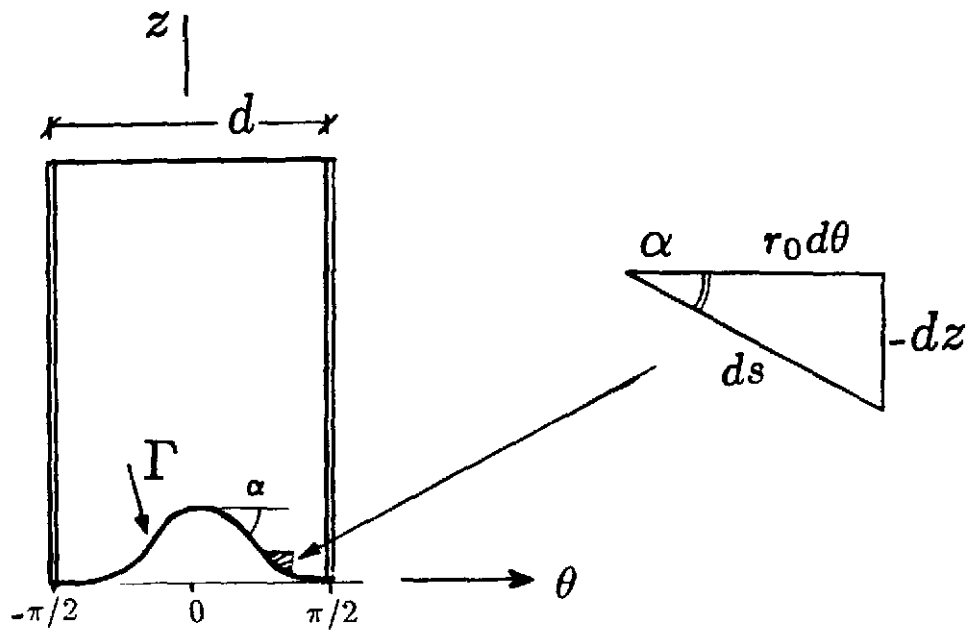

Figure 2.4

The intersection curve Γ on the lower edge of the unrolled nozzle describing the angle α.

$$\tan\alpha = \tan\phi \cos\theta \tag{2.3.19}$$

It is also possible to express the angle α in terms of γ as follows

$$\cos\alpha = \frac{r_0 d\theta}{ds} = \frac{r_0}{r_s} = \frac{\sin\gamma}{\sin\theta} \tag{2.3.20}$$

Differentiating (2.3.20) one can obtain the derivative

$$\frac{d\alpha}{d\gamma} = \frac{\sin\gamma\cos\theta(r_g/r_s) - \sin\theta\cos\gamma}{\sin\alpha\sin^2\theta} \tag{2.3.21}$$

which has the following values along the two major axes

$$\frac{d\alpha}{d\gamma} = \begin{cases} r_0/R & \text{if } \theta = 0 \\ -r_0/R & \text{if } \theta = \pi/2 \end{cases} \tag{2.3.22}$$

2.3.2 Approximate Representation of the Intersection Curve

It was mentioned in Chapter 1, that some investigators made certain approximations to the shape of the intersection curve for cases with small diameter ratios. The accuracy of such approximations is studied using four models with different d/D ratios. The nozzle radius of the four models is r_0. The vessel radius has a different value for each case such that

$$\frac{r_0}{R} = 0,\ .5,\ .8,\ 1.0 \tag{2.3.23}$$

The shape of the first quadrant of the intersection curve Γ on the unrolled vessel is plotted in Figure 2.5 for the four models. It is clear that for a diameter ratio up to 0.5, the opening can be represented by a circle. Larger diameter ratios are associated with intersection curves that can not be represented by a circle. In the case of the diameters of both cylinders being equal ($d/D = 1$), the intersection curve has a sharp corner along the transverse axis. The existence of this discontinuity in the slope of the intersection curve is one of the reasons the approach is not valid for d/D=1.

The same observations can be extended to the intersection curve on the lower edge of the unrolled nozzle. The edge may be assumed to be flat as long as the diameter ratio is less than 0.5 (see Figure 2.6).

§2.4 Directional Vectors

A set of orthonormal vectors is needed to describe the direction of actions on the boundary of each cylinder. For the vessel, the unit vectors $\vec{\mathbf{A}}_1$ and $\vec{\mathbf{A}}_2$ describe the vectors normal to the vessel surface and tangent to the intersection curve Γ respectively. These can be expressed as

$$\vec{\mathbf{A}}_1 = \sin\phi\,\vec{\mathbf{e}}_y + \cos\phi\,\vec{\mathbf{e}}_z \tag{2.4.1}$$

$$\vec{\mathbf{A}}_2 = \cos\alpha\,[-\sin\theta\,\vec{\mathbf{e}}_x + \cos\theta\,\vec{\mathbf{e}}_y - \tan\alpha\,\vec{\mathbf{e}}_z] \tag{2.4.2}$$

The vector $\vec{\mathbf{A}}_3$ is the unit vector normal to the intersection curve and tangent to the vessel midsurface. It can be evaluated by computing the cross product of the other two unit vectors $\vec{\mathbf{A}}_1$ and $\vec{\mathbf{A}}_2$.

$$\vec{\mathbf{A}}_3 = \cos\alpha\left[-\frac{\cos\theta}{\cos\phi}\,\vec{\mathbf{e}}_x - \sin\theta\cos\phi\,\vec{\mathbf{e}}_y + \sin\phi\sin\theta\,\vec{\mathbf{e}}_z\right] \tag{2.4.3}$$

For the nozzle boundary, $\vec{\mathbf{a}}_1$ represents the unit vector normal to the nozzle surface,

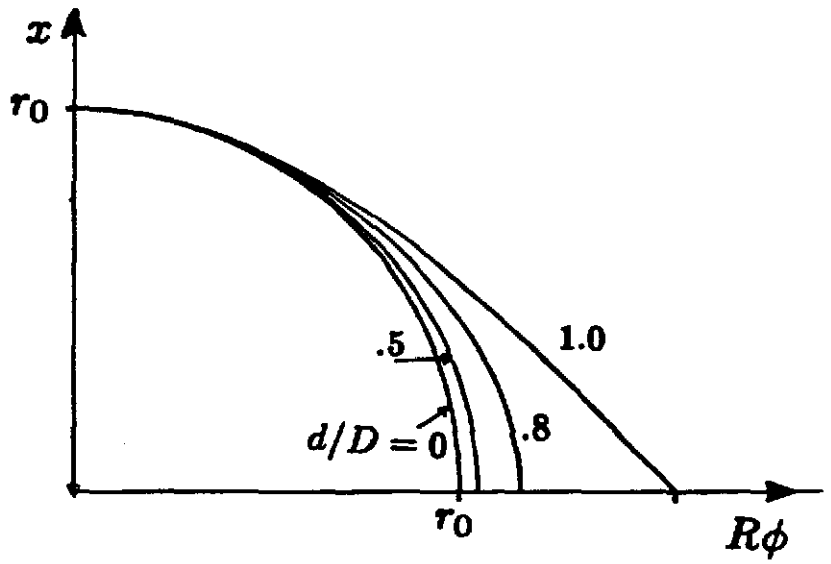

Figure 2.5

The first quadrant of the intersection curve Γ on the unrolled vessel for d/D= 0.0, 0.5, 0.8, and 1.0 .

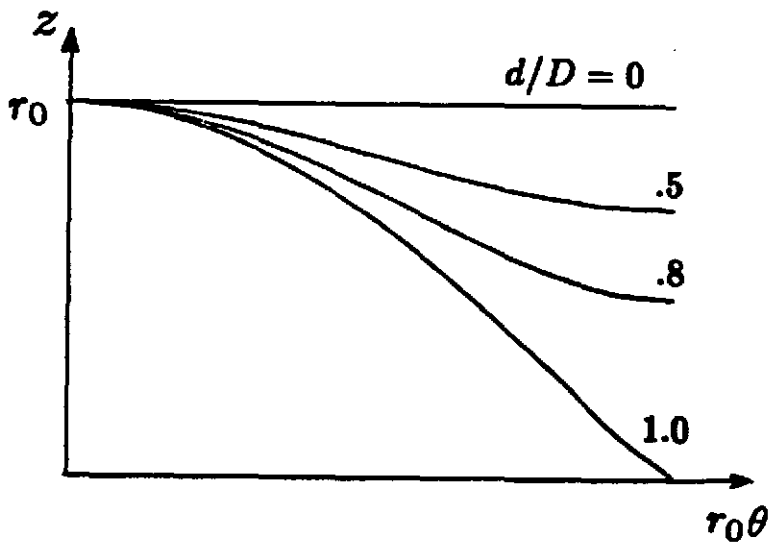

Figure 2.6

The first quadrant of the intersection curve Γ on the unrolled nozzle for d/D= 0.0, 0.5, 0.8, and 1.0 .

and $\vec{a}_2$ represents the unit vector tangent to the intersection curve. These can be defined as

$$\vec{a}_1 = \cos\theta\,\vec{e}_x + \sin\theta\,\vec{e}_y \tag{2.4.4}$$

$$\vec{a}_2 = \vec{A}_2 \tag{2.4.5}$$

The unit vector $\vec{a}_3$ is the vector normal to the intersection curve and tangential to the nozzle midsurface, defined as

$$\vec{a}_3 = -\sin\alpha\sin\theta\,\vec{e}_x + \sin\alpha\cos\theta\,\vec{e}_y + \cos\alpha\,\vec{e}_z \tag{2.4.6}$$

§2.5 Symmetry

By examining the geometry of the model and the effect of the different loading cases, it can be observed that for each loading case, certain symmetry requirements of the solution exist. For the cases of internal pressure, radial load on the nozzle, and axial force on the vessel ($Iload$= 0,1,5), the distribution of stresses is symmetric about both the longitudinal and transverse axes. Stresses are symmetric about the longitudinal axis but antisymmetric about the transverse axis for the case of a longitudinal moment on the nozzle. The opposite is true for the circumferential moment on the nozzle. Thus, the solution for only one quarter of the problem (e.g. 0 to $\pi/2$) is sufficient to evaluate the stresses around the complete junction. Since the solution will be in the form of a sum of a Fourier series, the selection of the appropriate trigonometric function depends on the loading configuration (see Table 2.2).

ILOAD	ISYM	Trigonometric Functions	
0,1,5	1	$\cos n\gamma$	($n = 0,\ 2,\ 4, \ldots$)
2	2	$\cos n\gamma$	($n = 1, 3,\ 5, \ldots$)
3	3	$\sin n\gamma$	($n = 1,\ 3,\ 5, \ldots$)
4	4	$\sin n\gamma$	($n = 2,\ 4,\ 6, \ldots$)

Table 2.2
Trigonometric functions of the Fourier expansion for the different loading cases. Either even or odd harmonics are needed depending on the symmetry.

العنوان:	STRESSES AT THE JUNCTION OF TWO NORMALLY INTERSECTING CIRCULAR CYLINDERS
المؤلف الرئيسي:	Khathlan, Abd Alrahman Abd Allah
مؤلفين آخرين:	Steele, Charles(Super)
التاريخ الميلادي:	1986
موقع:	ستانفورد
الصفحات:	1 - 156
رقم MD:	614792
نوع المحتوى:	رسائل جامعية
اللغة:	English
الدرجة العلمية:	رسالة دكتوراه
الجامعة:	Stanford University
الكلية:	College of Engineering
الدولة:	الولايات المتحدة الأمريكية
قواعد المعلومات:	Dissertations
مواضيع:	الهندسة المدنية، التصميمات الهندسية، الحاسب الآلي
رابط:	https://search.mandumah.com/Record/614792

Chapter 3

Solution for a Circular Cylinder

The elastic behavior of the circular cylinder has been investigated thoroughly over the past few decades more than other types of shells because of its simple geometry and common use. Circular cylinders were also studied in detail because they exhibit the characteristic load-resisting states of shells (i.e. membrane, inextensional, and edge bending). In this study, solutions for the circular cylinder are needed for use as the basic "building blocks" for the solution of the two intersecting shells. This chapter is devoted to the evaluation of stresses and strains in a circular cylinder due to edge loading. A set of simple, accurate equations for the cylinder is developed using one of the several possible approaches to the problem.

§3.1 Equilibrium Equations

A circular cylinder with midsurface radius R and constant thickness T is shown in Figure 3.1. The surface of the cylinder is free of any external loads, since interest is limited to edge loading only. For an element $ABCD$ (see Fig. (3.2)), the equations of force equilibrium in the x, y, z directions reduce respectively to

$$\begin{aligned} \frac{\partial N_x}{\partial x} + \frac{\partial N_{x\phi}}{R\partial\phi} &= 0 \\ \frac{\partial N_\phi}{R\partial\phi} + \frac{\partial N_{x\phi}}{\partial x} + \frac{Q_\phi}{R} &= 0 \end{aligned} \tag{3.1.1}$$

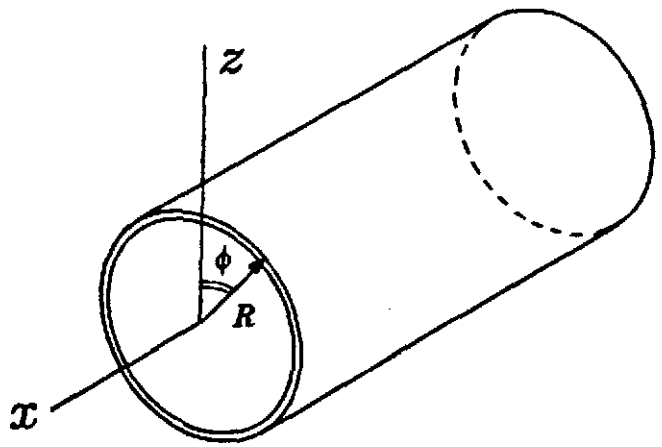

Figure 3.1

A thin circular cylindrical shell of mean radius R and thickness T.

$$\frac{\partial Q_\phi}{R\partial\phi} + \frac{\partial Q_{x\phi}}{\partial x} - \frac{N_\phi}{R} = 0$$

Similarly, the equations of moment equilibrium about the x and y axes are

$$\begin{aligned} \frac{\partial M_\phi}{R\partial\phi} + \frac{\partial M_{x\phi}}{\partial x} - Q_\phi &= 0 \\ \frac{\partial M_x}{\partial x} + \frac{\partial M_{x\phi}}{R\partial\phi} - Q_x &= 0 \end{aligned} \tag{3.1.2}$$

§3.2 Historical Review of Existing Solutions

Using stress-strain and strain-displacement relations, Flügge (1960) reduced the equations of equilibrium for a circular cylinder to a set of three differential

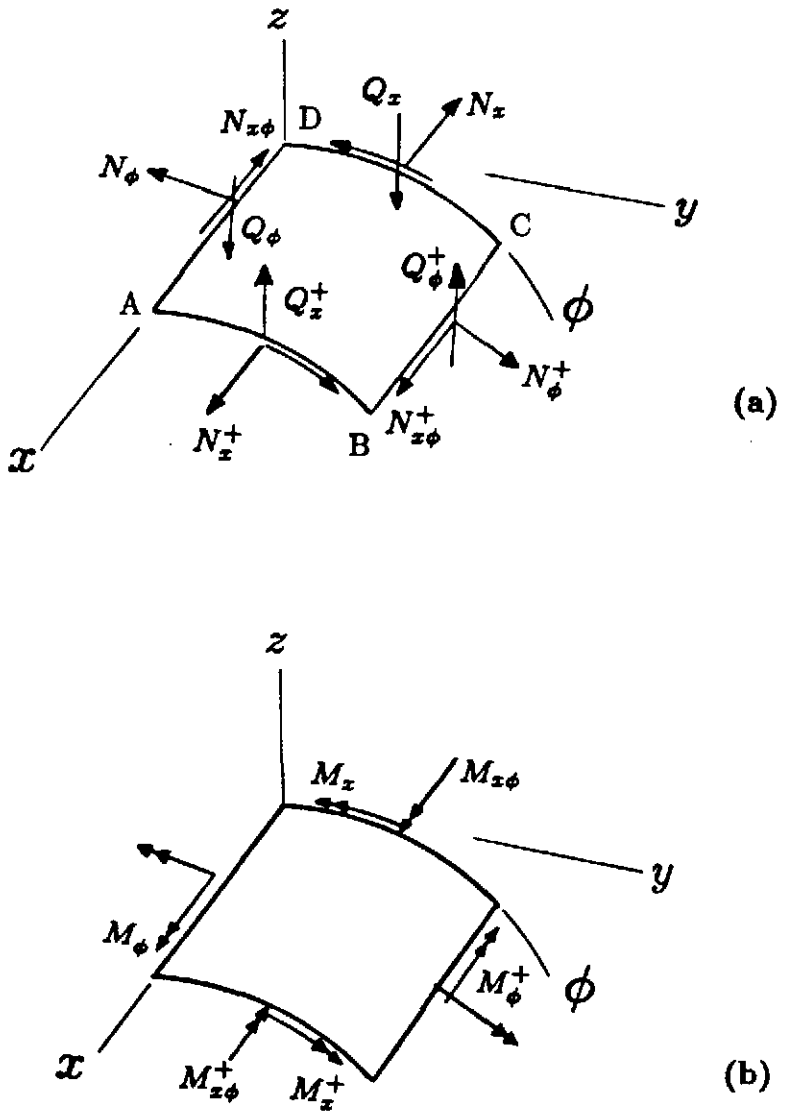

Figure 3.2

Stress resultants acting on the boundary of an infinitesimal element of the cylinder surface ($ABCD$), a) membrane stress resultants and transverse shears, b) bending and twisting moments.

equations in terms of the midsurface displacements u,v, and w. By retaining as many terms as feasible in the process, his equations reduce to

$$u_{xx} + \frac{1-\nu}{2}u_{\phi\phi} + \frac{1+\nu}{2}v_{x\phi} + \nu w_x + \frac{T^2}{12R^2}\left[\frac{1-\nu}{2}u_{\phi\phi} - w_{xxx} + \frac{1-\nu}{2}w_{x\phi\phi}\right] = 0$$

$$\frac{1+\nu}{2}u_{x\phi} + v_{\phi\phi} + \frac{1-\nu}{2}v_{xx} + w_\phi + \frac{T^2}{12R^2}\left[\frac{3}{2}(1-\nu)v_{xx} - \frac{3-\nu}{2}w_{xx\phi}\right] = 0$$

$$\nu u_x + v_\phi + w + \frac{T^2}{12R^2}\left[\frac{1-\nu}{2}u_{x\phi\phi} - u_{xxx} - \frac{3-\nu}{2}v_{xx\phi} + w_{xxxx}\right.$$

$$\left. + 2w_{xx\phi\phi} + w_{\phi\phi\phi\phi} + 2w\phi\phi + w\right] = 0 \qquad (3.2.1)$$

where

$$(\ldots)_x = R\frac{\partial(\ldots)}{\partial x} \quad , \quad (\ldots)_\phi = \frac{\partial(\ldots)}{\partial\phi}$$

Although this set of equations is accurate, it is also cumbersome and very difficult to solve, which explains why it has been avoided most of the time.

During his investigation of buckling of circular cylinders, Donnell (1933) derived a much simpler set of equations. His equations are considered equivalent to applying certain approximations to Flugge's equations. These approximations include neglecting terms of of order $(T/R)^2$ in the stress-strain relations, and neglecting the effect of the displacements u and v on the bending stresses. These assumptions produced a very simple set of equations described as

$$\Delta\Delta\Delta\Delta w + \left(\frac{1}{RC}\right)^2 \frac{\partial^4 w}{\partial x^4} = 0$$

$$\Delta\Delta u = \nu\frac{\partial^3 w}{\partial x^3} - \frac{\partial^3 w}{R^2\partial x\partial\phi^2} \qquad (3.2.2)$$

$$\Delta\Delta v = (2+\nu)\frac{\partial^3 w}{R\partial x^2 \partial\phi} + \frac{\partial^3 w}{R^3 \partial\phi^3}$$

in which

$$\Delta(\ldots) = \frac{\partial^2(\ldots)}{\partial x^2} + \frac{\partial^2(\ldots)}{R^2\partial\phi^2} \tag{3.2.3}$$

and the reduced thickness of the cylinder is

$$C = T/\sqrt{12(1-\nu^2)} \tag{3.2.4}$$

where ν is Poisson's ratio.

By examining (3.2.2) it is obvious that this set of equations is much simpler to solve than (3.2.1), which led to its popularity. However, as Hoff (1955) pointed out, the acquired simplicity in (3.2.2) leads in some specific cases to unacceptable errors. It was shown that the accuracy of the solution of (3.2.2) deteriorates as the wavelength of deformations increases. In other words, Donnell's equations are not accurate for handling the lower harmonics of the solution. This is exhibited by the absence of ring and beam bending solutions to the equations.

This led Morley (1959) to the development of another set of equations which matches the accuracy of (3.2.1) and the elegance and simplicity of (3.2.2). Using an *ad hoc* approach, he replaced the first equation in (3.2.2) by

$$\Delta\Delta(\Delta+1)^2 w + \left(\frac{1}{RC}\right)^2 \frac{\partial^4 w}{\partial x^4} = 0 \tag{3.2.5}$$

while retaining the same two equations for u and v. Numerical results showed that a significant improvement in the accuracy of the solution of (3.2.5) over (3.2.2).

As pointed out by Novozhilov (1964), another approach was used by Feinburg to develop equations for the cylinder using a complex formulation and the *static-geometric analogy* (see §3.3.2). This approach led to a single complex-valued equation

$$\Delta\Delta\Psi + \frac{i}{RC}\frac{\partial^2\Psi}{\partial x^2} = 0 \tag{3.2.6}$$

where the dependent variable Ψ is a complex stress-displacement function

$$\Psi = w - \frac{i}{ETC}\Phi \tag{3.2.7}$$

in which Φ is the Airy stress function and E is the modulus of elasticity.

One of the advantages of using (3.2.6) is that the order of the equation is half of that for (3.2.2), which leads to a reduction in the computation. Another advantage is the ease of prescribing stress boundary conditions because stress can be easily expressed in terms of the stress function Φ, in contrast to the more complicated stress-displacement relations. However, (3.2.6) has the same shortcomings of Donnell's equations, primarily that solutions for ring and beam bending are missing from the equation. As a result, Novozhilov proposed an improved equation that includes the missing solutions in which the dependent variable is composed of stresses and curvatures for the real and imaginary parts, respectively. His improved equation has an effect similar to that of Morley's improved equation.

§3.3 Sanders' Equations for the Circular Cylinder

Of the different formulations for the cylinder equations, it was decided that the equations derived by Sanders are the best choice for use in this study, because of their simplicity, consistency, and accuracy. These equations were derived using *exact* equilibrium equations, *exact* strain-displacement relations, and *approximate*

stress-strain relations. The use of these approximate relations is justified by the fact that the errors it introduces are of the same order of magnitude as the error that has already been introduced by using the Kirchhoff hypothesis.

3.3.1 Solution of Sanders' Equations

According to Simmonds (1966), using the stress-displacement function Ψ defined in (3.2.7), Sanders' equations can be reduced to

$$\Delta\Delta\Psi + \frac{\partial^2\Psi}{R^4\partial\theta^2} - \frac{i}{RC}\frac{\partial^2\Psi}{\partial x^2} = 0 \tag{3.3.1}$$

For a complete cylinder, the solution for (3.3.1) is periodic in ϕ. This permits the expression of Ψ in the form of a Fourier series

$$\Psi = \sum_{n=0,1,2,..}^{\infty} e^{\xi x/R}\,(A_n \cos n\phi + B_n \sin n\phi) \tag{3.3.2}$$

In the subsequent work, the solution is assumed to be symmetric about the longitudinal axis by retaining the $\cos n\phi$ term and dropping the $\sin n\phi$ term. However, $\sin n\phi$ may be used instead to represent the anti-symmetric cases about the longitudinal axis by replacing $\cos n\phi$ with $\sin n\phi$, and $\sin n\phi$ with $(-\cos n\phi)$ in all of the following equations.

Since the different harmonics of (3.3.2) are uncoupled, a general solution for each harmonic n is developed by dropping the summation sign. Using (3.3.2), it can be shown that

$$\frac{\partial^2\Psi}{\partial x^2} = \frac{\xi^2}{R^2}\, e^{\xi x/r} \cos n\phi = \frac{\xi^2}{R^2}\Psi \tag{3.3.3}$$

and

$$\frac{\partial^2 \Psi}{R^2 \partial \phi^2} = \frac{-n^2}{R^2} e^{\xi x/r} \cos n\phi = \frac{-n^2}{R^2} \Psi \tag{3.3.4}$$

In this case, the Laplacian reduces to

$$\Delta \Psi = \frac{1}{R^2} \left(\xi^2 - n^2\right) \Psi \tag{3.3.5}$$

Substituting the previous three equations in (3.3.1)

$$\left(\xi^2 - n^2\right)^2 - n^2 + \frac{iR}{C} \xi^2 = 0 \tag{3.3.6}$$

The complex quantities T_1, T_2, T_3, and T_4 are introduced such that

$$\begin{aligned} T_2(x,\xi) &= e^{\xi x/R} \\ T_1(x,\xi) &= \xi T_2 \\ T_3(x,\xi) &= \left(1 - \frac{\xi^2(\xi^2 - n^2)}{n^2(\xi^2 - n^2 + 1)}\right) T_2 \\ T_4(x,\xi) &= \xi T_3 \end{aligned} \tag{3.3.7}$$

The stresses and strains in the cylinder can be expressed using the complex quantities T_1, T_2, T_3, and T_4 as explained by Steele and Steele (1983).

a) Stress resultants:

$$
\begin{aligned}
N_x &= Im(-T_2)\cos n\phi \\
N_\phi &= Im(-T_3 + T_2)\cos n\phi \\
N_{x\phi} &= Im\left(\frac{T_1}{n}\right)\sin n\phi \\
M_x &= Re[-T_3 + (1-\nu)T_2]\cos n\phi \\
M_\phi &= Re[-(1-\nu)T_2 - \nu T_3]\cos n\phi \\
M_{x\phi} &= (1-\nu)Re\left(\frac{-T_1}{n}\right)\sin n\phi \\
Q_x &= Re\left(\frac{-T_4}{R}\right)\cos n\phi \\
Q_\phi &= Re\left(\frac{nT_3}{R}\right)\sin n\phi
\end{aligned}
\tag{3.3.8}
$$

where Re and Im indicate the real and imaginary parts of the function, respectively.

b) Curvatures and strains:

$$
\begin{aligned}
\epsilon_x &= \frac{1}{ETC}Im[(1+\nu)T_2 + \nu T_3]\cos n\phi \\
\epsilon_\phi &= \frac{1}{ETC}Im[-T_3 + (1+\nu)T_2]\cos n\phi \\
\kappa_x &= \frac{1}{ETC^2}Re(-T_3 + T_2)\cos n\phi \\
\kappa_\phi &= \frac{1}{ETC^2}Re(-T_2)\cos n\phi \\
\epsilon_{x\phi} &= \frac{(1+\nu)}{ETC}Im\left(\frac{-T_1}{n}\right)\sin n\phi \\
\tau &= \frac{1}{ETC^2}Re\left(\frac{T_1}{n}\right)\sin n\phi
\end{aligned}
\tag{3.3.9}
$$

where ϵ_x, ϵ_ϕ, $\epsilon_{x\phi}$ represent the midsurface strains, κ_x, κ_ϕ represent the curvature changes, and τ represents the twist.

On an edge $x =$ constant, four force quantities will be acting. These are;

$$M_x,\ N_x,\ N_{x\phi},\ V_x$$

where the last quantity (V_x) represents the effective Kirchhoff transverse shear

$$\begin{aligned} V_x &= Q_x + \frac{\partial M_{x\phi}}{R\partial\phi} \\ &= Re\left[-T_4 - (1-\nu)T_1\right]\frac{1}{R} \end{aligned} \tag{3.3.10}$$

The four force quantities are arranged in a force vector

$$\mathbf{F}_x(x,\xi) = \begin{Bmatrix} M_x \\ RV_x \\ CN_x \\ C\frac{\partial N_{x\phi}}{\partial\phi} \end{Bmatrix} = Re \begin{Bmatrix} -T_3 + (1-\nu)T_2 \\ -T_4 - (1-\nu)T_1 \\ iT_2 \\ -iT_1 \end{Bmatrix} \cos n\phi \tag{3.3.11}$$

Some of the elements in $\mathbf{F}_x$ have been multiplied by the constants R and C in order to simplify the algebra. For convenience, the derivative of the tangential shear $\frac{\partial N_{x\phi}}{\partial\phi}$ is used instead of $N_{x\phi}$ in order to express all elements of the force vector as functions of $\cos n\phi$ instead of having mixed $\cos n\phi$ and $\sin n\phi$ terms.

In a similar manner, the displacement vector $\mathbf{D}_x$ including the strain and curvature change measures at the edge of the cylinder, can be expressed as ;

$$\mathbf{D}_x(x,\xi) = \begin{Bmatrix} -ETC^2\frac{\partial\tau}{\partial\varphi} \\ ETC^2\kappa_\phi \\ ETCR\kappa_g \\ ETC\epsilon_\phi \end{Bmatrix} = Im \begin{Bmatrix} -iT_1 \\ iT_2 \\ T_4 + (1+\nu)T_1 \\ T_3 - (1+\nu)T_2 \end{Bmatrix} \cos n\phi \tag{3.3.12}$$

where κ_g represents the geodesic curvature.

In the displacement vector, strain and curvature measures were used instead of the displacements of the midsurface for several important reasons. One of the

reasons is the desired elimination of rigid body translation from $\mathbf{D}_x$. Another more important reason is the need to avoid singularities in the cylinder when edge displacements are prescribed (to be discussed in Chapter 4).

3.3.2 The Static-Geometric Analogy

Goldenveizer's (1961) *static-geometric analogy* is a useful tool for solving some elasticity problems. Whenever it is applied properly, it can reduce an eighth order problem to fourth order. The analogy is linked to the idea of stress functions in plane elasticity. It is based on the principle that there is a certain similarity between the equations of equilibrium and the equations of compatibility. This is illustrated by examining the equations for a shallow cylindrical shell

$$(RC)\Delta\Delta w + \frac{1}{ETC}\frac{\partial^2 \Phi}{\partial x^2} = 0 \tag{3.3.13}$$

$$\frac{-1}{ETC}\Delta\Delta\Phi + \frac{1}{RC}\frac{\partial^2 w}{\partial x^2} = 0 \tag{3.3.14}$$

The analogous structure of the two equations is evident, and makes it possible to combine both equations in one single complex equation

$$\Delta\Delta\Psi + \frac{i}{RC}\frac{\partial^2 \Psi}{\partial x^2} = 0 \tag{3.3.15}$$

where Ψ is given by (3.2.7).

Furthermore, by examining (3.3.11) and (3.3.12), it can be observed that each of the elements of $\mathbf{D}_x$ correspond to an element in $\mathbf{F}_x$, if ν is replaced by $-\nu$. The correspondence is as follows

$$M_x \Longleftrightarrow ETC\epsilon_\phi \quad , \quad RV_x \Longleftrightarrow ETCR\kappa_g \tag{3.3.16}$$

$$CN_x \Longleftrightarrow ETC^2\kappa_\phi \quad , \quad C\frac{\partial N_{x\phi}}{\partial \phi} \Longleftrightarrow -ETC^2\frac{\partial \tau}{\partial \phi}$$

§3.4 Solution for a Semi-infinite Cylinder

The solution for a semi-infinite circular cylinder, extending from $x = 0$ to $x = \infty$ is simplified by the fact that there is no coupling between the two edges. Thus, attention is limited to the solutions at $x = 0$ that decay along the length of the cylinder ($x \leq 0$).

For each harmonic n, the solution of (3.3.6) provides four values for the complex root ξ. However, only the two roots with positive real part (ξ_1, ξ_2) will be used, to accommodate the requirement that all quantities should decay exponentially along the axis of the cylinder.

By introducing four *real* arbitrary constants, (3.3.7-a) can be generalized as

$$T_2(x,\xi) = (c_1 + ic_2)\, e^{\xi_1 x/R} + (c_3 + ic_4)\, e^{\xi_2 x/R} \tag{3.4.1}$$

The force and displacement vectors $\mathbf{F}_x$, and $\mathbf{D}_x$ can be expressed in terms of the arbitrary constants. In matrix form, the relationships are

$$\mathbf{F}_x = \mathbf{FM}_x \times \mathbf{c} \tag{3.4.2}$$

$$\mathbf{D}_x = \mathbf{DM}_x \times \mathbf{c} \tag{3.4.3}$$

where

$$\mathbf{c} = \begin{Bmatrix} c_1 \\ c_2 \\ c_3 \\ c_4 \end{Bmatrix} \tag{3.4.4}$$

The matrices $\mathbf{FM}_x$, and $\mathbf{DM}_x$ are 4×4 matrices that were generated on a column-by-column basis by interchangeably computing the real and imaginary parts of $\mathbf{F}_x$

and $\mathbf{D}_x$ using

$$\xi = \xi_1, \xi_2 \qquad \text{, and} \quad x = 0$$

as illustrated in (3.4.5)

$$\mathbf{FM}_x = \left[\{Re\mathbf{F}_x(0,\xi_1)\}\ \{-Im\mathbf{F}_x(0,\xi_1)\}\ \{Re\mathbf{F}_x(0,\xi_2)\}\ \{-Im\mathbf{F}_x(0,\xi_2)\}\right]$$
$$\mathbf{DM}_x = \left[\{Re\mathbf{D}_x(0,\xi_1)\}\ \{-Im\mathbf{D}_x(0,\xi_1)\}\ \{Re\mathbf{D}_x(0,\xi_2)\}\ \{-Im\mathbf{D}_x(0,\xi_2)\}\right] \tag{3.4.5}$$

The four constants c_1, c_2, c_3, c_4 indicate that there are four arbitrary quantities to be prescribed at the edge (x=0) of the cylinder. In general, a combination of four of the elements of $\mathbf{F}_x$ and $\mathbf{D}_x$ are prescribed, provided that it satisfies equilibrium and compatibility (see §3.5). The choice of which elements are to be used is determined by the problem and the symmetry requirements along the transverse axis.

§3.5 Equilibrium and Compatibility

As stated earlier, the prescribed edge quantities need to satisfy the requirements of force and moment equilibrium, and deformation compatibility. It can be shown that any single harmonic periodic distribution of forces on the edge is self-equilibrating as long as

$$n \geq 2$$

By examining (3.3.6), it can be observed that for the two lowest harmonics (n = 0, 1), two of the roots (ξ_1, ξ_3) will be identically zero. So for these special cases,

the solution for the semi-infinite cylinder depends on one root only ξ_2, and has only two arbitrary constants instead of four.

3.5.1 Axisymmetric Distribution ($n = 0$)

This case represents the membrane behavior of a cylinder loaded along its axis. For this loading type to be self-equilibrating, the $N_x^{(0)}$ component of the solution has to vanish. Similarly, the tangential shear and the twist are also non-existent because of the axisymmetry of the solution. Thus,

$$\begin{aligned} (N_x)^{(0)} &= 0 \\ (N_{x\phi})^{(0)} &= 0 \\ \left(ETC^2\tau\right)^{(0)} &= 0 \\ \left(ETC^2\kappa_\phi\right)^{(0)} &= 0 \end{aligned} \tag{3.5.1}$$

where the superscript n indicates the Fourier coefficient of the nth harmonic.

3.5.2 Asymmetric Distribution ($n = 1$)

In order for a cylinder subjected to an asymmetric loading distribution to remain in equilibrium, it has to satisfy the moment equilibrium equation about the y-axis (Figure 3.3)

$$\int_0^{2\pi} M_x \cos\phi \, R d\phi + \int_0^{2\pi} N_x R \cos\phi \, R d\phi = 0 \tag{3.5.2}$$

This relation can be expressed in terms of the Fourier coefficients as

$$R(M_x)^{(1)} \int_0^{2\pi} \cos^2\phi \, d\phi + (N_x)^{(1)} R^2 \int_0^{2\pi} \cos^2\phi \, d\phi = 0 \tag{3.5.3}$$

which reduces to

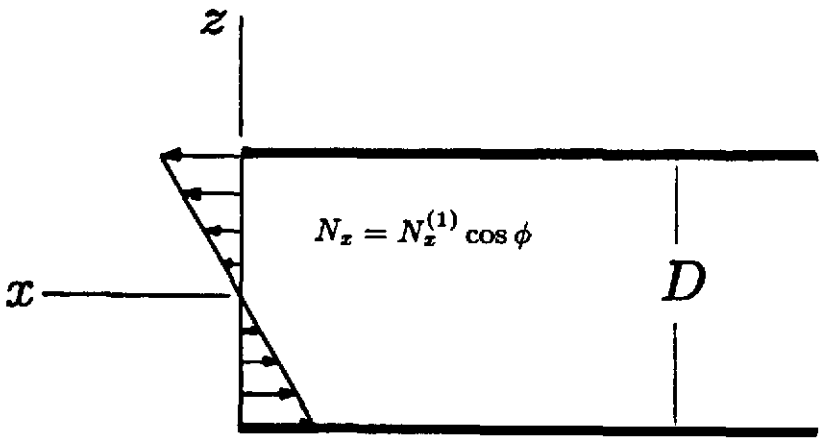

Figure 3.3

A circular cylinder subjected to an end asymmetric membrane stress resultant distribution $N_x = N_x^{(1)} \cos\phi$.

$$(N_x)^{(1)} = \frac{-1}{R}(M_x)^{(1)} \tag{3.5.4}$$

This indicates that the there is a dependency between the elements of the force vector $\mathbf{F}_x$. It can also be shown that a similar dependency exists between the elements of $\mathbf{D}_x$ .These dependencies are summarized as follows,

$$\begin{aligned}
(CN_x)^{(1)} &= \frac{-C}{R}(M_x)^{(1)} \\
\left(C\frac{\partial N_{x\phi}}{\partial\phi}\right)^{(1)} &= \frac{-C}{R}(RV_x)^{(1)} \\
\left(-ETC^2\frac{\partial\tau}{\partial\phi}\right)^{(1)} &= \frac{-C}{R}(ETCR\kappa_g)^{(1)} \\
(ETC^2\kappa_\phi)^{(1)} &= \frac{C}{R}(ETC\epsilon_\phi)^{(1)}
\end{aligned} \tag{3.5.5}$$

As a result, for the special case of n=0 and n=1, the order of the problem is halved and the force and displacement vectors reduce to

$$\mathbf{F}_x = \begin{pmatrix} M_x \\ RV_x \end{pmatrix} \qquad \mathbf{D}_x = \begin{pmatrix} ETCR\kappa_g \\ ETC\epsilon_\phi \end{pmatrix} \tag{3.5.6}$$

and the vector of the arbitrary constants becomes

$$\mathbf{c} = \begin{pmatrix} c_3 \\ c_4 \end{pmatrix} \tag{3.5.7}$$

العنوان:	STRESSES AT THE JUNCTION OF TWO NORMALLY INTERSECTING CIRCULAR CYLINDERS
المؤلف الرئيسي:	Khathlan, Abd Alrahman Abd Allah
مؤلفين آخرين:	Steele, Charles(Super)
التاريخ الميلادي:	1986
موقع:	ستانفورد
الصفحات:	1 - 156
رقم MD:	614792
نوع المحتوى:	رسائل جامعية
اللغة:	English
الدرجة العلمية:	رسالة دكتوراه
الجامعة:	Stanford University
الكلية:	College of Engineering
الدولة:	الولايات المتحدة الأمريكية
قواعد المعلومات:	Dissertations
مواضيع:	الهندسة المدنية، التصميمات الهندسية، الحاسب الآلي
رابط:	https://search.mandumah.com/Record/614792

Chapter 4

The Cut Method

In order to analyze the stress field at the junction of the two cylinders, it is essential to evaluate "stiffness" coefficients that relate the force quantities to the displacement quantities along the boundary of the opening in the vessel. Unlike the problem of a circular hole in a flat plate, stiffness coefficients for an opening in a cylindrical shell may be impossible to evaluate in a closed-form. This is due to the loss of the axisymmetry of the problem, and the complicated interaction between the bending, inextensional, and membrane behavior of the cylinder. This chapter is devoted to the description of the *cut method*, which is a new technique for generating the stiffness coefficients for the low harmonics of the solution.

§4.1 Description of the Method

The first step of the approach is to make a through-thickness circumferential cut at the top of the cylinder (see Figs. 4.1 and 4.2). This cut is located along the circumferential arc at midspan ($x=0$) and does not extend outside the region covered by the nozzle. As far as the physical wall of the vessel is concerned, the cut is fictitious, since it is made in the region of the opening. The size of the cut is defined using the angle β, where

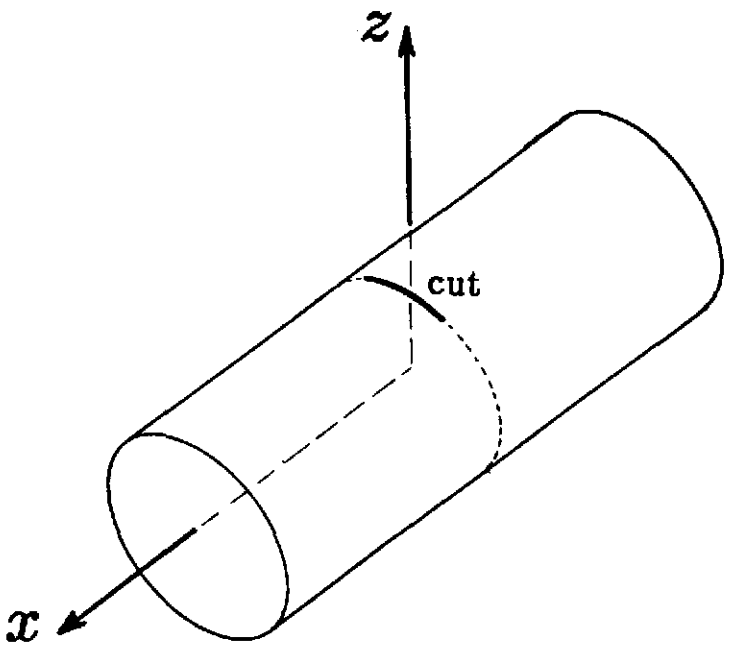

Figure 4.1

Position of the circumferential cut in the vessel surface extending inside the zone covered by the intersecting nozzle.

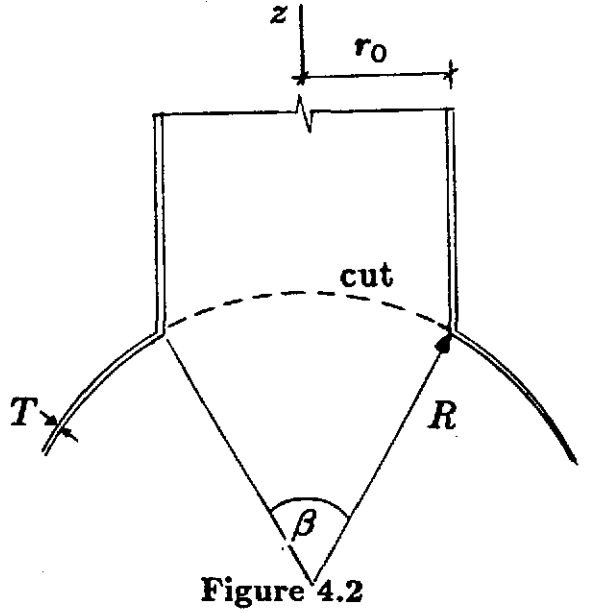

Figure 4.2

Cross section of the nozzle-vessel junction at $x = 0$, illustrating the position of the cut. The size of the cut is determined using the angle β; Eq. (4.1.1).

$$\beta = 2 \arcsin\left(\frac{r_0}{R}\right) \tag{4.1.1}$$

It is possible to visualize the vessel as two separate cylinders which are joined at $x = 0$. The first extends along $0 \leq x \leq L/2$ and the second along $-L/2 \leq x \leq 0$. At $x = 0$, the two cylinders are continuous *outside* the cut ($|\phi| \geq \beta/2$) but not inside the cut ($|\phi| \leq \beta/2$). Therefore, arbitrary distributions of force or displacement discontinuities may be precribed on the edges of the cut. However, these distributions must satisfy the continuity and regularity requirements on the circumference outside the cut, where the two cylinders are continuous.

For example, the functions $f_i(\phi)$, illustrated in Fig. 4.3, will be used in the cases where there is symmetry about the longitudinal axis ($Isym$=1,2). When the loading configuration is such that there is symmetry about the transverse axis ($Isym$=3,4), another set of functions $g_i(\phi)$ are used as the cut distributions (see Fig. 4.4).

By examining Figure 4.3, it can be seen that the functions $f_i(\phi)$ can be approximated as

$$f_i(\phi) \approx \begin{cases} \cos\frac{(2i-1)\pi\phi}{\beta} & \text{for } |\phi| < \beta/2; \\ 0 & \text{for } |\phi| \geq \beta/2 \end{cases} \qquad ;i = 1, 2, \cdots, 7 \tag{4.1.2}$$

The main difference is that the functions shown in Figure 4.3 are corrected to make the slope $f_i'(\phi)$ vanish at the ends of the cut. This makes the transition from inside to outside the cut much smoother and ultimately leads to faster convergence when the cut functions are expressed in the form of a Fourier series around the complete circumference.

For example, consider the function $f_1(\phi)$ and its approximate counterpart $\mathcal{F}_1(\phi)$, which are shown in Figure 4.5 . By expanding each function into a Fourier series, the Fourier coefficients can be evaluated. By comparing the two sets of

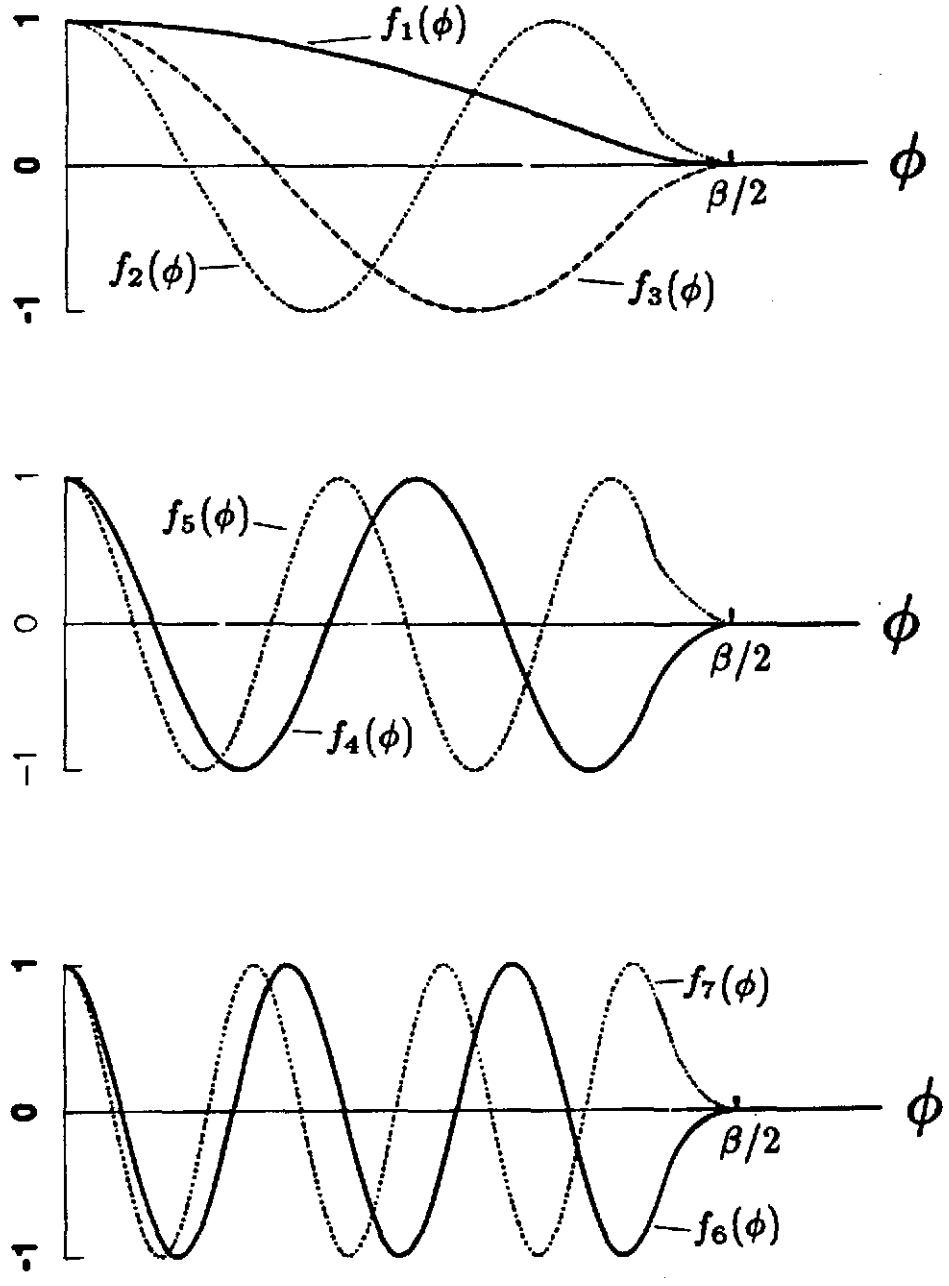

Figure 4.3

The cut distribution functions $f_i(\phi)$, for $Isym$=1 and 2. The value of all the functions is zero outside the cut ($|\phi| \geq \beta/2$). These functions are even about $\phi = 0$.

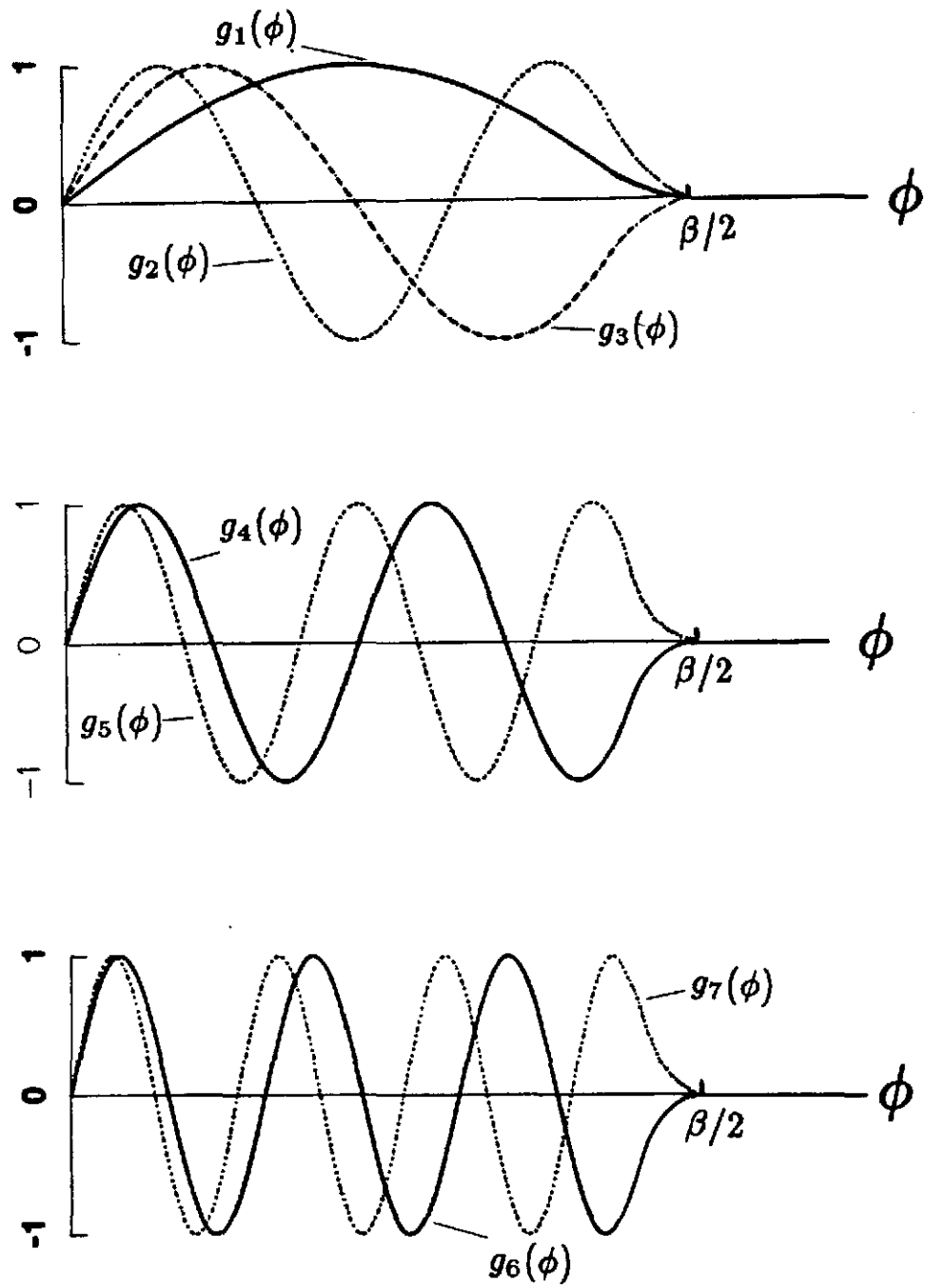

Figure 4.4

The cut distribution functions $g_i(\phi)$, for $Isym$=3 and 4. The value of all the functions is zero outside the cut ($|\phi| \geq \beta/2$). These functions are odd about $\phi = 0$.

n	$\mathcal{F}_1^{(n)}$	$f_1^{(n)}$
0	0.637	0.424
1	0 425	0.509
2	-0.085	0.073
3	0.036	-0.008
4	-0.020	0.002
5	0.013	-0.001
6	-0.009	0.000
7	0.007	0.000
8	-0.005	0.000
9	0.004	0.000
10	-0.003	0.000

Table 4.1
The lowest ten Fourier coefficients for the functions $\mathcal{F}_1(\phi)$ and $f_1(\phi)$ shown in Fig. 4.5 ($\beta = 60°$).

Fourier coefficients, listed in Table 4.1, one can observe that the smoother function $f_1(\phi)$ converges much faster than $\mathcal{F}_1(\phi)$.

§4.2 Discontinuities on the Cut

It was illustrated in §3.3 that for a semi-infinite circular cylinder, four distributions of force or displacement quantities can be prescribed at the edge $x=0$. For the cut method, these distributions will be composed of a set of cut functions $f_i(\phi)$ or $g_i(\phi)$, depending on the symmetry requirements. For example, in the case of $Isym$ =1 or 2 , these four edge distributions are

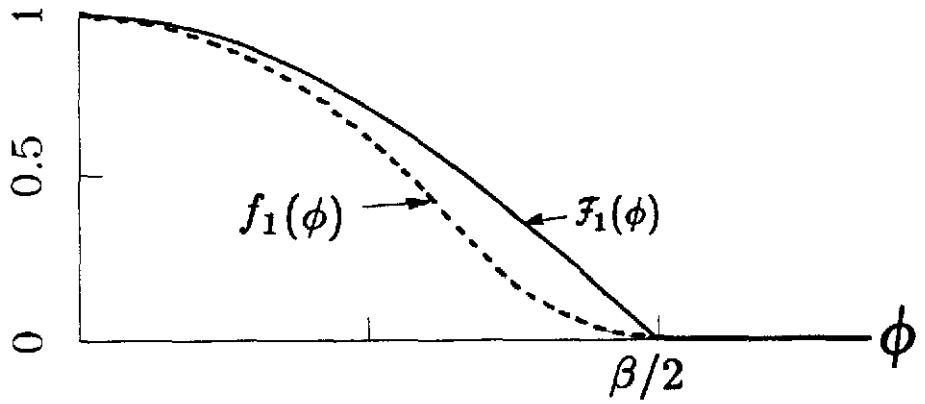

Figure 4.5

Comparison between two similar functions $f_1(\phi)$, which has a zero slope at $\phi = \beta/2$, and $\mathcal{F}_1(\phi)$ which has a nonzero slope at $\phi = \beta/2$ (see Table 4.1).

$$
\begin{aligned}
S_1(\phi) &= a_1 f_1(\phi) + \sum_{i=1}^{NHC} b_i f_{i+1}(\phi) \\
S_2(\phi) &= a_2 f_1(\phi) + \sum_{i=NHC+1}^{2\times NHC} b_i f_{i-NHC+1}(\phi) \\
S_3(\phi) &= a_3 f_1(\phi) + \sum_{i=2\times NHC+1}^{3\times NHC-1} b_i f_{i-2\times NHC+1}(\phi) \\
S_4(\phi) &= a_4 f_1(\phi) + \sum_{i=3\times NHC}^{4\times NHC-2} b_i f_{i-3\times NHC+2}(\phi)
\end{aligned}
\tag{4.2.1}
$$

where NHC is a parameter that indicates the number of harmonics to be handled by the *cut method* in the analysis. The significance of this parameter will be explained later, but for the current work it is sufficient to define it as

$$2 \leq NHC \leq 6 \tag{4.2.2}$$

In (4.2.1), a_i and b_i represent arbitrary constants. The first group is used to satisfy the regularity requirements of the solution, and the latter to generate the stiffness coefficients.

Each of the edge distributions $S_i(\phi)$ will correspond to one of the eight elements of the force and displacement vectors along the flat edge of the cylinder, $\mathbf{F}_x$ and $\mathbf{D}_x$, respectively (see (3.3.11)). The symmetry requirement for the solution dictates which quantities are to be used as the appropriate cut distributions according to Table 4.2 .

The quantities selected in Table 4.2 for each symmetry type represent the ones that have to be identically equal to zero outside the cut ($|\phi| \geq \beta/2$). For example, in the case of a longitudinal moment applied to the nozzle ($Isym$=2), continuity between the two semi-infinite cylinders requires that the midsurface displacements w and v along the the $x = 0$ plane must be zero. Using the following definitions of the circumferential curvature κ_ϕ and the circumferential strain ϵ_ϕ in terms of the midsurface displacements

$$\begin{aligned} \kappa_\phi &= -\frac{\partial^2 w}{R^2 \partial \phi^2} + \frac{1}{R}\frac{\partial v}{R \partial \phi} \\ \epsilon_\phi &= \frac{\partial v}{R \partial \phi} + \frac{w}{R} \end{aligned} \tag{4.2.3}$$

it can be concluded that κ_ϕ and ϵ_ϕ are also zero at midspan.

In addition, to satisfy equilibrium between the two semi-infinite cylinders, the moment and in-plane stress resultant have to be zero along the circumferential arc located at $x = 0$. As a result, for this symmetry case

$$M_x = N_x = \kappa_\phi = \epsilon_\phi = 0, \qquad \text{for} \qquad x = 0 \text{ and } \quad |\phi| \geq \beta/2 \tag{4.2.4}$$

$Isym$	$S_1(\phi)$	$S_2(\phi)$	$S_3(\phi)$	$S_4(\phi)$	Function
1	RV_x	$C\frac{\partial N_{x\phi}}{\partial \phi}$	$-ETC^2\frac{\partial \tau}{\partial \varphi}$	$ETCR\kappa_g$	$f_i(\phi)$
2	M_x	CN_x	$ETC^2\kappa_\phi$	$ETC\epsilon_\phi$	$f_i(\phi)$
3	RV_x	$C\frac{\partial N_{x\varphi}}{\partial \phi}$	$-ETC^2\frac{\partial \tau}{\partial \varphi}$	$ETCR\kappa_g$	$g_i(\phi)$
4	M_x	CN_x	$ETC^2\kappa_\phi$	$ETC\epsilon_\phi$	$g_i(\phi)$

Table 4.2
Force and displacement quantities to be used as cut distributions for each symmetry case.

which illustrates why these quantities were listed in Table 4.2 as the appropriate cut functions corresponding to $Isym = 2$.

The next step involves the expansion of the cut distributions $S_i(\phi)$ in the form of a finite Fourier series. This is necessary to be able to utilize the solution of the equations for the circular cylinder given in §3.3 .

For cases with $Isym$ =1 or 2, the Fourier series expansion is

$$S_i(\phi) = \sum_{n=0,1,2,}^{N} S_i^{(n)} \cos n\phi \quad ; \qquad i = 1,2,3,\cdots \tag{4.2.5}$$

where $S_i^{(n)}$ represents the Fourier coefficient of the n-th harmonic for the function $S_i(\phi)$. The parameter N is an arbitrary integer to determine the number of harmonics to be used in the series. However, since the *Fast Fourier Transform method* will be used to perform the Fourier series transformation, the restriction on N is that (see Brigham; 1974)

$$N = 2^J \quad , \qquad J = 1, 2, 3, \cdots \tag{4.2.6}$$

§4.3 Compatibility and Equilibrium Requirements

In Chapter 3 it was mentioned that arbitrary edge distributions may be prescribed along the flat edge of a cylinder as long as they satisfy the over-all equilibrium requirements for the cylinder and the requirements of compatibility between the prescribed deformations.

Using the appropriate functions from Table 4.2, it can be shown that (3.5.5-a,b) transform into

$$S_2^{(1)} = -\frac{C}{R} S_1^{(1)} \qquad \text{for} \qquad Isym = 2, 4 \tag{4.3.1}$$

and

$$S_2^{(1)} = \frac{C}{R} S_1^{(1)} \qquad \text{for} \qquad Isym = 1, 3 \tag{4.3.2}$$

Both relations can be summed into one general requirement which is valid for all values of the symmetry index

$$S_2^{(1)} + (-1)^{Isym} \frac{C}{R} S_1^{(1)} = 0 \qquad \text{for} \qquad Isym = 1, 2, 3, 4 \tag{4.3.3}$$

Similarly, the compatibility requirements (3.5.5-c,d) can be represented by

$$S_3^{(1)} - (-1)^{Isym} \frac{C}{R} S_4^{(1)} = 0 \qquad \text{for} \qquad Isym = 1, 2, 3, 4 \tag{4.3.4}$$

In addition to the previous over-all equilibrium and compatibility equations, the prescribed distributions ought to satisfy the regularity requirement of all quantities at the two tips of the cut ($|\phi| = \beta/2$). For example, when the derivative of the in-plane shear $\frac{\partial N_{x\phi}}{\partial \phi}$ is precribed on the cut, it is not sufficient to make it vanish outside the cut. It is also necessary to make the shear $N_{x\phi}$ equal to zero outside the cut. Therefore,

$$(N_{x\phi})_{\beta/2} = \int_0^{\beta/2} \frac{\partial N_{x\phi}}{\partial \varphi}\, d\phi = 0 \tag{4.3.5}$$

Using Table 4.2, the previous expansion can be written as

$$\int_0^{\beta/2} S_2(\phi)\, d\phi = 0 \qquad \text{for} \qquad Isym = 1,2,3,4 \tag{4.3.6}$$

Using the same argument on the prescribed displacement function $S_3(\phi)$, another requirement that has to be satisfied is

$$\int_0^{\beta/2} S_3(\phi)\, d\phi = 0 \qquad \text{for} \qquad Isym = 1,2,3,4 \tag{4.3.7}$$

The next step is to substitute the full series expansion of the four cut functions $S_i(\phi)$ (4.2.1) into the equilibrium, compatibility, and regularity equations. As a result, one can expand (4.3.6) as

$$\int_0^{\beta/2} \left[a_2 f_1(\phi) + \sum_{i=NHC+1}^{2\times NHC} b_i f_{i-NHC+1}(\phi) \right] d\phi = 0 \tag{4.3.8}$$

However, since

$$f_i(\phi) = 0 \qquad \text{for} \qquad |\phi| \geq \beta/2 \tag{4.3.9}$$

the upper limit of the integration can be replaced by π. Then by using the Fourier series expansion of the prescribed distributions, one can obtain

$$\int_0^{\pi} \sum_{n=0,1,2}^{N} \left[a_2 f_1^{(n)} + \sum_{i=NHC+1}^{2\times NHC} b_i f_{i-NHC+1}^{(n)} \right] \cos n\phi \, d\phi = 0 \tag{4.3.10}$$

which after integration yields

$$a_2 f_1^{(0)} + \sum_{i=NHC+1}^{2\times NHC} b_i f_{i-NHC+1}^{(0)} = 0 \tag{4.3.11}$$

By following the same procedure, it can be shown that (4.3.7) can be rewritten as

$$a_3 f_1^{(0)} + \sum_{i=2\times NHC+1}^{3\times NHC-1} b_i f_{i-2\times NHC+1}^{(0)} = 0 \tag{4.3.12}$$

Similarly, (4.3.1) can be written in terms of the Fourier coefficients of the cut functions as follows

$$a_2 f_1^{(1)} + \sum_{i=NHC+1}^{2\times NHC} b_i f_{i-NHC+1}^{(1)} + (-1)^{Isym} \left(\frac{C}{R}\right) \left[a_1 f_1^{(1)} + \sum_{i=1}^{NHC} b_i f_{i+1}^{(1)} \right] = 0 \tag{4.3.13}$$

and a similar relationship can also be obtained using (4.3.2).

By rearranging the previous identities, one can show that for any combination of cut distributions to be valid, the following identities must be satisfied

$$
\begin{aligned}
a_2 &= -\left[\sum_{i=NHC+1}^{2\times NHC} b_i f_{i-NHC+1}^{(0)}\right] / f_1^{(0)} \\
a_3 &= -\left[\sum_{i=2\times NHC+1}^{3NHC-1} b_i f_{i-2\times NHC+1}^{(0)}\right] / f_1^{(0)} \\
a_1 f_1^{(1)} &= -\sum_{i=1}^{NHC} b_i f_{i+1}^{(1)} - (-1)^{Isym}\frac{R}{C}\left[a_2 f_1^{(1)} + \sum_{i=NHC+1}^{2\times NHC} b_i f_{i-NHC+1}^{(1)}\right] \\
a_4 f_1^{(1)} &= -\sum_{i=3\times NHC}^{4\times NHC-2} b_i f_{i-3\times NHC+2}^{(1)} \\
&\quad + (-1)^{Isym}\frac{R}{C}\left[a_3 f_1^{(1)} + \sum_{i=2\times NHC+1}^{3\times NHC-1} b_i f_{i-2\times NHC+1}^{(1)}\right]
\end{aligned}
\tag{4.3.14}
$$

As a result, one can select any combination of the arbitrary constants b_i for the cut solutions in (4.2.1). Then using (4.3.14), the values of the constants a_i are evaluated in order to make the cut solutions self-equilibrating and compatible.

§4.4 Solutions at the Intersection Curve

In Chapter 3, the use of the exponential solutions of the equations for the circular cylinder to evaluate the components of force and displacement vectors $\mathbf{F}_x$ and $\mathbf{D}_x$ was explained. The solution was obtained by expressing the force and displacement quantities in terms of the complex quantities T_1, T_2, T_3, and T_4. Using such solutions, one can compute the forces and displacements acting on the intersection curve due to a prescribed edge distribution (see Fig. 4.6). These new force and displacement quantities are arranged in the two new vectors $\mathbf{F}$ and $\mathbf{D}$ respectively as follows

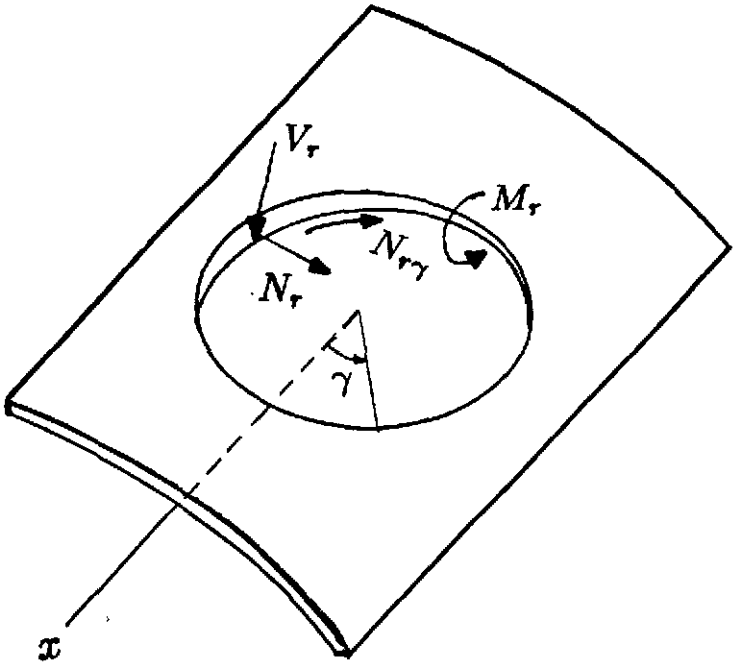

Figure 4.6

Bending and membrane stress resultants acting on the boundary of the opening in the vessel.

$$\mathbf{F} = \begin{pmatrix} M_r \\ r_0 V_r \\ C N_r \\ C \frac{\partial N_{r\gamma}}{\partial \gamma} \end{pmatrix} \qquad \mathbf{D} = \begin{pmatrix} -ETC^2 \frac{\partial \tau}{\partial \gamma} \\ ETC^2 \kappa_\gamma \\ ETC r_0 \kappa_g \\ ETC \epsilon_\gamma \end{pmatrix} \tag{4.4.1}$$

By comparing (4.4.1) to (3.3.11) it can be observed that the elements of $\mathbf{F}$ and $\mathbf{D}$ are similar to those in $\mathbf{F}_x$ and $\mathbf{D}_x$. The difference is that the former are expressed in the polar coordinates r-γ, while the latter are expressed in x-ϕ coordinates. In addition, two of the elements (V_r and κ_g) are normalized using the nozzle radius r_0 instead of the vessel radius R.

Using the principle of Mohr's circle (see Ugural and Fenster; 1975), it can be shown that at any point along the intersection curve defined by the angle γ, the

radial bending moment is

$$M_r = M_x \cos^2\gamma + M_\phi \sin^2\gamma + M_{x\phi} \sin 2\gamma \tag{4.4.2}$$

By substituting the definition of $M_x, M_\phi,$ and $M_{x\phi}$ from (3.3.8) into the previous equation produces

$$\begin{aligned} M_r = Re\Big\{ & -T_3 \cos n\phi + (1-\nu)\left[T_2 \cos^2\gamma + (T_3 - T_2)\sin^2\gamma\right]\cos n\phi \\ & - (1-\nu)\frac{T_1}{n}\sin 2\gamma \sin n\phi \Big\} \end{aligned} \tag{4.4.3}$$

Similarly, the twisting moment $M_{r\gamma}$ is

$$M_{r\gamma} = M_x(\cos^2\gamma - \sin^2\gamma) + (M_\phi - M_x)\frac{\sin 2\gamma}{2} \tag{4.4.4}$$

which can be expanded as,

$$M_{r\gamma} = -(1-\nu)Re\left\{\frac{T_1}{n}(\cos^2\gamma - \sin^2\gamma)\sin n\phi + \sin 2\gamma\left[T_2 - \frac{T_3}{2}\right]\cos n\phi\right\} \tag{4.4.5}$$

The next step involves the evaluation of the *equivalent* transverse shear V_r. According to Ugural (1981), it is defined as

$$V_r = Q_r + \frac{\partial M_{r\gamma}}{\partial s} \tag{4.4.6}$$

where Q_r is the actual transverse shear which can be evaluated using the equilibrium of a triangular element with Q_x and Q_ϕ acting on its sides. Using the definition of these shear quantities from (3.3.8) results in

$$Q_r = \frac{-T_3}{R}\left(\xi \cos\gamma \cos n\phi - n \sin\gamma \sin n\phi\right) \tag{4.4.7}$$

Then, by differentiating (4.4.5) with respect to γ and using the relationship

$$\frac{\partial(\cdots)}{\partial s} = \frac{1}{r_g}\frac{\partial(\cdots)}{\partial \gamma}$$

a formula for V_r in terms of T_1, T_2, T_3, and T_4 can be obtained.

The same approach can also be applied to derive similar formulas for the membrane stress resultants N_r and $N_{r\gamma}$. Also, by utilizing the Mohr's circle principle for strains and curvatures, the four displacement quantities in $\mathbf{D}$ can be evaluated. The final result is that the vectors $\mathbf{F}$ and $\mathbf{D}$ can be expressed as

$$\mathbf{F} = Re\begin{pmatrix} -V_3 + (1-\nu)V_2 \\ -V_4 - (1-\nu)V_1 \\ iV_2 \\ -iV_1(\frac{r_g}{R}) \end{pmatrix} \tag{4.4.8}$$

and

$$\mathbf{D} = Re\begin{pmatrix} V_1(\frac{r_g}{R}) \\ -V_2 \\ i[V_4 + (1+\nu)V_1] \\ i[V_3 - (1+\nu)V_2] \end{pmatrix} \tag{4.4.9}$$

where

$$
\begin{aligned}
V_1 &= \cos n\phi \left\{ (T_2 - \frac{1}{2}T_3)(-\xi \sin\gamma \sin 2\gamma + 2\frac{R}{r_g}\cos 2\gamma) + T_1 \cos\gamma \cos 2\gamma \right\} \\
&\quad - \sin n\phi \{ (T_2 - \frac{1}{2}T_3)(n \cos\gamma \sin 2\gamma) + \frac{T_1}{n}(\xi \sin\gamma \cos 2\gamma + 2\frac{R}{r_g}\sin 2\gamma) \} \\
V_2 &= \left[T_2 \cos^2\gamma + (T_3 - T_2)\sin^2\gamma \right] \cos n\phi - \left[\frac{T_1}{n} \sin 2\gamma \right] \sin n\phi \\
V_3 &= T_3 \cos n\phi \\
V_4 &= T_3(\xi \cos\gamma \cos n\phi - n \sin\gamma \sin n\phi)
\end{aligned}
\tag{4.4.10}
$$

In (4.4.1), the derivative of the shear and the twist were used as elements of $\mathbf{F}$ and $\mathbf{D}$, to be consistent with the notation used in $\mathbf{F}_x$ and $\mathbf{D}_x$ (see (3.3.11)). However, during the course of this study, it was concluded that it is more advantageous to use the values of the shear and the twist instead of their derivatives. The reason is that the derivative of a function expressed as a Fourier series is slower to converge than the function itself. Therefore, to improve accuracy and convergence, the fourth element in $\mathbf{F}$ and the first element in $\mathbf{D}$ are replaced by $CN_{r\gamma}$ and $-ETC^2\tau$, respectively.

The shear $N_{r\gamma}$ can be obtained by integrating its derivative given in (4.4.8-d), which produces

$$
CN_{r\gamma} = Re\left(-iV_5 \frac{r_g}{R}\right) \tag{4.4.11}
$$

where

$$
V_5 = \frac{R}{r_g}\left\{ \left(T_2 - \frac{1}{2}T_3 \right) \cos n\phi \sin 2\gamma + \frac{T_1}{n} \sin n\phi \cos 2\gamma \right\} \tag{4.4.12}
$$

Similarly, the twist can be evaluated using

$$-ETC^2\tau = Re\left(V_5\frac{r_g}{R}\right) \tag{4.4.13}$$

By comparing the relations for the force and displacement vectors for the opening on the wall of the cylinder (4.4.1) to those on the end of a cylinder (3.3.11), a strong similarity is observed. The complex quantities V_1, V_2, V_3, and V_4 for the boundary of the opening correspond to T_1, T_2, T_3, and T_4 for the circumference of the cylinder end. It is also important to note that the static-geometric analogy, which was observed in Chapter 3, is evident again in the equations for the boundary of an opening in a cylinder (see §3.3.1).

العنوان:	STRESSES AT THE JUNCTION OF TWO NORMALLY INTERSECTING CIRCULAR CYLINDERS
المؤلف الرئيسي:	Khathlan, Abd Alrahman Abd Allah
مؤلفين آخرين:	Steele, Charles(Super)
التاريخ الميلادي:	1986
موقع:	ستانفورد
الصفحات:	1 - 156
رقم MD:	614792
نوع المحتوى:	رسائل جامعية
اللغة:	English
الدرجة العلمية:	رسالة دكتوراه
الجامعة:	Stanford University
الكلية:	College of Engineering
الدولة:	الولايات المتحدة الأمريكية
قواعد المعلومات:	Dissertations
مواضيع:	الهندسة المدنية، التصميمات الهندسية، الحاسب الآلي
رابط:	https://search.mandumah.com/Record/614792

Chapter 5

Particular and Complementary Solutions for the Vessel

The investigation of stresses at the junction of two cylinders involves developing the solutions for each cylinder independently before the application of the continuity conditions at the junction. In this chapter, the particular and complementary solutions for the vessel are discussed. The *cut method*, which has been introduced in Chapter 4, is the main technique used for developing these solutions. However, membrane solutions and asymptotic methods will also be used in certain cases.

§5.1 The Particular Solution

In order to analyze the stresses at the junction, it is necessary to evaluate the particular part of the solution. This part includes the stresses and strains in the vessel due to the application of the loads with a resultant force or moment. If the vessel is subjected to internal pressure or an axial force ($Iload$ = 0, and 5), the particular solution is easy to obtain. Simple membrane solutions for the circular cylinder provide the stresses and strains along the intersection curve.

On the other hand, for the loading cases that involve external loads applied to the free end of the nozzle ($Iload$ = 1,2,3,4), the shell resists the loads through bending, inextensional, as well as membrane behavior. Therefore, there is no simple, exact procedure to evaluate the particular solution. In these cases, the *cut method* will be used to compute the particular solution.

5.1.1 Internal Pressure p ($Iload = 0$)

In this case, one needs to evaluate the stresses and strains along the intersection curve due to an internal pressure p in the vessel. The ends of the vessel are assumed to be closed to contain the pressure.

For a thin cylinder with internal pressure, it can be shown that the principal stress resultants in the shell are

$$\begin{aligned} N_x(x,\phi) &= \frac{1}{2}pR \\ N_\phi(x,\phi) &= pR \end{aligned} \tag{5.1.1}$$

Using Mohr's circle principle (see §4.4), stresses and strains at any point along the intersection curve Γ can be computed using the position angle γ as follows

$$\begin{aligned} N_r(\gamma) &= \frac{1}{2}pR(1+\sin^2\gamma) \\ N_{r\gamma}(\gamma) &= \frac{1}{4}pR\sin 2\gamma \\ \epsilon_\gamma(\gamma) &= \frac{pR}{2ET}\left[1+\cos^2\gamma-\nu(1+\sin^2\gamma)\right] \\ \kappa_g(\gamma) &= \frac{-pR}{2ETr_g}(1+\nu)\cos 2\gamma \end{aligned} \tag{5.1.2}$$

Because the pressure is resisted through membrane behavior of the cylinder, there are no bending stresses or curvatures in the cylinder. Thus, along the intersection curve

$$M_r(\gamma) = V_r(\gamma) = \kappa_\gamma(\gamma) = \tau(\gamma) = 0 \tag{5.1.3}$$

Henceforth, all the elements of the force and displacement vectors are determined, which completes the particular solution for this loading case.

5.1.2 Axial Force F_x ($Iload = 5$)

The same membrane solution that was used for the pressure loading will be used when the vessel is loaded by an axial force F_x. In this case the principal stress resultants are

$$\begin{aligned} N_x(x,\phi) &= F_x/(2\pi R) \\ N_\phi(x,\phi) &= 0 \end{aligned} \tag{5.1.4}$$

By following the same procedure in §5.1.1, it can be shown that along Γ

$$\begin{aligned} N_r &= \left(\frac{F_x}{2\pi R}\right)\cos^2\gamma \\ N_{r\gamma} &= \left(\frac{-F_x}{4\pi R}\right)\sin 2\gamma \\ \epsilon_\gamma &= \left(\frac{F_x}{2\pi RET}\right)\left[1-(1+\nu)\cos^2\gamma\right] \\ \kappa_g &= \left(\frac{F_x}{2\pi RET}\right)\frac{1+\nu}{r_g}\cos 2\gamma \end{aligned} \tag{5.1.5}$$

and

$$M_r(\gamma) = V_r(\gamma) = \kappa_\gamma(\gamma) = \tau(\gamma) = 0 \tag{5.1.6}$$

5.1.3 External Loads on the Nozzle ($Iload$=1,2,3,4)

The problem of a concentrated force or a couple on the surface of a cylindrical shell has been the subject of a number of studies. The complexity of the shell behavior and the existence of singularities beneath the applied loads have made such investigations very difficult and complex. Using separation of variables, Flügge and Conrad (1958) provided some results for the so-called *bending hot spots* in shallow cylindrical shells. Sanders and Simmonds (1970) also developed a solution for the

displacements in a shallow cylindrical shell subjected to concentrated forces. They developed a new function which can be used in combination with modified Bessel functions to evaluate the stress and strain measures.

§5.2 Application of the Cut Method

In Chapter 3, it was shown that the stresses and strains in a circular cylinder due to prescribed distributions along the edge of the cylinder can be evaluated. The *cut method* will be used to find a particular solution for the vessel when subjected to external concentrated actions. The resultant force or moment is replaced by statically equivalent distributions of load on the cut. The simplest cut solutions which have the desired resultants are considered the particular solutions.

5.2.1 The Particular Solution Using the Cut Method

In order to obtain the particular solution using the *cut method*, it is necessary to set all the integration constants b_i to zero in (4.2.1) and (4.3.14). The other constants a_i are also set to zero except a_1. This represents a distribution of either f_1 or g_1, depending on the symmetry index, along the cut. The value of a_1 is selected such that the prescribed cut distribution produces the same resultant as one half of the applied load (see Fig. 5.1). The reason is that because of symmetry about the transverse axis, it is sufficient to work with one half of the length of the vessel ($0 \geq x \geq -L/2$), which resists only one half of the load.

For example, in the case of a radial load P applied to the nozzle, the prescribed cut distribution is

$$RV_x = a_1 f_(\phi) = a_1 \sum_{n=0,1,2,}^{N} f_1^{(n)} \cos n\phi \tag{5.2.1}$$

In order to satisfy force equilibrium in the z-direction, the value of a_1 can be

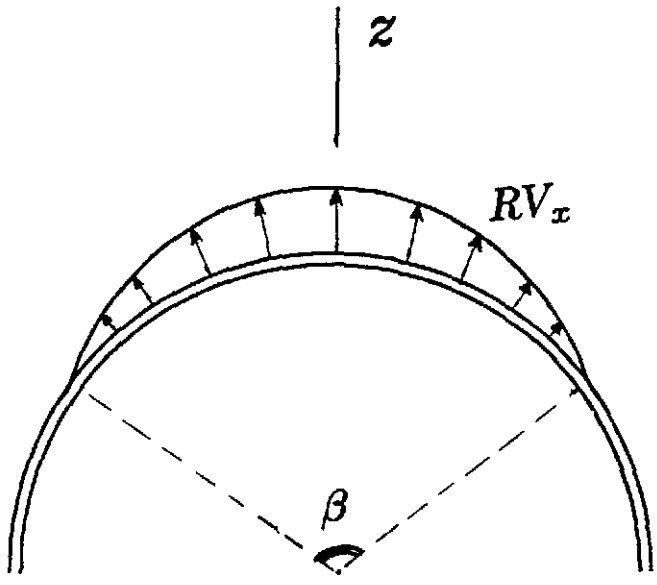

Figure 5.1

Application of the cut distribution function (transverse shear V_x) to the flat edge of the cylinder to represent an externally applied load P.

determined using

$$\frac{1}{R}\int_0^{2\pi}\left[a_1\sum f_1^{(n)}\cos n\phi\right]\cos\phi\, Rd\phi = P/2 \tag{5.2.2}$$

The integration causes all the Fourier coefficients $f_1^{(n)}$ to drop out except $f_1^{(1)}$, and this results in

$$a_1 = \frac{P}{2\pi f_1^{(1)}} \tag{5.2.3}$$

The same procedure is followed for the other remaining loading cases. The appropriate value of a_1 for each case was found to be as follows

$$a_1 = \begin{cases} P/2\pi f_1^{(1)} & \text{for} \quad Iload = 1 \\ M_L/2\pi R f_1^{(1)} & \text{for} \quad Iload = 2 \\ M_C/2\pi R g_1^{(1)} & \text{for} \quad Iload = 3 \\ M_T/2\pi R g_1^{(1)} & \text{for} \quad Iload = 4 \end{cases} \tag{5.2.4}$$

Once the value of a_1 is determined, the four cut distributions are defined using (4.2.1). These distributions can then be used to compute the stresses and strains along Γ as described in §4.4 .

In general, the use of the cut method to evaluate the particular solution for the vessel can be summarized by the following steps:

1) Using the value of the applied load, compute a_1 using (5.2.4).

2) Using (4.2.1), the four cut distributions S_1, S_2, S_3, and S_4 are determined by setting *all* the integration constants, except a_1, to zero.

3) Divide the circumference of the vessel into $2N$ intervals. These are used to discretize the cut distributions to prepare them for the use of FFT for the expansion in the form of a Fourier series.

4) For each harmonic n of the Fourier series, solve for the unknown constants c_1, c_2, c_3, and c_4 using the matrices $\mathbf{FM}_x$ and $\mathbf{DM}_x$ in (3.4.5).

5) Using these constants and the values of the coordinates x and ϕ for the point where the solution is needed, evaluate the complex quantities T_1, T_2, T_3, and T_4 which are the used to compute V_1, V_2, V_3, V_4, and V_5 using (4.4.10).

6) The Fourier coefficients of the elements of $\mathbf{F}$ and $\mathbf{D}$ can then be determined using (4.4.8) and (4.4.9). Then, steps 3 to 6 are repeated N times to evaluate the coefficients for all the harmonics. These are summed up in a Fourier series in terms of ϕ to produce the stresses and strains at one mesh point along Γ.

7) Repeat steps 5 and 6 $N1$ times to evaluate the stresses and strains at all the mesh points along one quarter of the intersection curve. Each of these distributions is then expanded in a Fourier series in terms of γ.

8) The *nonzero* Fourier coefficients of the forces and displacements are then arranged, in the same order given for $\mathbf{F}$ and $\mathbf{D}$, into the particular solution force and displacement vectors $\mathbf{F}_p$ and $\mathbf{D}_p$.

5.2.2 Example of a Typical Particular Solution

In this example, the particular solution for the vessel when subjected to a radial load P is evaluated. First, by following steps 1 and 2, the four cut distributions will be defined as (see Fig. 5.2-a)

$$RV_x(0,\phi) = \frac{P}{2\pi f_1^{(1)}} f_1(\phi) \tag{5.2.5}$$

$$N_{x\phi}(0,\phi) = \tau(0,\phi) = \kappa_g(0,\phi) = 0 \tag{5.2.6}$$

Using step 4, the four other quantities along the edge of the cylinder, M_x, CN_x, $ETC^2\kappa_\phi$, and $ETC\epsilon_\phi$ can be calculated. Their distributions along a segment of the circumference is plotted in Fig. 5.2-b. It should be noted that these four quantities do not show any slope discontinuity at the tip of the cut (at $\phi = \beta/2$). This is a direct result of the careful choice of the cut distributions to avoid having singularities near the tip of the cut.

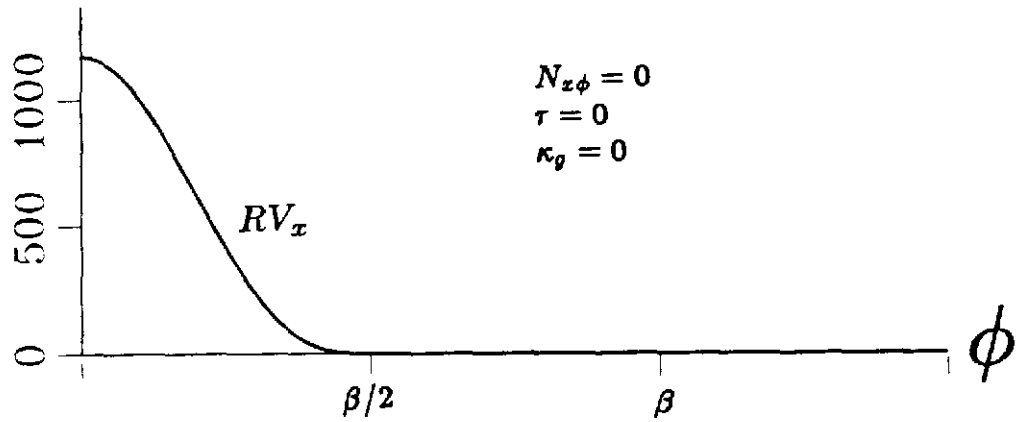

(a)

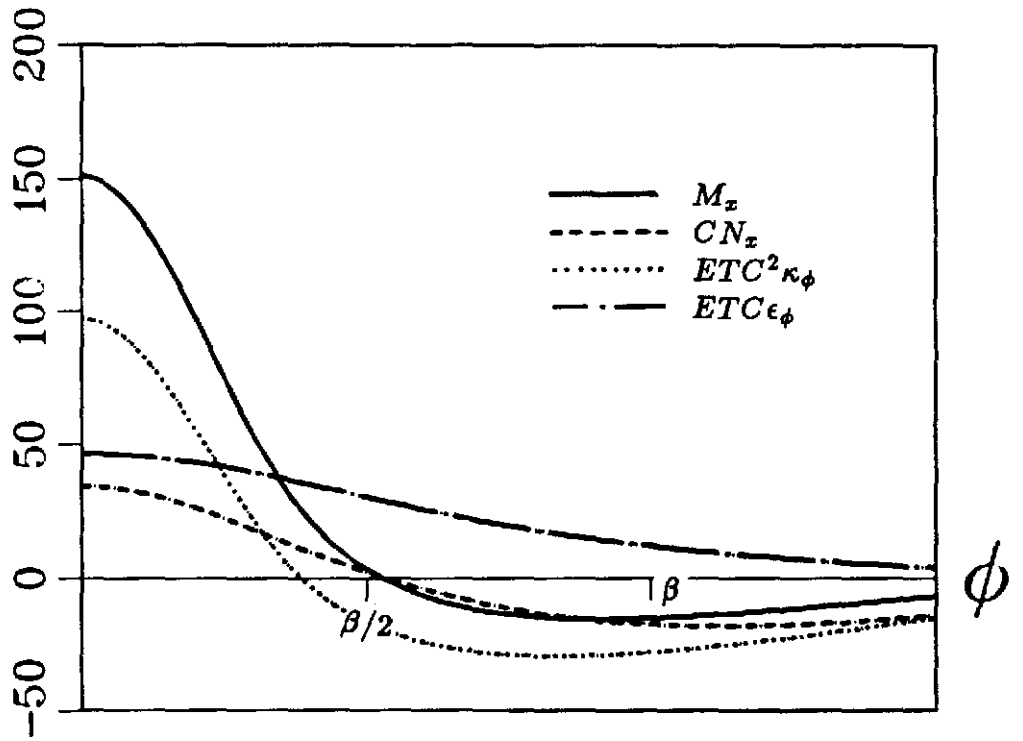

(b)

Figure 5.2

Distribution of force and displacement quantities along the edge of the vessel (at $x = 0$), corresponding to the particular solution for the example in §5.2.2 ($Iload = 1$, $P = 1000$ lbs, $R = 10$ in., $r_0 = 5$ in., $T = 1.0$ in., $\nu = 0.3$) : a) Distribution of the prescribed quantities; b) Distribution of the computed quantities.

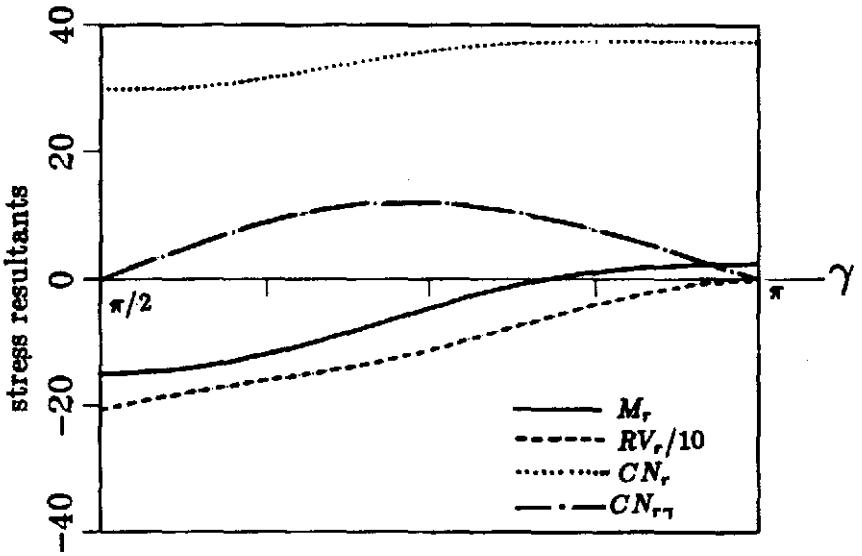

(a)

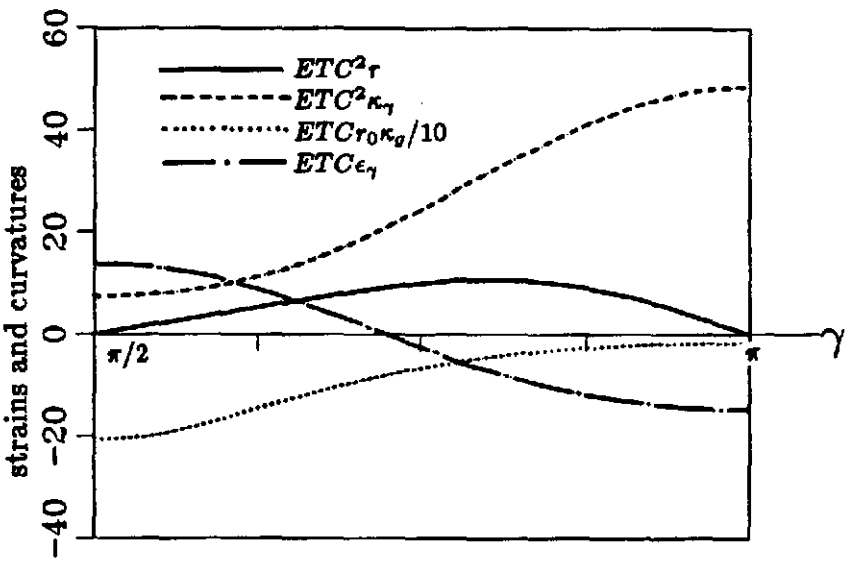

(b)

Figure 5.3

Distribution of the elements of the particular solution force and displacement vectors, $\mathbf{F}_p$ and $\mathbf{D}_p$, around the intersection curve ($\pi/2 \leq \gamma \leq \pi$) for the example in §5.2.2.

The next step involves the computation of the elements of **F** and **D** along one quarter of the intersection curve. By following steps 5-7, each of these quantities will be represented as the sum of a Fourier series. For example, the bending moment can be computed using

$$M_r = \sum_{m=0,1,2,}^{N} M_r^{(m)} \cos m\phi \tag{5.2.7}$$

Figure 5.3 shows the distribution of the force and displacement quantities between $\gamma = \pi/2$ and $\gamma = \pi$. The smoothness of these distributions at $\gamma = \pi/2$ indicates that singular behavior at the crack tip is avoided.

The force and displacement quantities are then decomposed into finite Fourier series in terms of γ, using *FFT*. For example, the radial moment and the curvature along Γ will be expressed as

$$\begin{aligned} M_r(\gamma) &= \sum_{n=0,2,4,}^{2(N1-1)} M_r^{(n)} \cos n\gamma \\ ETC^2\kappa_\gamma(\gamma) &= ETC^2 \sum_{n=0,2,4,}^{2(N1-1)} \kappa_\gamma^{(n)} \cos n\gamma \end{aligned} \tag{5.2.8}$$

The Fourier series includes the even values of n only because for this loading case the solution is doubly symmetric, which means that all the coefficients of the odd harmonics are zero.

In terms of the even Fourier coefficients of the force and displacement quantities, the particular solution vectors are

$$\mathbf{F}_p = \begin{pmatrix} M_r^{(0)} \\ r_0 V_r^{(0)} \\ CN_r^{(0)} \\ CN_{r\gamma}^{(0)} \\ M_r^{(2)} \\ r_0 V_r^{(2)} \\ \vdots \end{pmatrix} \qquad \mathbf{D}_p = ETC \begin{pmatrix} C\tau^{(0)} \\ C\kappa_\gamma^{(0)} \\ r_0 \kappa_g^{(0)} \\ \epsilon_\gamma^{(0)} \\ C\tau^{(2)} \\ C\kappa_\gamma^{(2)} \\ \vdots \end{pmatrix} \tag{5.2.9}$$

§5.3 The Complementary Solution for the Vessel

The complementary solution for the vessel is composed of a group of self-equilibrating sinusoidal distributions around the boundary of the opening. This section is related to the low harmonics of such solutions. As mentioned earlier, these harmonics are usually coupled together in a complicated fashion which makes them difficult to solve. However, as will be illustrated in this section, the *cut method* has proven to be a very useful technique for handling these harmonics.

The method includes the use of the procedure outlined in §4.3 . First, a value of NHC is selected, which defines the number of harmonics that will be investigated using this approach. By examining (4.2.1), it can be seen that we will be dealing with $4 \times NHC - 2$ independent solutions. Each one of these solution is associated with one of the constants b_i, and will be handled independently from the others by setting the corresponding b_i to unity and all the others to zero. Using (4.3.14), the appropriate values of the constants a_i are evaluated for each case which uniquely defines the four cut distributions S_1, S_2, S_3, and S_4.

Using the example given in §5.2.2, assume that it is desired to handle the lowest two harmonics ($n = 0, 2$) using the *cut method*. This corresponds to $NHC = 2$.

As a result, a total of six different cut solutions will be needed. The first of these solutions is obtained by using

$$b_1 = 1$$

$$b_2 = b_3 = b_4 = b_5 = b_6 = 0 \tag{5.3.1}$$

Using 4.3.4, it can be shown that

$$a_1 = -b_1 f_2^{(1)} / f_1^{(1)} \tag{5.3.2}$$

and

$$a_2 = a_3 = a_4 = 0 \tag{5.3.3}$$

Upon substituting these values in (4.2.1), the four cut distributions would be defined as

$$S_1(\phi) = \left(-b_1 f_2^{(1)} / f_1^{(1)}\right) f_1(\phi) + f_2(\phi) \tag{5.3.4}$$

$$S_2(\phi) = S_3(\phi) = S_4(\phi) = 0$$

At this stage, the same procedure which was applied to the particular solution is used here by following steps 3-7 discussed in §5.2.1. However, in this case the nonzero Fourier coefficients of forces and displacements are stored in the first columns of the new matrices **FM1** and **DM1**, respectively.

The next step is to repeat the previous steps using $b_2 = 1$, while all the other b_i equal to zero. The Fourier coefficients of this solutions are placed in the second columns of **FM1** and **DM1**. The same process is repeated for a total of $4 \times NHC - 2$ times. The final result will be two matrices **FM1** and **DM1** relating

the Fourier coefficients of the unknown forces and displacements to the integration constants. In matrix formulation, this can be expressed as

$$\mathbf{F}_c = \mathbf{FM1} \times \mathbf{b}$$

$$\mathbf{D}_c = \mathbf{DM1} \times \mathbf{b} \tag{5.3.5}$$

where

$$\mathbf{b} = \begin{pmatrix} b_1 \\ b_2 \\ \vdots \\ b_{4 \times NHC-2} \end{pmatrix} \tag{5.3.6}$$

The vectors $\mathbf{F}_c$ and $\mathbf{D}_c$ represent the force and displacement vectors for the complementary solution, respectively. They include Fourier coefficients arranged in the same order as $\mathbf{F}_p$ and $\mathbf{D}_p$ (see (5.2.9)).

§5.4 Remarks about the Cut Method

The previous section provided a description of the use of *cut method* for evaluating the complementary solution for an opening in a cylindrical shell. Unfortunately, this method is not useful for handling all the harmonics of the solution for several reasons.

First, it was found that the method tends to break down if an attempt is made to use it for handling high harmonics. This is due to the fact that in order to generate solutions for high harmonics around the intersection curve, more cut distributions with very rapid circumferential variation will be needed. In accordance with shell behavior, these rapidly varying functions will decay within a very short distance from the cut. This leaves a large portion of Γ unaffected by the cut distributions, which results in similar force and displacement distributions along the intersection

curve, for different cut distributions. As a result, some of the columns in **FM1** and **DM1** will be dependent which could lead to numerical difficulties during the solution.

Another reason is the high cost of the cut solutions in terms of computer *CPU* time. It was mentioned earlier that to generate the solutions for a single harmonic, four cut solutions are needed. Although the *Fast Fourier Transform* and symmetry were used whenever possible to minimize the amount of computation, a large number of mathematical operations are required. Possibilities for improving the efficiency have not yet been explored.

العنوان:	STRESSES AT THE JUNCTION OF TWO NORMALLY INTERSECTING CIRCULAR CYLINDERS
المؤلف الرئيسي:	Khathlan, Abd Alrahman Abd Allah
مؤلفين آخرين:	Steele, Charles(Super)
التاريخ الميلادي:	1986
موقع:	ستانفورد
الصفحات:	1 - 156
رقم MD:	614792
نوع المحتوى:	رسائل جامعية
اللغة:	English
الدرجة العلمية:	رسالة دكتوراه
الجامعة:	Stanford University
الكلية:	College of Engineering
الدولة:	الولايات المتحدة الأمريكية
قواعد المعلومات:	Dissertations
مواضيع:	الهندسة المدنية، التصميمات الهندسية، الحاسب الآلي
رابط:	https://search.mandumah.com/Record/614792

Chapter 6

The Asymptotic Solution for the Vessel

The previous chapter included a description of the method used for handling the complementary solution for the vessel. It was concluded that it is desirable to minimize the number of harmonics to which the *cut method* is applied. Therefore, another method will be needed to handle the high harmonics of the solution. Because one will be dealing with distributions of rapid variation in a thin shell, asymptotic methods present themselves as the most logical alternative.

Steele (1965) worked out the asymptotic solution for a shell of revolution with edge loads of rapid variation. Influence coefficients for shells with positive and negative curvatures were investigated. These were found to represent a transition between shell and flat plate behavior. This chapter includes the application of this general solution to the special case of a circular cylinder. It also provides a description of the approach to be used for utilizing such solutions to generate stiffness coefficients for the boundary of an opening in a cylinder.

§6.1 Solution for Circular Cylinders

In Chapter 3, it was shown that the *shallow shell equation* for a circular cylinder of radius R and thickness T is

$$\Delta\Delta\psi + \frac{i}{RC}\frac{\partial^2\psi}{\partial x^2} = 0 \tag{6.1.1}$$

where

$$\Delta(\cdots) = \frac{\partial^2(\cdots)}{\partial x^2} + \frac{\partial^2(\cdots)}{R^2\partial\phi^2} \tag{6.1.2}$$

Although (6.1.1) is written in terms of the x-ϕ coordinates, it is desirable to obtain solutions which oscillate around the intersection curve. Therefore, the solution will be expressed in the polar coordinates (r-γ).

The solution for the nth harmonic is assumed to be in the form

$$\psi = exp\left[-\xi\mu \pm in\gamma\right] \tag{6.1.3}$$

where μ is the distance normal to the boundary measured from the boundary outwards, divided by $\sqrt{2CD}$. The reason for this normalization is to simplify the upcoming mathematical equations. The parameter ξ is an unknown complex function that is to be evaluated. It is assumed that $\xi(\gamma)$ is a slowly varying function relative to the rapidly varying nature of the general solution (see Fig. 6.1). With this assumption one may neglect the derivative of $\xi(\gamma)$ with respect to γ.

Using the definition of μ and γ, their derivatives with respect to x are

$$\begin{aligned}\frac{\partial\mu}{\partial x} &= \frac{\cos\gamma}{\sqrt{2CD}} \\ \frac{\partial\gamma}{\partial x} &= \frac{-\sin\gamma}{r_g}\end{aligned} \tag{6.1.4}$$

Using these derivatives to differentiate-by-part (6.1.3) with respect to x produces

$$\frac{\partial\psi}{\partial x} = \frac{-1}{\sqrt{2CD}}\left[\xi\cos\gamma \pm i\aleph\sin\gamma\right]\psi \tag{6.1.5}$$

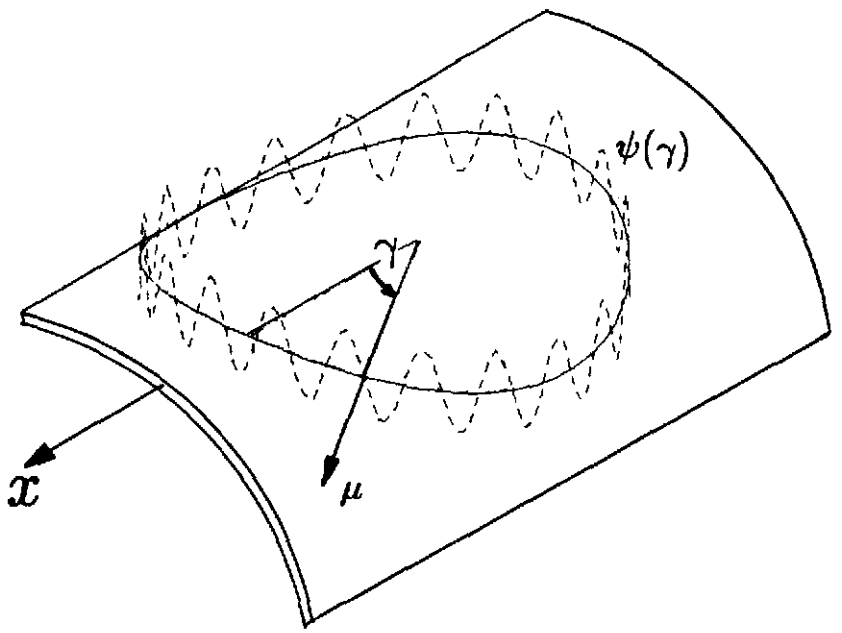

Figure 6.1

A typical rapidly varying distribution $\psi(\gamma)$ around the opening in the vessel, which is to be handled using the asymptotic solution.

where

$$\aleph = \frac{n\sqrt{2CD}}{r_g} \tag{6.1.6}$$

Differentiating (6.1.5) again with respect to x produces

$$\frac{\partial^2 \psi}{\partial x^2} = \frac{1}{2CD} \left[\xi \cos\gamma \pm i\aleph \sin\gamma\right]^2 \psi \tag{6.1.7}$$

Similarly, differentiating (6.1.3) twice with respect to ϕ yields

$$\frac{\partial^2 \psi}{R^2 \partial \phi^2} = \frac{1}{2CD} \left[-\xi \sin\gamma \pm i\aleph \cos\gamma\right]^2 \psi \tag{6.1.8}$$

By substituting (6.1.7) and (6.1.8) in (6.1.2), the laplacian operator Δ can be expressed as

$$\Delta\psi = \frac{1}{2CD} \left(\xi^2 - \aleph^2\right) \psi \tag{6.1.9}$$

Substituting (6.1.7) and (6.1.9) in the *shallow shell equation* for the cylinder (6.1.1) produces the *eikonal equation* for the unknown function $\xi(\gamma)$

$$\frac{-i}{4}(\xi^2 - \aleph^2)^2 + (\xi \cos\gamma \pm i\aleph \sin\gamma)^2 = 0 \tag{6.1.10}$$

This equation has eight different complex roots, four of which correspond to solutions which decay away from the opening, i.e., for positive μ. Only the four roots which have positive real parts can produce such a decay. These four roots are

$$
\begin{aligned}
\xi_1 &= \sqrt{-i}\cos\gamma + (-i\cos^2\gamma + \aleph^2 + 2\aleph\sqrt{i}\sin\gamma)^{1/2} \\
\xi_2 &= \sqrt{-i}\cos\gamma + (-i\cos^2\gamma + \aleph^2 - 2\aleph\sqrt{i}\sin\gamma)^{1/2} \\
\xi_3 &= -\sqrt{-i}\cos\gamma + (-i\cos^2\gamma + \aleph^2 - 2\aleph\sqrt{i}\sin\gamma)^{1/2} \\
\xi_4 &= -\sqrt{-i}\cos\gamma + (-i\cos^2\gamma + \aleph^2 + 2\aleph\sqrt{i}\sin\gamma)^{1/2}
\end{aligned}
\tag{6.1.11}
$$

Using these roots, the corresponding solutions of (6.1.1) are

$$
\begin{aligned}
\psi_1 &= exp(-\xi_1\mu + in\gamma) \\
\psi_2 &= exp(-\xi_2\mu - in\gamma) \\
\psi_3 &= exp(-\xi_3\mu + in\gamma) \\
\psi_4 &= exp(-\xi_4\mu - in\gamma)
\end{aligned}
\tag{6.1.12}
$$

§6.2 Symmetry Requirements of the Solution

By examining the four complex solutions ψ_1, ψ_2, ψ_3, and ψ_4 it can be observed that none of them possess any symmetry features. However, what is needed is the development of solutions that satisfy the symmetry requirements for each of the loading cases investigated in this study. Such solutions can be obtained using linear combinations of the functions ψ_1, ψ_2, ψ_3, and ψ_4.

The behavior of the roots of the *eikonal equation* is illustrated in Fig. 6.2. It shows the values of the four complex roots ξ_1, ξ_2, ξ_3, and ξ_4 corresponding to the 11-th harmonic for a hole in a circular cylinder (R=10, r_0=5, T=1.). By examining these roots, it can be observed that the four roots are related to each other in the following manner

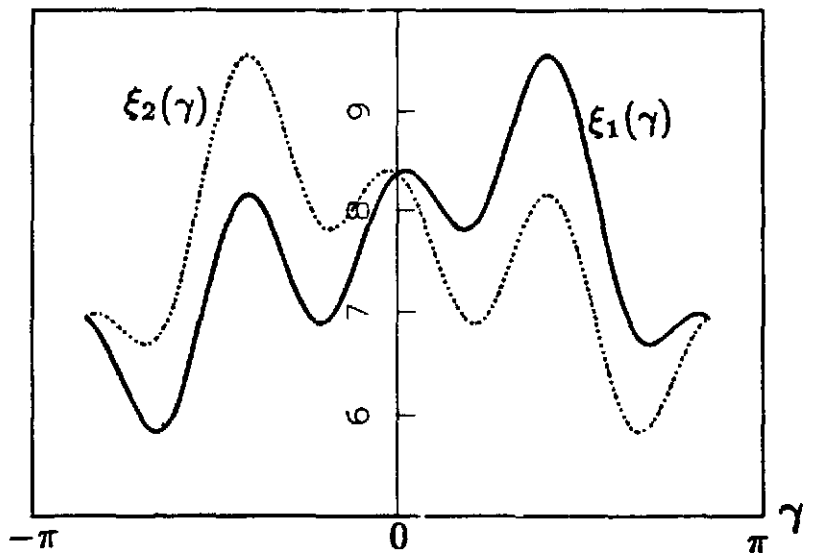

(a)

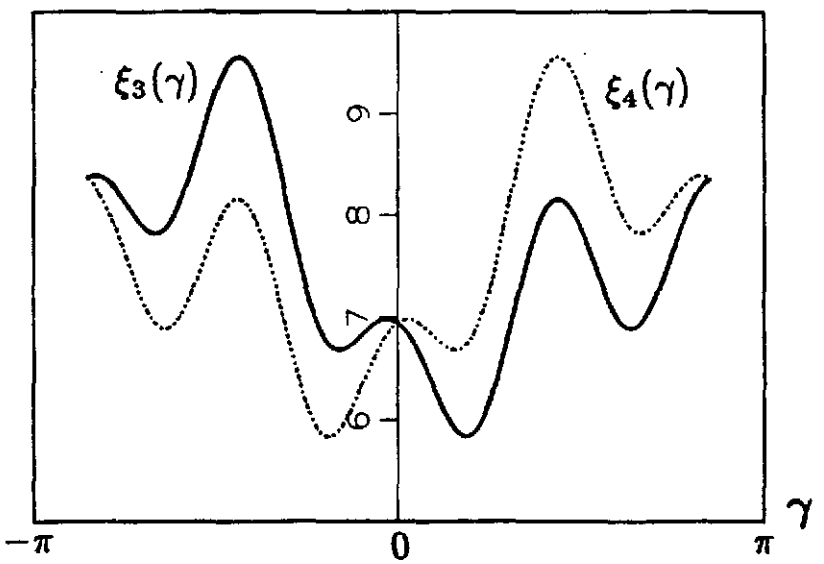

(b)

Figure 6.2

Variation of the roots of the *eikonal* equation (6.1.10) around the intersection curve ($R = 10$ in., $r_0 = 5$ in., $T = 1.0$ in., $n = 11$): a) roots $\xi_1(\gamma)$ and $\xi_2(\gamma)$, b) roots $\xi_3(\gamma)$ and $\xi_4(\gamma)$.

$$\begin{aligned} \xi_2(-\gamma) &= \xi_1(\gamma) \\ \xi_4(-\gamma) &= \xi_3(\gamma) \\ \xi_3(\gamma) &= \xi_1(\pi+\gamma) \\ \xi_4(\gamma) &= \xi_2(\pi+\gamma) \end{aligned} \tag{6.2.1}$$

Using these relationships, it can be shown that depending on whether n is odd or even, different combinations of the four solutions ψ_1, ψ_2, ψ_3, and ψ_4 produce new function which possess symmetry characteristics. These combinations are:

$$\begin{aligned} \Psi_1 &= \psi_1 + \psi_2 + \psi_3 + \psi_4 \\ \Psi_2 &= \psi_1 + \psi_2 - \psi_3 - \psi_4 \\ \Psi_3 &= \psi_1 - \psi_2 - \psi_3 + \psi_4 \\ \Psi_4 &= \psi_1 - \psi_2 + \psi_3 - \psi_4 \end{aligned} \tag{6.2.2}$$

Table 6.1 provides the appropriate functions to be used for each value of the symmetry index depending the harmonic number n.

Isym	Symmetry about θ=0	Symmetry about $\theta = \pi/2$	Even n	Odd n
1	symmetric	symmetric	Ψ_1	Ψ_2
2	symmetric	anti-symmetric	Ψ_2	Ψ_1
3	anti-symmetric	symmetric	Ψ_3	Ψ_4
4	anti-symmetric	anti-symmetric	Ψ_4	Ψ_3

Table 6.1
The appropriate complex functions Ψ_1, Ψ_2, Ψ_3, and Ψ_4, to be used for different values of *Isym* and for even or odd harmonic numbers.

§6.3 Evaluation of Forces and Displacements

The advantage of obtaining an asymptotic solution for the *shallow shell* equation is evident during the evaluation of the force and displacement quantities along the intersection curve. The force and displacements vectors (see (4.4.1)) can be expressed in terms of a new set of complex functions $\mathcal{V}_1$, $\mathcal{V}_2$, $\mathcal{V}_3$, $\mathcal{V}_4$, and $\mathcal{V}_5$, which are similar to the ones developed for the *cut method* (4.4.10). However, in the *cut method*, the development of these functions was a painstaking process. In that case, solution in the x-ϕ coordinates were obtained first and then transfered to the r-γ coordinates. By utilizing the asymptotic solution of the shallow shell equation, it is possible to develop approximate formulas for $\mathcal{V}_1$, $\mathcal{V}_2$, $\mathcal{V}_3$, and $\mathcal{V}_4$ in the r-γ coordinates directly, with relative ease. This leads to a tremendous saving in the amount of computations involved in the analysis.

Let s_1 and s_2 be the two vectors tangent and normal to a smooth boundary curve on the surface of a circular cylinder. It can be shown that for such a boundary, the following relations can be used in conjunction with (4.4.8) and (4.4.9)

$$
\begin{aligned}
\mathcal{V}_1 &= (2CD)R\frac{\partial}{\partial s_2}\left(\frac{\partial^2\psi}{\partial s_1^2}\right) \\
\mathcal{V}_2 &= (2CD)\left(\frac{\partial^2\psi}{\partial s_1^2}\right) \\
\mathcal{V}_3 &= (2CD)\Delta\psi = (2CD)\left(\frac{\partial^2\psi}{\partial s_1^2}+\frac{\partial^2\psi}{\partial s_2^2}\right) \\
\mathcal{V}_4 &= (2CD)R\frac{\partial(\Delta\psi)}{\partial s_2} \\
\mathcal{V}_5 &= (2CD)R\frac{\partial^2\psi}{\partial s_1\partial s_2}
\end{aligned}
\tag{6.3.1}
$$

where ψ is the general form of the solution of (6.1.1).

In this study, s_1 will correspond to the arc length around the intersection curve, which results in

$$\frac{\partial(\cdots)}{\partial s_1} = \frac{1}{r_g}\frac{\partial(\cdots)}{\partial \gamma} \tag{6.3.2}$$

On the other hand, s_2 will be the distance normal to the intersection curve. Using the definition of the normalized distance μ, it can be shown that

$$\frac{\partial(\cdots)}{\partial s_2} = \frac{1}{\sqrt{2CD}}\frac{\partial(\cdots)}{\partial \mu} \tag{6.3.3}$$

By substituting the general form of ψ from (6.1.3) into (6.3.1), and using (6.3.2) and (6.3.3), the four complex functions can be expressed as;

$$\begin{aligned}
\mathcal{V}_1 &= -\aleph^2 \cdot \psi \\
\mathcal{V}_2 &= \frac{R}{\sqrt{2CD}}\aleph^2 \xi \cdot \psi \\
\mathcal{V}_3 &= (\xi^2 - \aleph^2) \cdot \psi \\
\mathcal{V}_4 &= \frac{R}{\sqrt{2CD}}\aleph^2(\xi^2 - \aleph^2) \cdot \psi \\
\mathcal{V}_5 &= \pm\frac{R}{r_g} i\aleph\xi \cdot \psi
\end{aligned} \tag{6.3.4}$$

These relations, in conjunction with (4.4.8) and (4.4.9) completely define the elements of the force and displacement vectors in terms of ψ, the solution of the *shallow shell equation.*

§6.4 Application of the Asymptotic Solution

The theory presented in the previous sections will be used to develop the stiffness coefficients of the high harmonics for the boundary of the opening in the vessel. This section gives a description of the procedure for the specific case of a doubly symmetric distribution ($Isym = 1$). The same procedure is valid for other symmetry cases with very minor changes.

In order to generate the solution for a specific harmonic n, where n is an even integer, it is necessary to utilize solutions corresponding to both n and $n-1$. By examining Table 6.1, it can be observed that for this specific symmetry case, the corresponding solutions are Ψ_1 and Ψ_2. A linear combination of these two solutions is the general solution for this symmetry case. It can be written in the form

$$\Psi_{tot} = (c_1 + ic_2)\Psi_1 + (c_3 + ic_4)\Psi_2 \tag{6.4.1}$$

where c_1, c_2, c_3, and c_4 represent arbitrary integration constants. The force and displacement quantities can be evaluated in terms of these constants by substituting (6.4.1) into (6.3.4).

The next step is to repeat the same process for higher harmonics $n+2$, $n+4$, $\cdots$ etc., to cover the whole range of harmonics which are to be included in the analysis. Each of these harmonics will be associated with four new integration constants. Finally, the complementary force and displacement vectors can be written in terms of these integration constants. In matrix formulation, this is

$$\begin{aligned} \mathbf{F}_c &= \mathbf{FM2} \times \mathbf{c} \\ \mathbf{D}_c &= \mathbf{DM2} \times \mathbf{c} \end{aligned} \tag{6.4.2}$$

where $\mathbf{F}_c$ and $\mathbf{D}_c$ are the same vectors defined in §5.3, and $\mathbf{c}$ is a vector including the integration constants in the following order

$$\mathbf{c} = \begin{pmatrix} c_1 \\ c_2 \\ c_3 \\ c_4 \\ c_5 \\ c_6 \\ \vdots \end{pmatrix} \tag{6.4.3}$$

The matrices **FM2** and **DM2** will be used in combination with the previously

evaluated **FM1** and **DM1** to compute the stiffness coefficients for the opening in the vessel.

العنوان:	STRESSES AT THE JUNCTION OF TWO NORMALLY INTERSECTING CIRCULAR CYLINDERS
المؤلف الرئيسي:	Khathlan, Abd Alrahman Abd Allah
مؤلفين آخرين:	Steele, Charles(Super)
التاريخ الميلادي:	1986
موقع:	ستانفورد
الصفحات:	1 - 156
رقم MD:	614792
نوع المحتوى:	رسائل جامعية
اللغة:	English
الدرجة العلمية:	رسالة دكتوراه
الجامعة:	Stanford University
الكلية:	College of Engineering
الدولة:	الولايات المتحدة الأمريكية
قواعد المعلومات:	Dissertations
مواضيع:	الهندسة المدنية، التصميمات الهندسية، الحاسب الآلي
رابط:	https://search.mandumah.com/Record/614792

Chapter 7

The Total Solution Including Nozzle Flexibility

The previous chapters provided a description of the cut and asymptotic solutions. The first part of this chapter illustrates the procedure used to eliminate the dependency between the Fourier coefficients in the force and displacement vectors, which is a direct result of the equilibrium and compatibility requirements of the solutions. In addition, this chapter includes a description of the procedure used to combine the complementary parts of the solution evaluated by the *cut method* and the asymptotic solution to generate the needed stiffness coefficients for the vessel.

The solution for the nozzle is also included in this chapter. To some extent, the analysis is similar to that for the vessel, though simpler. The solution is divided into particular and complementary parts. Then, another version of the *cut method* is used to handle both parts of the solution. Finally, by applying continuity conditions at the junction of the two cylinders, the unknown stress and strain distributions around the intersection curve can be solved for.

§7.1 Equilibrium and Compatibility of the Vessel Solution

The force and displacement vectors **F** and **D** represent the Fourier coefficients of the force and displacement quantities acting on the boundary of the opening in the vessel. These quantities are known to satisfy the requirements of equilibrium and compatibility. As a result, it is expected that the four force stress resultants

are related in order to satisfy the equilibrium of the cylinder. Similarly, one expects the four strain and curvature measures to be related in a similar fashion. These relations are very simple in the case of an opening in a flat plate. However, in the case of an opening in a circular cylinder, these relations are difficult to visualize because of the complicated geometry of the boundary.

For example, consider the first symmetry case corresponding to $Isym = 1$. Figure 7.1 shows the stress resultants acting on the boundary of a circular flat plate, which is the limiting case of a very small nozzle intersecting a vessel ($d/D \approx 0$). For these stress resultants to satisfy the equilibrium of forces in the z-direction, the axisymmetric transverse shear has to be zero. In terms of Fourier coefficients of the transverse shear, this can be written as;

$$V_r^{(0)} = 0 \tag{7.1.1}$$

In addition, because there is no external twisting moment, the lowest harmonic of the in-plane shear is;

$$N_{r\gamma}^{(0)} = 0 \tag{7.1.2}$$

These two coefficients correspond to the second and fourth elements of $\mathbf{F}$, and are known to be zero. Consequently, all the elements in the second and fourth rows in **FM1** and **FM2** are equal to zero. The existence of these null rows makes the matrices singular. So in order to avoid the resulting numerical difficulties, both the second and fourth rows are deleted from all the force vectors and matrices $\mathbf{F}_c, \mathbf{F}_p$, **FM1**, and **FM2**.

The same principle can be extended to the case of the intersection curve in a circular cylinder (Fig. 7.2). Unlike the case of a flat plate, all three forces acting on the boundary V_r, N_r, and $N_{r\gamma}$ contribute to the vertical equilibrium of the shell. The contribution of these quantities can be evaluated by using the directional

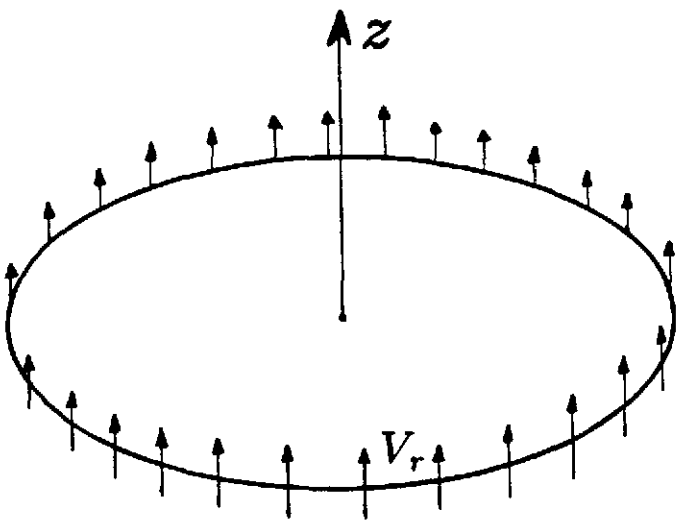

Figure 7.1

Equilibrium of a circular plate with axisymmetric transverse shear V_r acting on the boundary. Other stress resultants do not contribute to vertical equilibrium.

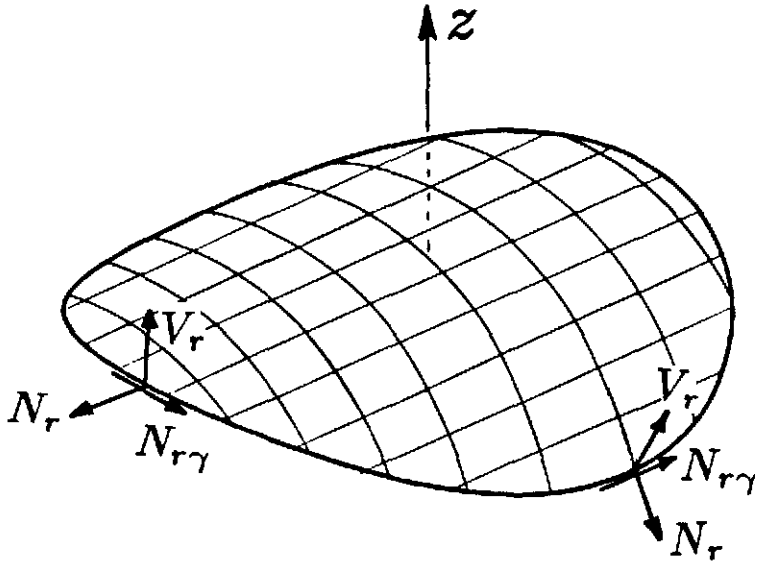

Figure 7.2

Equilibrium of a segment of the vessel surface. The three stress resultants (V_r, N_r, $N_{r\gamma}$) contribute to vertical equilibrium in this case.

cosines of the vectors $\vec{\mathbf{A}}_1$, $\vec{\mathbf{A}}_2$, and $\vec{\mathbf{A}}_3$ (see §2.4). The total vertical resultant is obtained by integrating the contribution of these stress resultants over the length of the boundary. Therefore, the equation of equilibrium in the z-direction is:

$$\int_0^{2\pi} V_r \cos\phi \cdot r_g d\gamma - \int_0^{2\pi} N_r \sin\phi \sin\gamma \cdot r_g d\gamma - \int_0^{2\pi} N_{r\gamma} \sin\phi \cos\gamma \cdot r_g d\gamma = 0 \quad (7.1.3)$$

Substituting the Fourier series expansion of the three stress resultants in (7.1.3) yields

$$\int_0^{2\pi} r_g \cdot \Bigg[\cos\phi \sum_{n=0,2,}^{N1} V_r^{(n)} \cos n\gamma - \sin\phi \sin\gamma \sum_{n=0,2,}^{N1} N_r^{(n)} \cos n\gamma - \sin\phi \cos\gamma \sum_{n=2,4,}^{N1} N_{r\gamma}^{(n)} \sin n\gamma \Bigg] d\gamma = 0 \quad (7.1.4)$$

As a result, it is possible to write the lowest harmonic of the transverse shear $V_r^{(0)}$ in terms of all the other Fourier coefficients. Thus, $V_r^{(0)}$ can not be assumed to be an unknown which justifies dropping it from all the force matrices and vectors.

The same principle can also be applied to the strain and curvature quantities which have to satisfy the deformation compatibility requirements. This results in the elimination of two of the Fourier coefficients for the displacement quantities corresponding to $n = 0$.

In summary, it is necessary to delete the second and fourth rows of all the force vectors and matrices $\mathbf{F}_c, \mathbf{F}_p, \mathbf{FM1}$, and $\mathbf{FM2}$ which correspond to $V_r^{(0)}$ and $N_{r\gamma}^{(0)}$. Similarly, the first and third rows, corresponding to $\tau^{(0)}$ and $\kappa_g^{(0)}$, are also deleted from $\mathbf{D}_c, \mathbf{D}_p, \mathbf{DM1}$, and $\mathbf{DM2}$. As a result, the new arrangement for the Fourier coefficients in a typical force or displacement vector is:

$$\mathbf{F}_p = \begin{pmatrix} M_r^{(0)} \\ CN_r^{(0)} \\ M_r^{(2)} \\ r_0 V_r^{(2)} \\ CN_r^{(2)} \\ CN_{r\gamma}^{2)} \\ \vdots \end{pmatrix} \qquad \mathbf{D}_p = ETC \begin{pmatrix} C\kappa_\gamma^{(0)} \\ \epsilon_\gamma^{(0)} \\ C_T{}^{(2)} \\ C\kappa_\gamma^{(2)} \\ Cr_0\kappa_g^{(2)} \\ \epsilon_\gamma^{(2)} \\ \vdots \end{pmatrix} \tag{7.1.5}$$

From now on, these new vectors will replace the old ones described in (5.2.9).

§7.2 Stiffness Matrix for the Opening in the Vessel

Both the *cut method* and the asymptotic solution will be used in this section to evaluate the stiffness coefficients for the boundary of the opening in the vessel. These stiffness coefficients will be used to express the stress resultants along the boundary in terms of the strains and curvatures.

A brief discussion of the stiffness matrix is also found in this section. It illustrates the different characteristics of different parts of the stiffness matrix in light of the different methods used in the analysis, and the different response of the shell for different harmonic indices.

7.2.1 Computation of the Stiffness Matrix

In Chapter 5, the *cut method* was used to handle the low harmonics of the complementary solution, which correspond to the top few harmonics in $\mathbf{F}_c$ and $\mathbf{D}_c$. The results were expressed in the form

$$\begin{aligned} \mathbf{F}_c &= \mathbf{FM1} \times \mathbf{b} \\ \mathbf{D}_c &= \mathbf{DM1} \times \mathbf{b} \end{aligned} \tag{7.2.1}$$

In addition, the application of the asymptotic methods to the *shallow shell* equation produced

$$\begin{aligned} \mathbf{F}_c &= \mathbf{FM2} \times \mathbf{c} \\ \mathbf{D}_c &= \mathbf{DM2} \times \mathbf{c} \end{aligned} \tag{7.2.2}$$

By observing that (7.2.1) is for the low harmonics and that (7.2.2) is for the high harmonics, both relations can be combined into

$$\begin{aligned} \mathbf{F}_c &= \mathbf{FM} \times \mathbf{B} \\ \mathbf{D}_c &= \mathbf{DM} \times \mathbf{B} \end{aligned} \tag{7.2.3}$$

where **FM** and **DM** are square matrices which include the submatrices **FM1**, **FM2** and **DM1**, **DM2** assembled next to each other in the following way

$$\begin{aligned} \mathbf{FM} &= \Big[[\mathbf{FM1}]\ [\mathbf{FM2}] \Big] \\ \mathbf{DM} &= \Big[[\mathbf{DM1}]\ [\mathbf{DM2}] \Big] \end{aligned} \tag{7.2.4}$$

and **B** represents a vector of the combined unknown constants b_i and c_i.

$$\mathbf{B} = \begin{Bmatrix} \{\mathbf{b}\} \\ \{\mathbf{c}\} \end{Bmatrix} \tag{7.2.5}$$

Multiplying (7.2.3-b) by $\mathbf{DM}^{-1}$ yields

$$\mathbf{B} = \mathbf{DM}^{-1} \times \mathbf{D}_c \tag{7.2.6}$$

which when substituted in (7.2.3-a) produces

$$\mathbf{F}_c = \mathbf{K} \times \mathbf{D}_c \tag{7.2.7}$$

where

$$\mathbf{K} = \mathbf{FM} \times \mathbf{DM}^{-1} \tag{7.2.8}$$

Thus, the square matrix $\mathbf{K}$ is the "stiffness" matrix for the opening since it relates the force quantities to the displacement quantities.

7.2.2 Characteristics of the Stiffness Matrix

In Chapter 4 it was mentioned that the complexity of the problem stems from the complicated manner in which the shells resist the external loads at the junction. Consequently, this is inherited by the stiffness matrix of the vessel because it reflects the response of the vessel to prescribed edge distortions. To understand this, it is desirable to take a close look at the stiffness matrix $\mathbf{K}$. Unfortunately, because of its large size, it is not practical to present the individual coefficients in $\mathbf{K}$. However, by examining the global picture of $\mathbf{K}$, a general idea about the coupling between the harmonics can be given.

A typical stiffness matrix for the boundary of the opening in the vessel is shown in Fig. 7.3. It can be observed that there is significant coupling between the lower harmonics, which are located at the top left-hand corner. Of course, this behavior is not surprising because the existence of such coupling was the main reason for selecting the *cut method* to handle the low harmonics. However, by moving down along the diagonal (increasing n), it can be observed that the level of coupling between the harmonics is decaying. This is the range where the asymptotic solution was used. In the bottom right-hand corner, which corresponds to the very high harmonics, there is no significant coupling at all between the different harmonics.

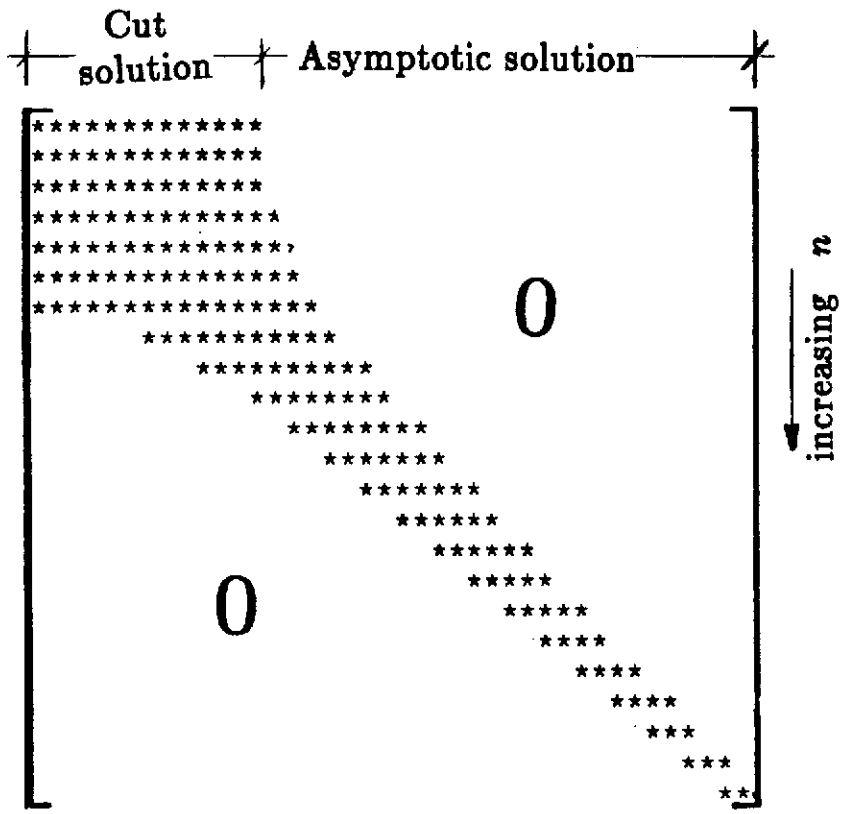

Figure 7.3

A Typical stiffness matrix **K** for the boundary of the opening in the vessel indicating significant coupling between the low harmonics (top left-hand corner), and no coupling between the high harmonics (lower right-hand corner).

This is indicative of flat-plate behavior which has been known to exist in shells of revolution with a high harmonic index (see Steele; 1965).

For the boundary of a circular hole of radius r_0 in a flat plate, each harmonic of the solution is completely independent of the other harmonics. Therefore, it is possible to derive a 4×4 stiffness for the nth harmonic that relate the Fourier coefficients of forces to displacements. This relationship can be expressed as

$$\begin{pmatrix} M_r^{(n)} \\ r_0 V_r^{(n)} \\ CN_r^{(n)} \\ CN_{r\gamma}{}^{(n)} \end{pmatrix} = \begin{bmatrix} 2 & 1+\nu & 0 & 0 \\ -n(1+\nu) & -2n & 0 & 0 \\ 0 & 0 & -2\varrho/n & (-1+\nu)\varrho \\ 0 & 0 & \varrho(1-\nu)/n & 2\varrho \end{bmatrix} \begin{pmatrix} -ETC^2\tau^{(n)} \\ ETC^2\kappa_\gamma^{(n)} \\ ETCr_0\kappa_g^{(n)} \\ ETC\epsilon_\gamma^{(n)} \end{pmatrix} \tag{7.2.8}$$

where $\varrho = \frac{1}{(1+\nu)(3-\nu)}$.

The flat plate stiffness matrix can be useful for the verification of the numerical values of the computed stiffness coefficients in $\mathbf{K}$ for high values of n.

§7.3 Solution for the Nozzle

So far, the analysis has been confined to only one of the two cylinders that compose the joint. The previous chapters illustrated the use of the *cut method* and the application of the asymptotic methods to develop the particular and complementary parts of the solution for the vessel. Up to this point, the effect of the nozzle has not been included. This limits the range of problems that can be handled to the two limiting cases of a very rigid inclusion or a hole in the vessel. Actually, some of the earlier investigators have elected to ignore the effect of the nozzle and solve for these two limiting cases only.

However, in this study the contribution of the nozzle to the flexibility and stresses of the joint will be included. This section provides a brief description of

the nozzle analysis. The solution will be divided into particular and complementary parts. The particular solution will be obtained by representing the applied load by a set of membrane stresses that produce the same resultant. The complementary solution will be used to generate stiffness coefficients for the boundary of the lower edge of the nozzle. Both parts of the solution utilize the general solution for the equations of a circular cylinder given in §3.3 , and are much easier to develop than the particular and complementary solutions for the vessel.

7.3.1 The Governing Equations

Figure 7.4 shows a circular cylinder of radius r_0 and thickness t, which represents the unrolled nozzle before its lower edge is machined to fit on the vessel surface (edge # 1). The figure also shows the shape of the lower edge of the nozzle when it intersects a larger cylinder of radius R (edge # 2). The approach will utilize solutions for the flat edge (# 1) of a complete cylinder to generate solutions along the actual lower edge (# 2) of the intersecting nozzle.

The solution of the equations for a semi-infinite circular cylinder was discussed in detail in Chapter 3. In general, those same equations will be used for the analysis of the nozzle. However, the coordinates and the dimensions of the nozzle should be used here instead of those for the vessel. This implies that for the analysis of the nozzle, the axis of the cylinder is z, the circumferential angle is θ, r_0 is the radius, t is the thickness, and E_n is the modulus of elasticity. As a result, the equivalent of (3.3.6) for the nozzle is

$$\left(\xi^2 - n^2\right)^2 - n^2 + \frac{ir_0}{c}\xi^2 = 0 \tag{7.3.1}$$

where c, the reduced thickness of the nozzle, is

$$c = t/\sqrt{12(1-\nu^2)} \tag{7.3.2}$$

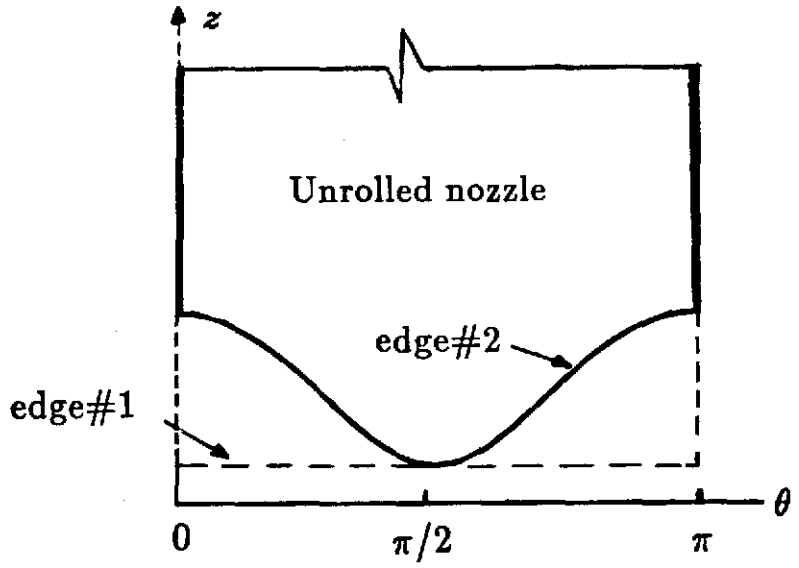

Figure 7.4

Half of the unrolled nozzle with edge #1 representing the flat edge of the cylinder before it is machined to fit the vessel. Edge #2 represents the actual edge of the nozzle when it intersects the other cylinder.

By following the same procedure detailed in §3.3 , it can be shown that the stresses and strains in the nozzle can be expressed in terms of the complex quantities T_1, T_2, T_3, and T_4. For the nozzle,

$$T_2(z,\xi) = (c_1 + ic_2)e^{\xi_1 z/r_0} + (c_3 + ic_4)e^{\xi_2 z/r_0} \tag{7.3.3}$$

where ξ_1 and ξ_2 are the two roots of (7.3.1) which have positive real parts. The remaining complex quantities T_2, T_3, and T_4 can be expressed in terms of T_2 using the same relations given in §3.3.

The next step is to develop relations that can be used to compute stresses and strains along the intersection curve (edge # 2). This goal is achieved by using the Mohr's circle principle by following the same steps detailed in §4.4. The result is

that the force vector for the nozzle $\mathbf{f}$ can be expressed as

$$\mathbf{f} = \begin{pmatrix} M_n \\ r_0 V_n \\ cN_n \\ cN_{n\gamma} \end{pmatrix} = Re \begin{pmatrix} -U_3 + (1-\nu)U_2 \\ -U_4 - (1-\nu)U_1 \\ iU_2 \\ -iU_5(\frac{r_g}{r_0}) \end{pmatrix} \tag{7.3.4}$$

and the displacement vector

$$\mathbf{d} = \begin{pmatrix} -E_n t c^2 \hat{\tau} \\ E_n t c^2 \hat{\kappa}_\gamma \\ E_n t c r_0 \hat{\kappa}_g \\ E_n t c \hat{e}_\gamma \end{pmatrix} = Re \begin{pmatrix} U_5(\frac{r_g}{r_0}) \\ -U_2 \\ i[U_4 + (1+\nu)U_1] \\ i[U_3 - (1+\nu)U_2] \end{pmatrix} \tag{7.3.5}$$

where

$$\begin{aligned}
U_1 &= \cos n\theta \left\{ (T_2 - \frac{1}{2}T_3)(-\xi \sin\alpha \sin 2\alpha + 2\frac{r_0}{r_g}\cos 2\alpha) + T_1 \cos\alpha \cos 2\alpha \right\} \\
&\quad - \sin n\theta \left\{ (T_2 - \frac{1}{2}T_3)(n \cos\alpha \sin 2\alpha \frac{d\,\alpha}{d\,\gamma}) + \frac{T_1}{n}(\xi \sin\alpha \cos 2\alpha + 2\frac{R}{r_g}\sin 2\alpha) \right\} \\
U_2 &= \left[T_2 \cos^2\alpha + (T_3 - T_2)\sin^2\alpha\right]\cos n\theta - \frac{T_1}{n}\sin 2\alpha \sin n\theta \\
U_3 &= T_3 \cos n\theta \\
U_4 &= T_3(\xi \cos\alpha \cos n\theta - n \sin\alpha \sin n\theta) \\
U_5 &= \frac{r_0}{r_g}\left[(T_2 - \frac{1}{2}T_3)\cos n\theta \sin 2\alpha + \frac{T_1}{n}\sin n\theta \cos 2\alpha\right]
\end{aligned} \tag{7.3.6}$$

7.3.2 The Particular Solution for the Nozzle

In order to evaluate the particular solution for the nozzle, membrane stress resultants need to be applied to the edges of the shell. These membrane stress resultants have to produce the same resultant as the applied loads. The membrane equations for the cylinder are represented by the special cases of $n = 0$ and $n = 1$ for the general equation for the cylinder (see §3.5). These solutions correspond to the cases when the root of (7.3.1) is $\xi = 0$, indicating that the solutions do not decay along the axis of the cylinder.

For example, in the case of internal pressure p, the axisymmetric membrane stress resultants in the nozzle are:

$$\begin{aligned} N_z &= \frac{1}{2} p r_0 \\ N_\theta &= p r_0 \end{aligned} \tag{7.3.7}$$

On the other hand, all the bending stresses and curvatures are known to be zero. As a result, by using (3.3.11) it can be shown that

$$T_1 = T_4 = Re(T_2) = Re(T_3) = 0 \tag{7.3.8}$$

and

$$\begin{aligned} Im(T_2) &= -cN_z \\ Im(T_3 - T_2) &= -cN_\theta \end{aligned} \tag{7.3.9}$$

Substituting (7.3.7) in (7.3.9) yields

$$\begin{aligned} T_2 &= -\frac{1}{2} c p r_0 i \\ T_3 &= -\frac{3}{2} c p r_0 i \end{aligned} \tag{7.3.10}$$

Iload	n	N_z	N_θ	T_2	T_3
0	0	$\frac{1}{2}pr_0$	pr_0	$-\frac{1}{2}cpr_0i$	$-\frac{3}{2}cpr_0i$
1	0	$\frac{P}{2\pi r_0}$	0	$-\frac{cPi}{2\pi r_0}$	$-\frac{cPi}{2\pi r_0}$
2	1	$\frac{M_L}{\pi r_0^2}\cos\theta$	0	$-\frac{cM_Li}{\pi r_0^2}$	$-\frac{cM_Li}{\pi r_0^2}$
3	1	$-\frac{M_C}{\pi r_0^2}\sin\theta$	0	$\frac{cM_Ci}{\pi r_0^2}$	$\frac{cM_Ci}{\pi r_0^2}$

Table 7.1
Membrane stress resultants in the nozzle and the corresponding complex quantities T_2 and T_3, for use in the particular solution of the nozzle.

These values are then substituted in (7.3.6) to evaluate the complex quantities U_1, U_2, U_3, U_4, and U_5 in terms of the pressure p, and using;

$$n = 0 \qquad \text{,and} \qquad \xi = 0$$

At this stage, all the force and displacement quantities can be evaluated at any point on the intersection curve by using (7.3.4) and (7.3.5). These can be expressed as the sum of a finite Fourier series, the harmonics of which are stored in the particular solution force and displacement vectors $\mathbf{f}_p$ and $\mathbf{d}_p$, respectively (see §5.2.2).

For the other loading cases, the same procedure is followed. The membrane stresses N_z and N_θ are different for each case. Table 7.1 lists the appropriate

stresses and the corresponding values for T_2 and T_3 in terms of the applied load. The values of T_3 and T_4 are known to be zeros for all the loading configurations. No particular solution for the nozzle is given in the case of an axial force on the vessel ($Iload = 5$) because in this case there is no external load being applied to the nozzle itself.

7.3.3 The Complementary Solution for the Nozzle

The complementary solution for the nozzle will be evaluated using the same equations that were used in the particular solution. This means that each harmonic will be handled separately, which greatly reduces the amount of computation involved. This is in contrast to the complementary solution for the vessel for which the *cut method* was used. In that case, each single cut solution was expanded into N harmonics and the contribution of each harmonic was summed up to produce the complementary solution at a high cost in CPU time (see §5.4).

To evaluate the complementary solution for a single harmonic n, four independent solutions are used. Each of these solutions corresponds to one of the integration constants c_1, c_2, c_3, and c_4 in (7.3.3). First, c_1 is set equal to unity while setting the other three constants to zero. Using these constants, T_1, T_2, T_3 and T_4 can be determined, which are then substituted in (7.3.6) to produce the eight force and displacement quantities on the intersection curve. The nonzero Fourier coefficients of these forces and displacements are stored in the first columns of the matrices **fm** and **dm**, respectively.

The same procedure is repeated four times to cover the four corresponding integration constants. After that, using the next higher harmonic, the whole cycle is repeated untill all the required harmonics are covered. The final result will be in the form

$$\begin{aligned} \mathbf{f_c} &= \mathbf{fm} \times \mathbf{c} \\ \mathbf{d_c} &= \mathbf{dm} \times \mathbf{c} \end{aligned} \tag{7.3.11}$$

where $\mathbf{c}$ is a vector that includes the constants c_1, c_2, c_3, and c_4 for all the harmonics.

The stiffness matrix for the nozzle can be computed by eliminating the unknown vector $\mathbf{c}$ from (7.3.11) using the same method that was applied to the vessel (see §7.2.1). In the nozzle case, the relation is

$$\mathbf{f_c} = \mathbf{k} \times \mathbf{d_c} \tag{7.3.12}$$

where the nozzle stiffness matrix is

$$\mathbf{k} = \mathbf{fm} \times \mathbf{dm}^{-1} \tag{7.3.13}$$

§7.4 Transformation of Force and Displacement Quantities

Up to this stage, the analysis of each of the two cylinders was performed separately. However, the final analysis of the problem will involve combining the equations for both cylinders. As a result, it is necessary to make the force and displacement vectors for the vessel and the nozzle compatible.

For example, compare the elements of the force vector of the vessel $\mathbf{F}$ (4.4.1) to the force vector for the nozzle $\mathbf{f}$ (7.3.4). By examining the directional vectors for both shells (see §2.4), one can observe that the vector tangent to the boundary of the opening in the vessel is the same as the tangent to the nozzle ($\vec{\mathbf{A}}_1 = \vec{\mathbf{a}}_1$). As a result, it can be concluded that the bending moment components in the nozzle M_n and the vessel M_r must be equal (see Fig. 7.5). Similarly, the two in-plane shears

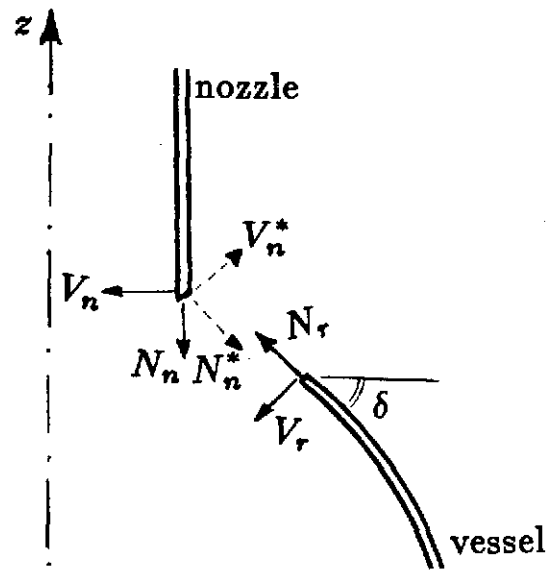

Figure 7.5

Cross section of the junction along the transverse axis. The figure illustrates the transformation of the nozzle shears V_n and N_n to the new quantities V_n^* and N_n^* which are compatible with the vessel coordinates.

$N_{r\gamma}$ and $N_{n\gamma}$ are the same. On the other hand, the other two stress resultants in the nozzle, V_n and N_n, have different lines of action from those for the vessel, V_r and $N_{r\gamma}$.

In essence, the force quantities for the nozzle need to be transfered to a new set of actions that have the same directions as the vessel force quantities. The new force quantities for the nozzle, which will be distinguished by an asterisk, are related to the original elements of $\mathbf{f}$ as follows;

$$\begin{aligned} M_n^* &= M_n \\ N_{n\gamma}^* &= N_{n\gamma} \\ V_n^* &= -V_n \sin\delta - N_n \cos\delta \\ N_n^* &= -V_n \cos\delta + N_n \sin\delta \end{aligned} \tag{7.4.1}$$

where δ is the angle defined as

$$\begin{aligned} \sin\delta &= \vec{\mathbf{A}}_1 \cdot \vec{\mathbf{a}}_1 \\ &= \sin\theta \sin\phi \end{aligned} \tag{7.4.2}$$

Using (7.4.1), the four force quantities in the nozzle force vector $\mathbf{f}$ can be transformed into their new counterparts which are compatible with the vessel force quantities. The new force quantities can then be arranged in the new force vector for the nozzle,

$$\mathbf{f}^* = \begin{Bmatrix} M_n^* \\ r_0 V_n^* \\ C N_n^* \\ C N_{n\gamma}^* \end{Bmatrix} \tag{7.4.3}$$

Note that some of the elements in $\mathbf{f}^*$ are normalized in a different way from $\mathbf{f}$ in (7.3.4). The two in-plane stress resultants are multiplied by the vessel reduced thickness C instead of that for the nozzle c. This is essential to ensure that $\mathbf{f}^*$ is normalized in the exact way used for normalizing $\mathbf{F}$.

Using the static-geometric analogy, the strains and curvatures can also be transformed in the same way. In this case, the new displacement quantities will be normalized using E, T and C instead of E_n, t, and c.

The final result will be the transformation of all the intermediate results for the nozzle $\mathbf{f}_c, \mathbf{d}_c, \mathbf{f}_p, \mathbf{d}_p$, and $\mathbf{k}$ to $\mathbf{f}_c^*, \mathbf{d}_c^*, \mathbf{f}_p^*, \mathbf{d}_p^*$, and $\mathbf{k}^*$ which are compatible with those for the vessel.

§7.5 Continuity Conditions and the Final Solution

The previous work is finally reduced to a single equilibrium equation for each of the two cylinders independently. For the vessel, assume that the unknown forces and displacement vectors at the junction are $\mathbf{F}_u$ and $\mathbf{D}_u$. Using the definition of

the complementary solution as the difference between the total solution and the particular solution, (7.2.7) can be written as

$$(\mathbf{F}_u - \mathbf{F}_p) = \mathbf{K} \times (\mathbf{D}_u - \mathbf{D}_p) \tag{7.5.1}$$

Similarly, the equation of the nozzle is

$$(\mathbf{f}_u^* - \mathbf{f}_p^*) = \mathbf{k}^* \times (\mathbf{d}_u^* - \mathbf{d}_p^*) \tag{7.5.2}$$

where $\mathbf{f}_u^*$ and $\mathbf{d}_u^*$ are the unknown forces and displacements in the nozzle, at the junction.

The continuity of the structure at the junction of the two cylinders implies that the stress resultants and strains are continuous between the two shells. As a result, the unknown force and displacement vectors for the two cylinders are the same, which gives

$$\begin{aligned} \mathbf{f}_u^* &= \mathbf{F}_u \\ \mathbf{d}_u^* &= \mathbf{D}_u \end{aligned} \tag{7.5.3}$$

Substituting (7.5.3) in (7.5.2) yields

$$\mathbf{F}_u = \mathbf{k}^* \times \mathbf{d}_u^* - \mathbf{k}^* \times \mathbf{d}_p^* + \mathbf{f}_p^* \tag{7.5.4}$$

Eliminating $\mathbf{F}_u$ from (7.5.4) produces

$$(\mathbf{K} - \mathbf{k}^*) \times \mathbf{D}_u = \mathbf{K} \times \mathbf{D}_p - \mathbf{k}^* \times \mathbf{d}_p^* + \mathbf{f}_p^* - \mathbf{F}_p \tag{7.5.5}$$

The displacement vector $\mathbf{D}_u$, which is the only unknown in (7.5.5), can be easily solved for. Then it can be substituted in (7.5.1) to evaluate the unknown force

vector $\mathbf{F}_u$. Because $\mathbf{F}_u$ and $\mathbf{D}_u$ include Fourier coefficients, their elements have to be back-transformed to produce the unknown force and displacement quantities evaluated at the mesh points along the intersection curve.

العنوان:	STRESSES AT THE JUNCTION OF TWO NORMALLY INTERSECTING CIRCULAR CYLINDERS
المؤلف الرئيسي:	Khathlan, Abd Alrahman Abd Allah
مؤلفين آخرين:	Steele, Charles(Super)
التاريخ الميلادي:	1986
موقع:	ستانفورد
الصفحات:	1 - 156
رقم MD:	614792
نوع المحتوى:	رسائل جامعية
اللغة:	English
الدرجة العلمية:	رسالة دكتوراه
الجامعة:	Stanford University
الكلية:	College of Engineering
الدولة:	الولايات المتحدة الأمريكية
قواعد المعلومات:	Dissertations
مواضيع:	الهندسة المدنية، التصميمات الهندسية، الحاسب الآلي
رابط:	https://search.mandumah.com/Record/614792

Chapter 8

Results and Comparisons

FAST3 is a new FORTRAN code for the analysis of cylinder-to-cylinder junctions that incorporates the theoretical work discussed in the previous chapters. The major parts of the code have been checked independently to insure their validity. The cut solution and the asymptotic solution for the vessel, and the solution for the nozzle, have been found to produce the expected results during the testing phase. In addition, the complete code was tested using a variety of geometries and loading configurations. Results showed excellent agreement with other published results using different approaches.

In this chapter, the convergence and numerical stability of FAST3 are discussed. The relationship between the size of the nozzle and the validity of the numerical results is explained in light of the decay distance principle for shells. The chapter also includes some of the comparisons performed between FAST3 results and those obtained by other investigators. The final part of the chapter includes the analysis of stresses at the junction of two cylinders with $d/D \geq 0.5$. Some of these results are used to complement existing design tables obtained using the Bessel functions solution of the problem (FAST2).

§8.1 Convergence of the Solution

FAST3 was designed to handle a wide range of geometrical parameters ranging

from nozzles which may be considered very small to those that are about as large as the vessel. However, there is a limit for the validity of FAST3 that can be defined as follows

$$0.05 \leq d/D \leq 0.90 \tag{8.1.1}$$

$$D/T \leq 200$$

In certain cases, FAST3 can be used with geometries that do not fulfill the requirement of (8.1.1), but the accuracy of the solution for such cases is not guaranteed.

In general, the convergence of the solution for the junction problem was found to be entirely dependent on the convergence of the solution for the vessel. The convergence of the vessel solution can be measured by the sensitivity of the vessel stiffness matrix $\mathbf{K}$ to small changes in the the total number of harmonics handled by the *cut method*. Therefore, an investigation of the effect of NHC on the stability of $\mathbf{K}$ is required.

8.1.1 Stability of the Cut Method

By reviewing the analysis of the vessel, one can observe that the parameter NHC identifies the specific harmonic at which the use of the *cut method* is terminated and the use of the asymptotic solution commences. Because NHC is an arbitrary number to be specified by the user, the solution of the physical problem should be insensitive , to some extent, to the prescribed value of NHC. As a result, to reach convergence the stiffness matrix $\mathbf{K}$ should not be greatly affected by slightly changing the value of NHC.

During this study, it was observed that for each problem there is an ideal range of values of NHC to be used in the analysis. This range of values defines the minimum number of cut solutions needed to obtain a converging solution. These values are listed in Table 8.1 for different geometric parameters. For example, for

the analysis of a model with $d/D = 0.7$ and $D/T = 40$, the convergence of the results ia achieved at $NHC = 3$ or 4. Higher values for NHC makes the solution more expensive in terms of CPU time and may lead to numerical instability.

D/T	$d/D = 0.5$	$d/D = 0.7$	$d/D = 0.9$
20	2-3	3-4	5-6
40	3-4	4-5	6
100	5-6	5-6	≥ 6

Table 8.1
Recommended values of the number of harmonics NHC to be handled by the *cut method* in the analysis for different values of d/D and D/T.

8.1.2 Nozzle Size Parameter

For an opening in a circular cylinder, there are two geometric parameters, the diameter ratio d/D, and the diameter to thickness ratio D/T. However, several investigators (Van Dyke; 1965, Steele and Steele; 1983) have concluded that the behavior is mainly dependent on only a single parameter. This parameter is referred to as the *nozzle size parameter* and defined as

$$\lambda = d/\sqrt{DT} \tag{8.1.2}$$

The significance of λ is understood by comparing it to the *decay distance* for shells. The *decay distance* for a shell, δ_d, is defined as the distance from the boundary

beyond which edge bending stresses and curvatures can be considered very small ($< 5\%$). For a circular cylinder of radius R and thickness T (see Flügge; 1960)

$$\delta_d = \sqrt{RT} \tag{8.1.3}$$

Therefore, by examining (8.1.2) and (8.1.3) it can be deduced that the nozzle size parameter λ is proportional to the ratio of the nozzle diameter to the vessel decay distance, which reflects the vessel response to the existence of the opening.

The nozzle size parameter is also useful for deciding whether a certain cylinder-to-cylinder model is within the range of the validity of FAST3. In addition to (8.1.1), the diameter to thickness ratio (D/T) also contributes to the convergence of FAST3 solution. Using Table 8.1 and (8.1.2), it can be shown that the range of validity of FAST3 in terms of λ is

$$0.22 \leq \lambda \leq 9.0 \tag{8.1.4}$$

§8.2 Computation of Stresses

The solution of (7.5.5) provides the distribution of the four stress resultants acting on the boundary of the opening M_r, V_r, N_r, and $N_{r\gamma}$. In addition, the solution also yields the distribution of the displacement quantities $\tau, \kappa_\gamma, \kappa_g$, and ϵ_γ. However, there is always interest in the values of the stress resultants in the circumferential direction M_γ and N_γ, which are yet to be determined.

The bending moment-curvature relationships are (see Ugural;1981)

$$M_r = ETC^2(\kappa_r + \nu\kappa_\gamma) \tag{8.2.1}$$

$$M_\gamma = ETC^2(\kappa_\gamma + \nu\kappa_r) \tag{8.2.2}$$

Eliminating the unknown curvature κ_r from (8.2.2) produces

$$M_\gamma = \nu M_r + (1-\nu^2)ETC^2\kappa_\gamma \tag{8.2.3}$$

Similarly, the tangential stress resultant is

$$N_\gamma = \nu N_r + (1-\nu^2)ETC\epsilon_\gamma \tag{8.2.4}$$

In general, the most important stress resultants at the junction of two cylinders are M_r, N_r, M_γ, and N_γ. The transverse shear V_r and the in-plane shear $N_{r\gamma}$ usually produce negligible stress levels compared to the other stress resultants. Therefore, most of the results reported in this chapter will include the bending and membrane stress resultants only.

The magnitude of these stress resultants can be easily understood if they are normalized in terms of the applied load and the geometry of the junction. The same method used by Mershon, et al. (1984), Steele and Steele (1983) for normalizing the stress resultants is applied here. Table 8.2 lists the appropriate normalized stress resultants $\bar{M}_r, \bar{N}_r, \bar{M}_\gamma$, and $\bar{N}_\gamma$ for each loading case.

In general, it desirable to present the bending and the membrane stress resultants independently. The reason is that designers sometimes apply a different safety factor to the bending resultant than that for the membrane resultants. However, in some cases, the stresses at the outer and inner fibers of the vessel are also of interest. These stresses, in the radial and tangential directions, can be determined using

$$\sigma_r = \frac{N_r}{T} \pm \frac{6M_r}{T^2} \tag{8.2.5}$$

$$\sigma_\gamma = \frac{N_\gamma}{T} \pm \frac{6M_\gamma}{T^2} \tag{8.2.6}$$

$ILOAD$	Applied load	$\bar{M}_r$	$\bar{N}_r$	$\bar{M}_\gamma$	$\bar{N}_\gamma$
0	p	M_r/pRT	N_r/pR	M_θ/pRT	N_θ/pR
1	P	M_r/P	N_rT/P	M_θ/P	$N_\theta T/P$
2	M_L	$M_r d/M_L$	$N_r dT/M_L$	$M_\theta d/M_L$	$N_\theta dT/M_L$
3	M_C	$M_r d/M_C$	$N_r dT/M_C$	$M_\theta d/M_C$	$N_\theta dT/M_C$
5	F_z	$M_r \pi D/F_z T$	$N_r \pi D/F_z$	$M_\theta \pi D/F_z T$	$N_r \pi D/F_z$

Table 8.2
Normalized stress resultants in the vessel for the five different loading configurations.

where $+$ is used for the evaluation of the outer stresses, and $-$ is used for the inner stresses.

§8.3 Solution for Rigid Inclusions and Openings

It was mentioned in Chapter 1 that the early stages of research have been confined to the limiting cases of a rigid inclusion or a hole in a circular cylinder. These cases are of some importance because they resemble situations in which the nozzle thickness to vessel thickness ratio (t/T) is very large or very small. These two limiting cases can actually be solved using the analysis discussed in §7.5. This is possible by imagining the existence of a nozzle and adjusting its modulus of elasticity to a very high or very low value to represent a rigid inclusion or an opening. However, this approach is not the most efficient one because an analysis

of the fictitious nozzle is performed which consumes additional computer time. Therefore, an alternative approach which excludes the nozzle analysis is needed for handling these two limiting cases.

In the case of a rigid inclusion in the surface of a circular cylinder, all the strain and curvature quantities included in the displacement vector $\mathbf{D}$ are known to be zero. As a result, at the boundary between the rigid inclusion and the cylinder;

$$\mathbf{D}_u = 0 \tag{8.3.1}$$

Using (7.5.1), it can be shown that

$$\mathbf{F}_u = \mathbf{F}_p - \mathbf{K} \times \mathbf{D}_p \tag{8.3.2}$$

which yields the values of the stress resultants at the boundary.

In the case of a hole in a cylinder, the boundary of the hole is known to be free of tractions. Thus, the substitution of $\mathbf{F}_u = 0$ in (7.5.1) yields

$$\mathbf{D}_u = \mathbf{D}_p - \mathbf{K}^{-1} \times \mathbf{D}_p \tag{8.3.3}$$

Because of the absence of the radial stresses along the boundary, tangential stresses at the boundary can be evaluated using (8.2.3) and (8.2.4).

§8.4 Effect of the Vessel Length

In this section, the effect of the vessel length L on the stress field will be discussed. This effect can range from completely insignificant to very significant depending on the loading configurations.

It was stated in §2.1 that the vessel is assumed to be long enough to justify neglecting any coupling between the stresses at the joint and the vessel ends. However, in certain cases if the vessel is too long, the results may be slightly misleading.

For example, in the case of a radial load on the nozzle ($Iload$=1) if L is too large, the stresses at midspan due to the beam bending behavior of the vessel can be of the same order of magnitude as the stresses due to the existence of the nozzle. As a result, the vessel length is considered to be very significant for the radial load case.

A vessel length parameter which relates the vessel length to the decay distance was used by Steele and Steele (1983) to understand the effect of the vessel length. Its principle is similar to the nozzle size parameter (see §8.1.2) and can be defined as

$$\Lambda = L/\sqrt{DT} \tag{8.4.1}$$

Steele and Steele also indicated that the beam bending effect can be neglected when the vessel length parameter Λ is less than a critical value Λ_{cr} defined as;

$$\Lambda_{cr} = \begin{cases} D/T, & \text{for } Iload = 1; \\ (D/T)^2, & \text{for } Iload = 3. \end{cases} \tag{8.4.2}$$

Results obtained using FAST3 indicate that this criterion is valid for models with $d/D \geq 0.5$.

§8.5 Testing FAST3

The computer code FAST3 has gone through an extensive testing program to verify its validity. FAST3 results have been compared to a large set of results obtained by several investigators. These included results evaluated through different analytical, experimental, and finite element analysis. The testing procedure

also covered a wide range of geometrical parameters and loading configurations. Unfortunately, most of the results available in the literature are for models with $d/D \leq 0.5$. As a result, it was not possible to do an extensive checking for models with larger nozzles. This section provides a summary of some of the comparisons between FAST3 and results from other approaches.

8.5.1 Comparison with Analytical Results

First, to test the validity of the vessel solution, an analysis of a circular cylinder with a circular hole was performed. Van Dyke (1965) solved this problem for the pressure and axial tension loadings. He used Hankel function solutions of the shallow shell equations to evaluate the bending and membrane stresses in the circumferential direction as a function of the opening size parameter λ. For the purpose of comparison, four different sizes of the opening in a cylinder ($D/T = 100$) were used. The sizes of the opening for the four models are

$$d/D = 0.1,\ 0.2,\ 0.3, \quad \text{and } 0.4$$

Using (8.1.2), it can be shown that the values of λ for the four models are 1.0, 2.0, 3.0, and 4.

Comparison between the membrane stress resultant $\bar{N}_\gamma$, at $\theta = 0°$ and $90°$, computed by Van Dyke and FAST3 is given in Figs. 8.1 and 8.2. Figure 8.1 includes the results for internal pressure loading, while Fig. 8.2 is for the axial tension loading on the cylinder. FAST3 results for both cases have been computed using (8.3.3), and the agreement with Van Dyke's results for all models is good.

The next step was to test FAST3 using cylinder-to-cylinder junctions to verify the solution of the nozzle discussed in Chapter 7, and the continuity conditions between the two cylinders.

Eringen, et al (1969), used an infinite series solution of Donnell's equations

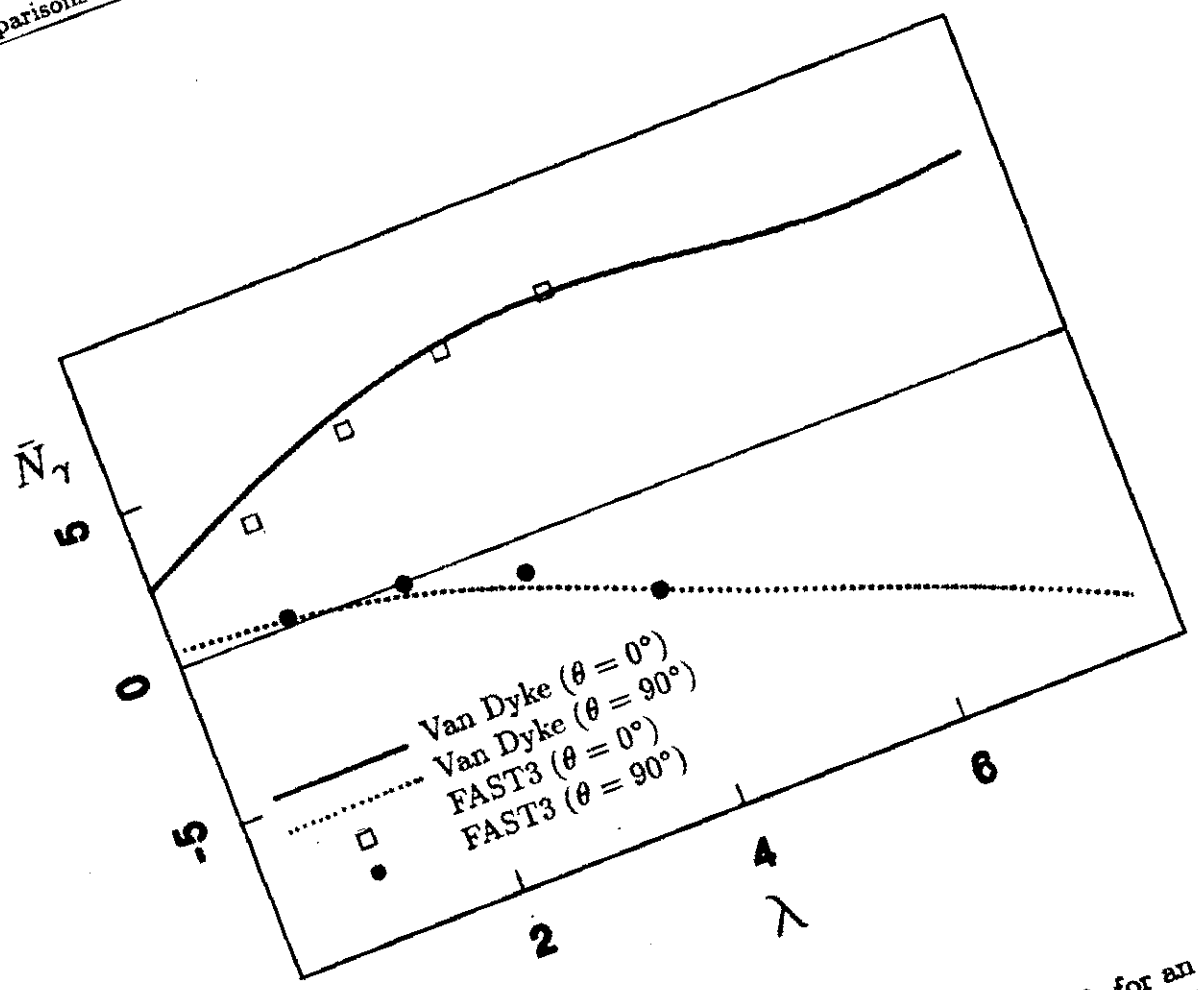

Figure 8.1

Tangential stress concentration factors at $\theta = 0°$ and $\theta = 90°$, for an opening in a cylinder subjected to internal pressure. Lines represent results obtained by Van Dyke (1965). Points represent FAST3 results using four different hole sizes ($d/D = 0.1, 0.2, 0.3, 0.4$) in a circular cylinder (D/T=100).

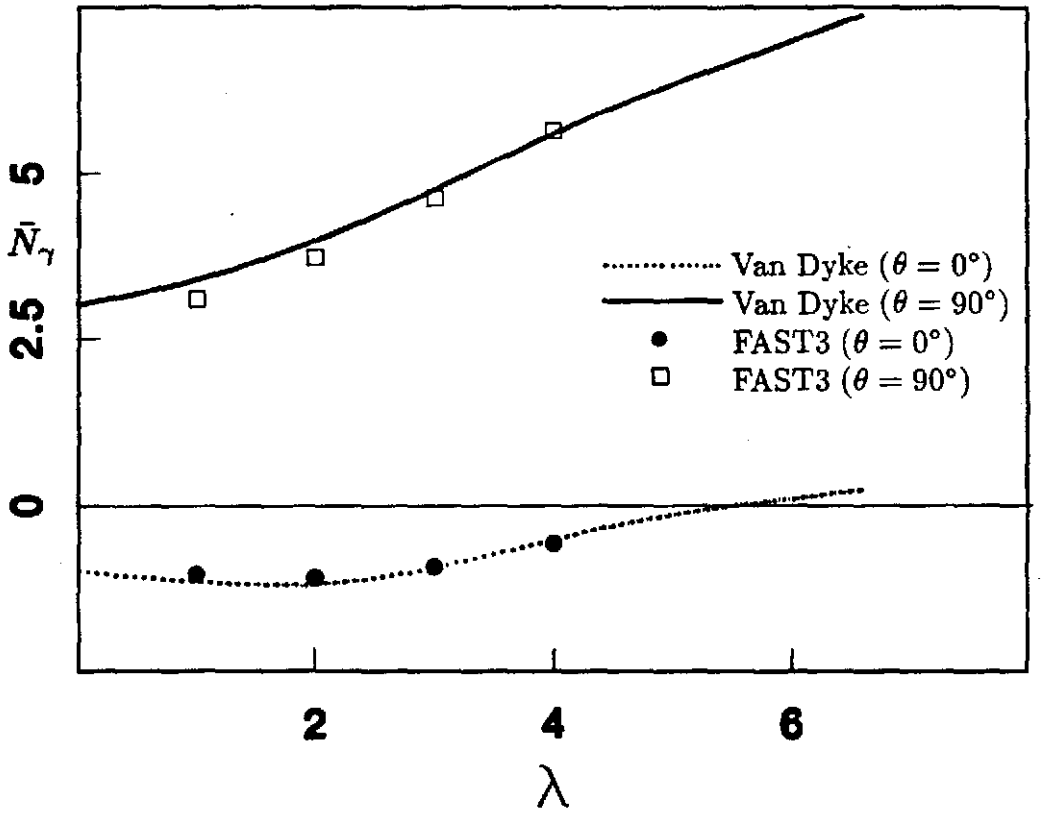

Figure 8.2

Tangential stress concentration factors at $\theta = 0°$ and $\theta = 90°$, for an opening in a cylinder subjected to axial tension. Lines represent results obtained by Van Dyke (1965). Points represent FAST3 results using four different hole sizes ($d/D = 0.1, 0.2, 0.3, 0.4$) in a circular cylinder (D/T=100).

to compute the stresses in cylinder-to-cylinder joints with $d/D \leq 0.33$ subject to internal pressure. Stress concentration factors for several models were published in *Welding Research Council Bulletin No. 139* (WRC-139). Three models with different d/t ratios were selected for the purpose of comparison with FAST3. The geometries of these three models are as follows;

$$D/T = 25 \quad , \quad d/D = 0.25,$$

$$d/t = 12.5,\ 25.0,\ \text{and}\ 50.0\ .$$

A comparison between the tangential stress resultant in the vessel $\bar{N}_\gamma$ computed by Eringen, et al., FAST2, and FAST3 is given in Table 8.3. The agreement is fair.

The next step was to compare FAST3 results to the data available in *Welding Research Council Bulletin No. 279*. Based on the numerical results from FAST2, WRC-297 was developed by Mershon, et al. (1984) for design utilization. It includes results for three different loading cases, but results will be presented for the longitudinal moment case only ($Iload = 2$). Four different models with small nozzle sizes and a thickness ratio $T/t = 2$, are used for the comparison. The normalized tangential moment $\bar{M}_\gamma$ for the four models , including the limiting cases of a very rigid and very flexible nozzle, are plotted in Figure 8.3 next to WRC-297 results. The tangential membrane resultant $\bar{N}_\gamma$ is given in Fig. 8.4. The agreement between FAST3 and WRC-297 is very good for the four geometries including the two limiting cases of the nozzle rigidity.

8.5.2 Comparison with Experimental Results

In addition to other analytical approaches, FAST3 results can be compared to experiments. Although the agreement is not as good as it was with the analytical results, FAST3 results are very close to those obtained by strain gauge measurements, given the difficulty of manufacturing and testing thin shell models.

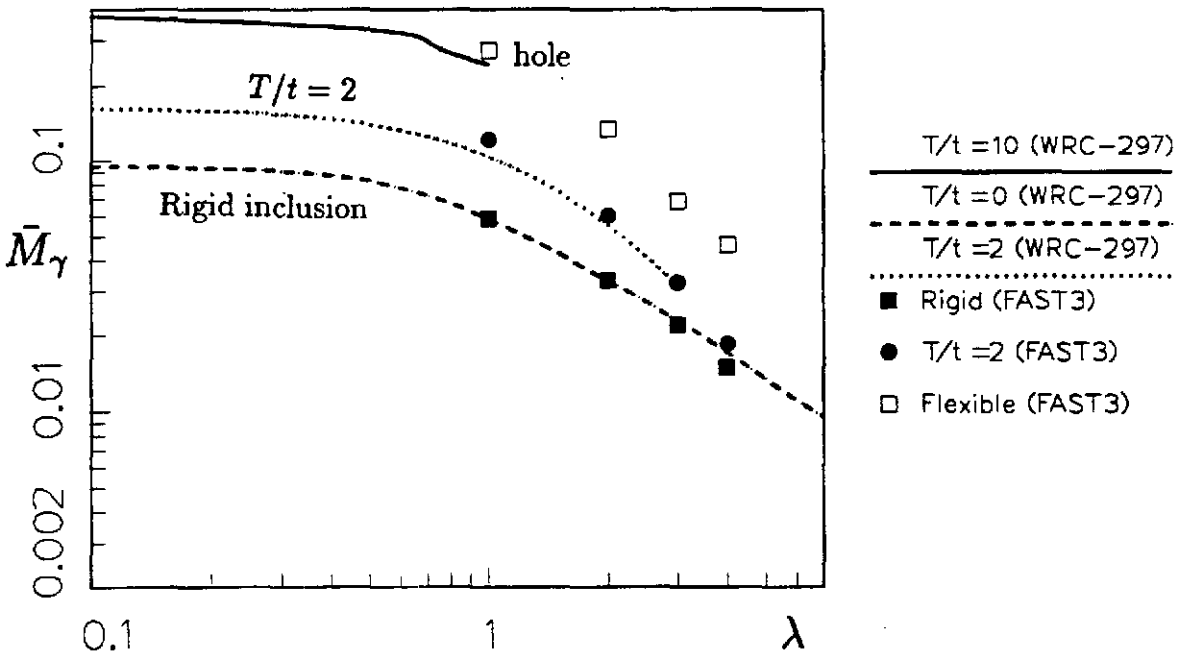

Figure 8.3

Normalized bending stress resultant in the tangential direction ($\bar{M}_\gamma$) due to an external longitudinal moment on the nozzle for different geometries. Points represent FAST3 results for a rigid inclusion (T/t=0), cylinder-to-cylinder models (T/t=2), and an opening in the vessel ($T/t = \infty$). Lines represent results from WRC-297 (Mershon, et al.; 1984) for T/t= 0, 2, and 10.

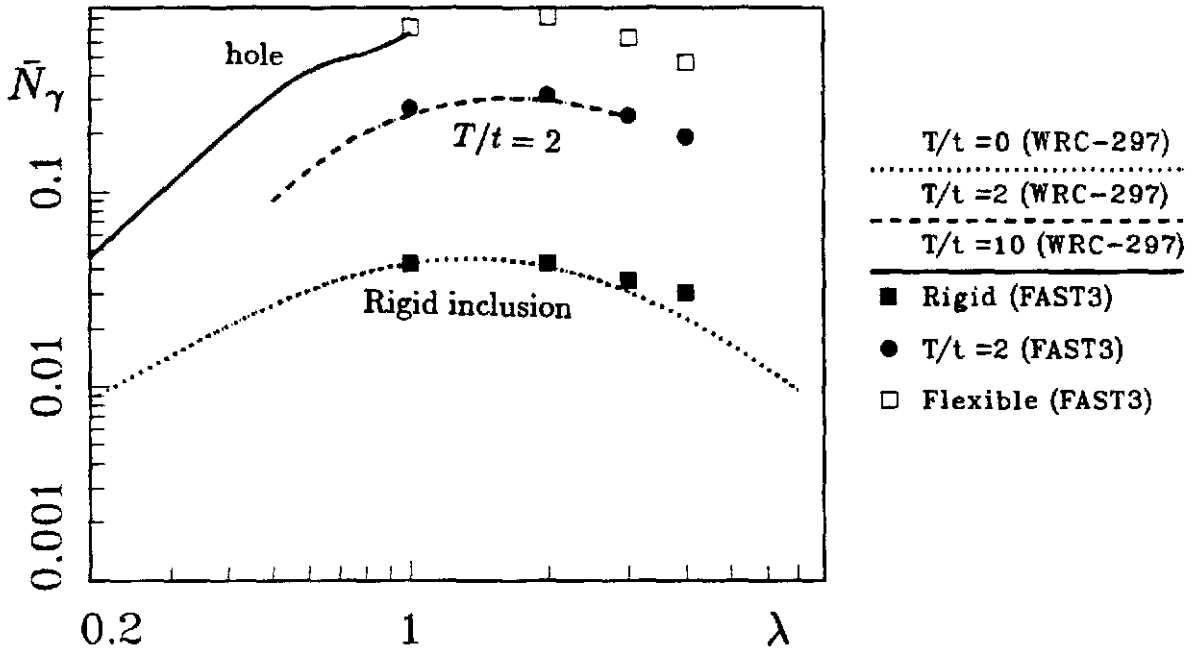

Figure 8.4

Normalized membrane stress resultant in the tangential direction ($\bar{N}_\gamma$) due to an external longitudinal moment on the nozzle for different geometries. Points represent FAST3 results for a rigid inclusion (T/t=0), cylinder-to-cylinder models (T/t=2), and an opening in the vessel ($T/t = \infty$). Lines represent results from WRC-297 (Mershon, et al.; 1984) for T/t= 0, 2, and 10.

	$\theta = 0^o$			$\theta = 90^o$		
Geometry	WRC-139	**FAST2**	**FAST3**	WRC-139	**FAST2**	**FAST3**
$d/t = 12.5$	2.70	2.03	2.60	0.30	0.76	0.58
$d/t = 25.0$	3.50	2.84	3.21	0.40	0.60	0.62
$d/t = 50.0$	4.00	3.51	3.54	0.40	0.48	0.62

Table 8.3
Comparison of tangential stress concentration factors in the vessel due to internal pressure, computed by WRC-139, FAST2, and FAST3 ($D/T = 25$, $d/D = 0.25$).

First, stress distributions at the junction of two cylinders computed by FAST3 were compared to similar stress distributions measured experimentally by Riley (1965). The dimensions of the tested model are as follows:

$$D = 24.0 \text{ in.}, \; T = .104 \text{ in.}, \; d = 12.0 \text{ in.}, \; t = .102 \text{ in.}$$

Riley reported the distribution of the radial and circumferential stresses in the outer fibers of the vessel around the junction for different loading configurations. Figure 8.5 compares FAST3 results to the strain gauge measurements when the nozzle is subjected to a longitudinal moment. Stress distributions for the same case computed using FAST2 (Steele, and Steele; 1983) are also plotted in the same figure.

By examining Fig. 8.5, it can be observed that the peak stresses, which are

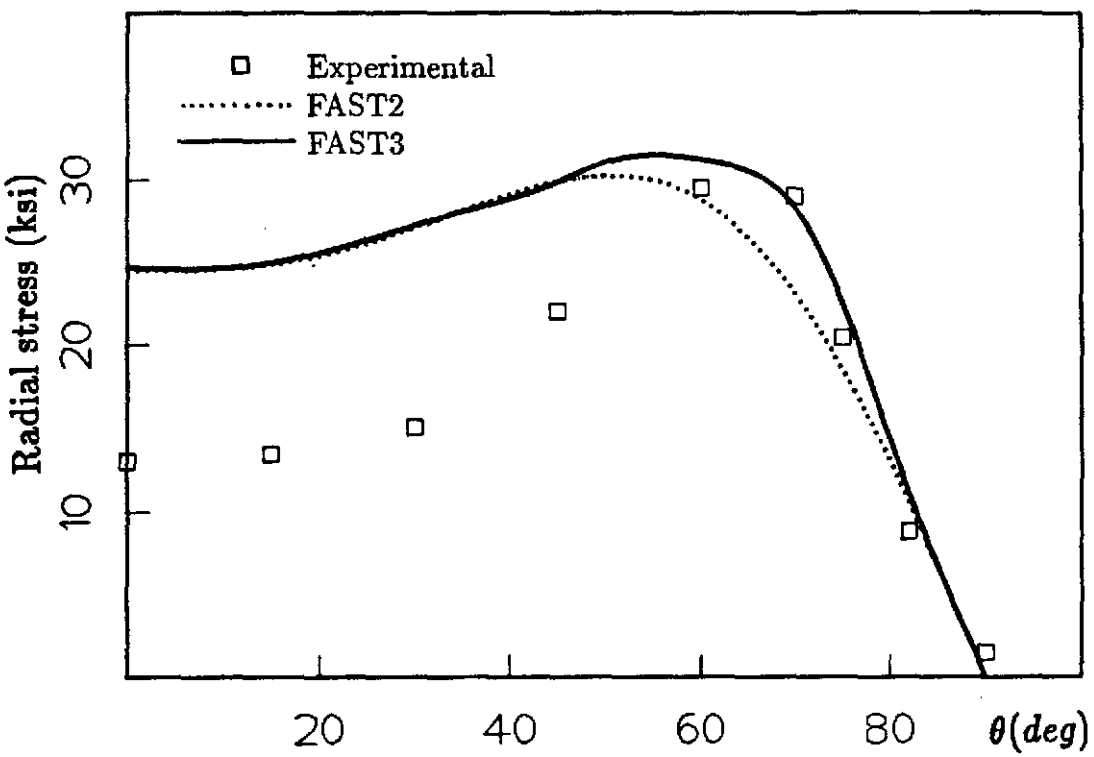

Figure 8.5

Distribution of radial stress in the outer fibers of a cylinder-to-cylinder model (D= 24.0 in., T= .104 in., d= 12.0 in., t= .102 in.) subjected to an in-plane moment on the nozzle (M_L = 18 Kip-in.). Comparison is between strain gauge measurements by Riely(1965) and numerical results using FAST2 (Steele and Steele; 1983) and FAST3.

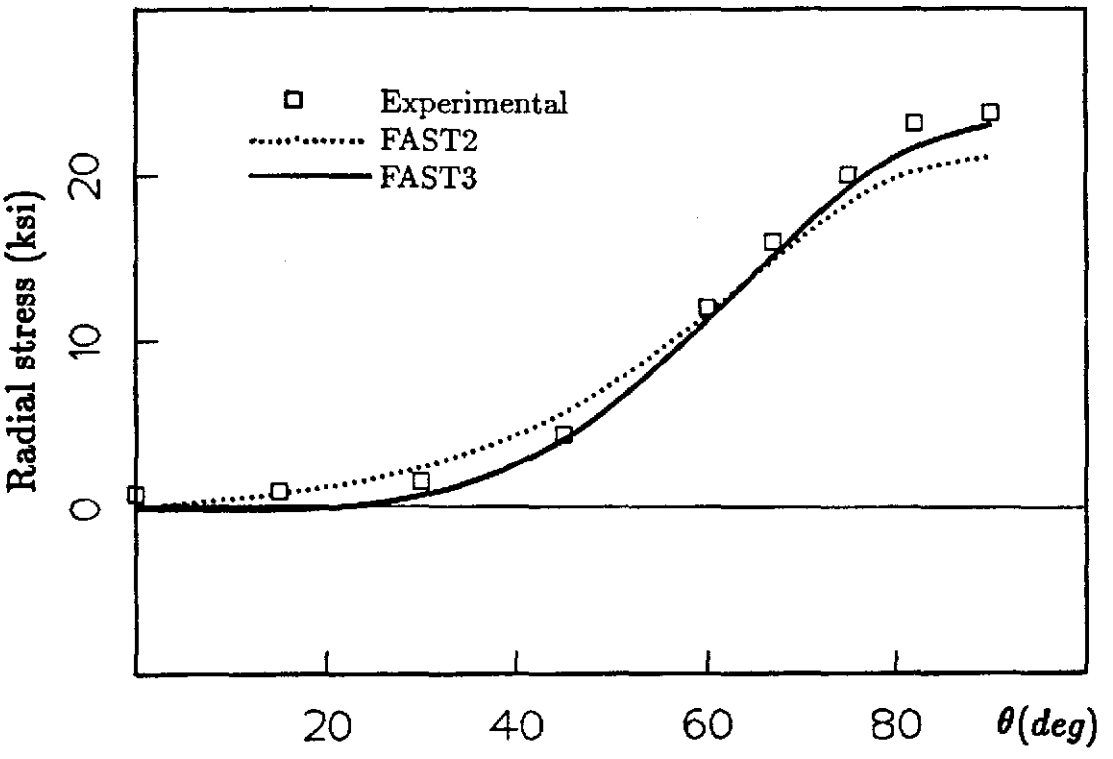

Figure 8.6

Distribution of radial stress in the outer fibers of a cylinder-to-cylinder model (D= 24.0 in., T= .104 in., d= 12.0 in., t= .102 in.) subjected to an out-of-plane moment on the nozzle (M_C = 18 Kip-in.). Comparison is between strain gauge measurements by Riely(1965) and numerical results using FAST2 (Steele and Steele; 1983) and FAST3.

Method	$\bar{M}_r$	$\bar{N}_r$	$\bar{M}_\gamma$	$\bar{N}_\gamma$
Experimental	.039	.046	.016	.19
FAST2	.033	.015	.014	.17
FAST3	.029	.020	.016	.167

Table 8.4
Normalized stress resultants in the vessel for model ORNL-1 subjected to an in-plane moment ($Iload = 2$). Results evaluated experimentally by Gwaltney, et al. (1976), and numerically using FAST2 and FAST3.

Method	$\bar{M}_r$	$\bar{N}_r$	$\bar{M}_\gamma$	$\bar{N}_\gamma$
Experimental	.120	.10	.07	.25
FAST2	.138	.052	.076	.132
FAST3	.114	.067	.067	.153

Table 8.5
Normalized stress resultants in the vessel for model ORNL-1 subjected to an out-of-plane moment ($Iload = 3$). Results evaluated experimentally by Gwaltney, et al. (1976), and numerically using FAST2 and FAST3.

located at $\theta \approx 60°$, are the same for the three different distributions. However, the stress level at $\theta = 0°$ reported by Riley is significantly lower than that computed by FAST3 and FAST2. The reason for this discrepancy is not understood. The geometry is at the limit of the "safe" range of FAST2, and the end stiffness constraint is not included in FAST3. This specific problem deserves further attention.

On the other hand, more satisfactory results for the same model are obtained for the circumferential moment loading case. Peak stresses, as well as the stress distributions, in the radial and tangential directions evaluated experimentally and using FAST3 show excellent agreement (see Fig. 8.6).

Another careful experiment was performed at the Oak Ridge National Laboratory by Gwaltney, et al. (1976), using four different cylinder-to-cylinder models. Two of these models had a diameter ratio d/D= .129, and the third d/D =1.0 . The dimensions of the fourth model (ORNL-1) are;

$$D = 10.0\text{in.}, \quad d = 5.0\text{in.}, \quad T = 0.10\text{in.}, \quad t = 0.05\text{in.}$$

This model was selected for testing FAST3 because its geometry is within the range covered by FAST3 The other three models diameter ratio are either too small or too large.

Normalized stress resultants for model ORNL-1 when the nozzle is loaded with a longitudinal moment, evaluated experimentally and numerically using FAST2 and FAST3, are given in Table 8.4. In addition, Table 8.5 includes the normalized stress resultant for the same model when subjected to an out-of-plane moment. In both loading cases, the agreement between the experimental and numerical results is considered good for a relatively thin model ($D/T = 100$).

More recently, Khan and Woods (1984) presented a comparative study of the stress distribution at the junction of two cylinders using experimental measurements and finite element analysis. Two models with identical geometries ($d/D =$

	$Isym = 2$		$Isym = 3$	
Method	$\bar{\sigma}_r$	$\bar{\sigma}_\theta$	$\bar{\sigma}_r$	$\bar{\sigma}_\theta$
Experimental	7.2	5.3	18.5	10.0
Finite Element	8.5	5.2	22.0	10.5
FAST3	7.0	4.7	24.0	9.5

Table 8.6
Stress concentration factors in the radial and tangential directions in a cylinder-to-cylinder model ($d/D = 0.68, D/T = 23.7,\ d/t = 19.05$). FAST3 results are compared to experimental and finite element analysis results reported by Khan and Woods (1984) for the in-plane and out-of-plane moment loadings.

0.68, $D/T = 23\ 7$, $d/t = 19.05$) were used. One of the models was reinforced at the junction while the other had no such reinforcement. Stress concentration factors evaluated experimentally and using finite element analysis for the *unreinforced* model are listed in Table 8.6, for the in-plane and out-of-plane moment loadings. By examining Table 8.6, the excellent agreement between FAST3 results and the experimental and finite element results, for both loading cases, is evident.

§8.6 Results for Large Diameter Ratios

The previous few sections of this chapter illustrated the validity of FAST3 results for a variety of geometrical and loading parameters. The next step involves the use of FAST3 to investigate the stress fields at the junction of cylinder-to-cylinder models with $d/D \geq 0.5$.

8.6.1 Development of Design Tables

The Welding Research Council Bulletin No. 297(see Mershon, et al.; 1984) is used for the evaluation of stresses at the junction of two cylinders. The WRC-297 provides the four principal stress resultants in the vessel $\bar{M}_r$, $\bar{N}_r$, $\bar{M}_\gamma$, $\bar{N}_\gamma$ for a very wide range of geometrical parameters, but limited to $d/D \leq 0.5$. As a result, it is desirable to utilize FAST3 for the development of a new set of tables that complement the results presented in WRC-297, for $d/D \geq 0.5$.

For each loading case, WRC-297 provides results for different models by keeping d/t and T/t constant and varying the nozzle size parameter λ. For consistency, the same scheme will be used for the application of FAST3. The values of the geometrical parameters used for the development of these tables are;

$$d/t = 20,\ 30,\ 50,\ 100,\ 200$$

$$T/t = 0.5,\ 1.0,\ 2.0,\ 5.0,\ 10.0$$

$$\lambda = d/\sqrt{DT}\ ;\ \text{evaluated at intervals of } 0.5$$

$$\Lambda = L/\sqrt{DT}\ =\ 20.0$$

with the following limitations

$$0.45 \leq d/D \leq 0.90$$

$$20 \leq D/T \leq 200$$

These geometries were used for each of the five important loading cases included in this study, internal pressure, radial load on the nozzle, in-plane moment on the nozzle, out-of-plane moment on the nozzle, and axial force on the vessel. For each model, and every loading case, the maximum values of the normalized stress resultants in the vessel ($\bar{M}_r$, $\bar{N}_r$, $\bar{M}_\gamma$, $\bar{N}_\gamma$) are listed in Appendix A. The position of the maximum stress in the vessel is different for different loading cases. For example,

in the case of internal pressure ($Iload = 0$), maximum stress is located along the longitudinal axis, but in the case of an axial force on the vessel ($Iload = 5$), the maximum stress is located along the transverse axis.

8.6.2 Distribution of Stresses

The previous section and Appendix A provide the designer with maximum values of the stress resultants at the junction of two cylinders. Although this is generally considered the most important piece of information, sometimes it is useful to examine the distribution of stresses around the junction and how this distribution changes as d/D increases.

To investigate this, five different models are used for comparison. The dimensions of the vessel in the five models are the same ($D=$ 20 in., $T=$ 0.5 in.), and the nozzle thickness is also the same ($t=$ 0.5 in.). The nozzle diameter for the five models are $d=$ 10, 12, 14, 16, and 18 inches.

First, these five models were investigated for the in-plane moment loading case ($Iload = 2$). The distributions of the radial stress in the outside surface of the vessel along the intersection curve are plotted in Figure 8.7. By examining Figure 8.7, it can be observed that the level of the stress drops as the diameter ratio (d/D) increases. One can also observe that the position of the peak stress shifts away from the longitudinal axis for larger values of d/D. For very small values of d/D, the peak stress is known to be located along the longitudinal axis ($\theta = 0°$). According to Fig. 8.7, the peak stress shifts to $\theta = 40°$ for d/D=0.5, and is located at $\theta = 77°$ for $d/D=$ 0.9 .

The previous analysis of these five models was repeated again using the out-of-plane moment loading case ($Iload = 3$), and the results are plotted in Figure 8.8. A comparison of Figures 8.7 and 8.8 reveals that for the same geometry, the stress level produced by an out-of-plane moment is at least twice as high as that produced by an in-plane moment of the same magnitude. This underlines the significance of the

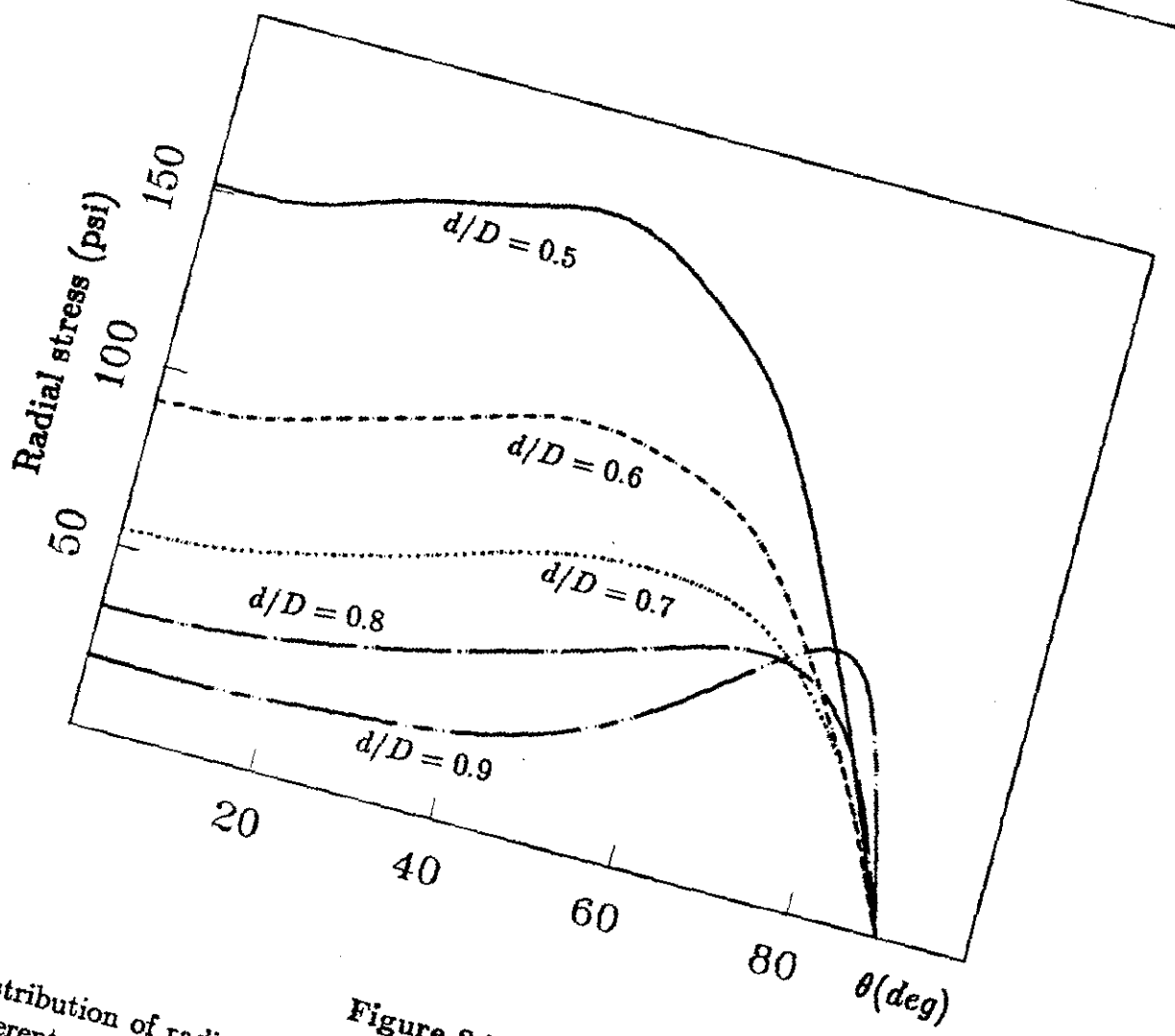

Figure 8.7

Distribution of radial stress in the outer fibers of the vessel for five different cylinder-to-cylinder models subjected to in-plane moment (M_L = 1000 lb-in.) using FAST3. The vessel dimensions and the nozzle thickness are the same for the five models (D= 20.0 in., T= 0.5 in., t= 0.5 in.). The nozzle diameters for the five models are d= 10, 12, 14, 16, and 18 in., respectively.

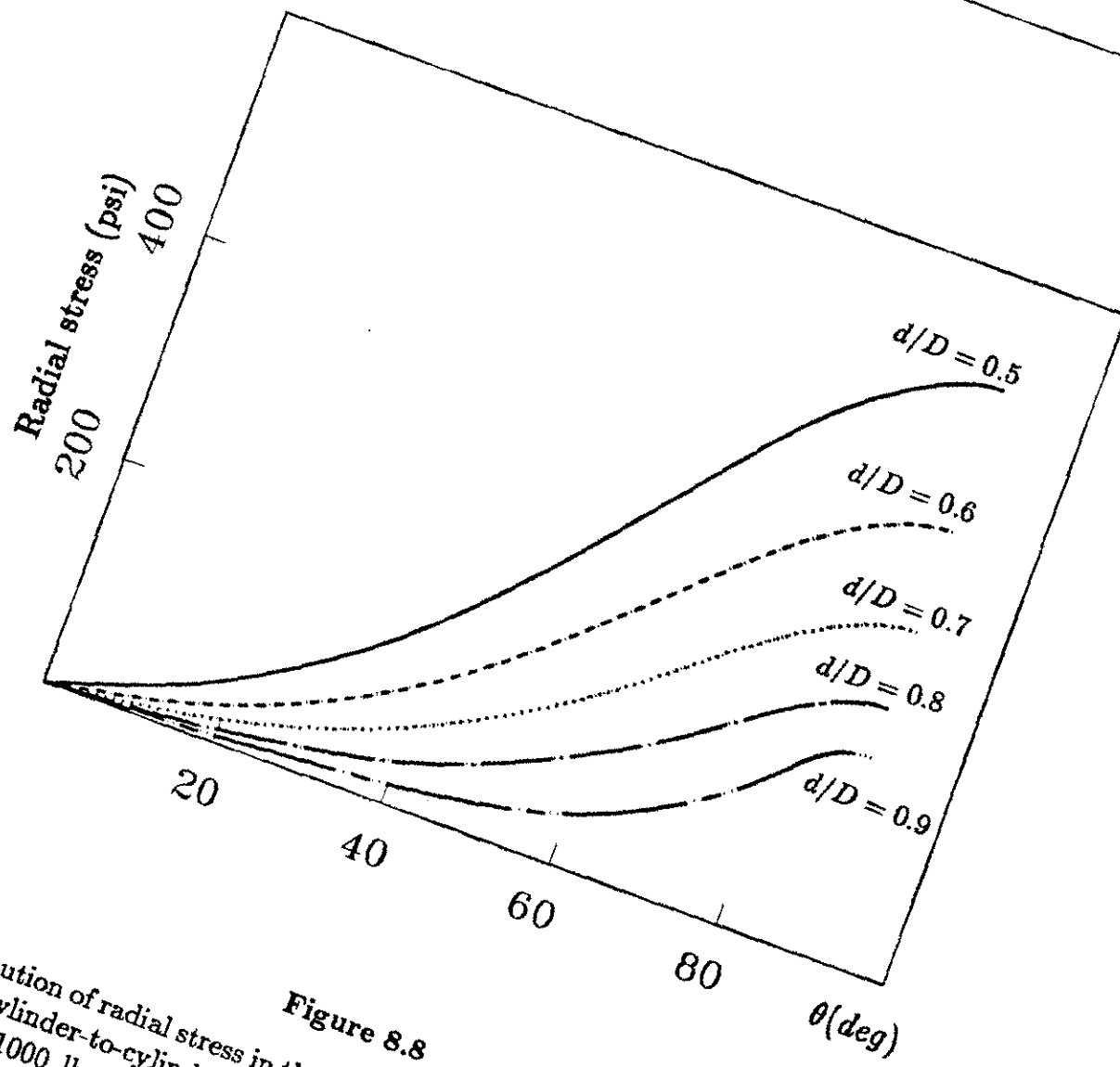

Figure 8.8

Distribution of radial stress in the outer fibers of the vessel for five different cylinder-to-cylinder models subjected to out-of-plane moment (M_C = 1000 lb-in.) using FAST3. The vessel dimensions and the nozzle thickness are the same for the five models (D= 20.0 in., T= 0.5 in., t= 0.5 in.). The nozzle diameters for the five models are d= 10, 12, 14, 16, and 18 in., respectively.

out-of-plane moment loading case and the high stresses that are usually associated with it. Also, unlike the in-plane moment loading, the position of the maximum stress in the vessel is stationary and is always located along the transverse axis for the out-of-plane moment loading.

العنوان:	STRESSES AT THE JUNCTION OF TWO NORMALLY INTERSECTING CIRCULAR CYLINDERS
المؤلف الرئيسي:	Khathlan, Abd Alrahman Abd Allah
مؤلفين آخرين:	Steele, Charles(Super)
التاريخ الميلادي:	1986
موقع:	ستانفورد
الصفحات:	1 - 156
رقم MD:	614792
نوع المحتوى:	رسائل جامعية
اللغة:	English
الدرجة العلمية:	رسالة دكتوراه
الجامعة:	Stanford University
الكلية:	College of Engineering
الدولة:	الولايات المتحدة الأمريكية
قواعد المعلومات:	Dissertations
مواضيع:	الهندسة المدنية، التصميمات الهندسية، الحاسب الآلي
رابط:	https://search.mandumah.com/Record/614792

Chapter 9

Conclusions and Recommendations

The previous chapters include the basis for the development of FAST3, a computer code for the analysis of stress distributions at the junction of two normally intersecting cylinders.

It was mentioned in Chapter 1 that during the development of FAST3, emphasis was directed towards minimizing the required user set-up time. This was achieved by the utilization of the exact thin shell equations in the analysis. The philosophy was to treat each of the two intersecting cylinders as a very large finite element. Each of the two "elements" has its own stiffness matrix at the junction. This is in contrast to the standard Finite Element Method, in which a very large number of elements are needed for the analysis. The process of mesh selection and generation, which could be a very painstaking process in FEM, is not required for the use of FAST3. As a result, only two to three minutes of user set-up time are needed for each run.

In addition, FAST3 is relatively inexpensive in terms of CPU time. Depending on the geometry of the model, each run requires about one to four minutes of CPU on a DEC-20 system. However, huge savings in CPU time can be achieved through the careful choice of the number of cut solutions to be included in the analysis (see Table 8.1).

The main obstacle during this study was the development of an approach that

can be used to generate stiffness coefficients for the boundary of large openings in the cylinder. It was discussed in Chapter 1 that some stiffness coefficients have been obtained in the past for small openings using shallow shell theory and Bessel functions. However, the development of a closed-form solution for openings that extend into the steep part of the shell is still a formidable task. This is the reason for considering the *cut method* a breakthrough in this field, despite its shortcomings. Additional work is needed to improve the *cut method* and reduce the large number of iterations needed to transfer solutions from the flat edge of the cylinder to the boundary of the opening.

In Chapter 6, the asymptotic solution of the shallow shell equations was found to be a very useful technique for handling the rapidly varying part of the solution. The approach is relatively simple and very inexpensive in terms of CPU time. Results indicated that the stiffness coefficients for high harmonics generated using the asymptotic solution are identical to these for a flat plate. The accuracy and simplicity of the asymptotic solution makes it the ideal complement to the *cut method.*

Some of the examples used to test the validity of FAST3 were presented in Chapter 8. These represent a subset of a large number of examples and experiments that have been investigated by other researchers. All the comparisons were found to have reasonable agreement over a wide range of geometries and for all the loading configurations included in this study. In certain cases, the agreement with experimental results was not very good. This could be attributed to several reasons. One of these reasons is the difficulty of manufacturing and testing very thin shell models. Slight imperfections in the wall thickness could introduce significant errors. Also, because FAST3 assumes that the junction is free of any welds or reinforcement, the existence of fillet welds between the two cylinders in the tested models may have contributed to the discrepancies in the results.

Finally, the development and use of FAST3 showed that the following conclu-

sions can be made :

1) The *cut method* is a useful numerical approach for the evaluation of the stiffness coefficients for the boundary of a large opening in a cylindrical shell.

2) The asymptotic solution of the shallow shell equations is a useful alternative to the *cut method* for handling the high harmonics of the solutions.

3) FAST3, which incorporates the *cut method*, the asymptotic solution, the nozzle solution and the continuity conditions, is a useful tool for the investigation of stress distributions at the junction of two cylinders with a diameter ratio $.05 \leq d/D \leq 0.90$.

4) The shallow shell solution for the problem (FAST2) developed by Steele and Steele (1983), which was designed to be valid only for $d/D \leq 0.5$, is not seriously in error for $0.5 \leq d/D \leq 0.7$.

5) The effect of the vessel length L on the stresses observed by other investigators for $d/D \leq 0.5$, can be generalized to models with larger diameter ratios.

The following recommendations for future work can also be given:

1) To improve the *cut method* by reducing the amount of computation needed for each harmonic. It is also desirable to extend the range of validity of the approach to $d/D \geq 0.9$.

2) Additional investigation of the suitability of the *cut method* for handling openings of other shapes is needed. This may prove to be useful for studying junctions in which the nozzle intersects the vessel at an oblique angle. In addition, this might be extended to include the effect of neighboring nozzles on the stress field.

3) Additional features need to be added to FAST3 to improve its versatility. This includes the ability to handle models which have reinforcement at the junction or in which the nozzle intersects the vessel at a position close to the supports.

4) The buckling loads and the dynamic behavior of cylinder-to-cylinder junctions is another field to be investigated. FAST3 can be improved to handle such tasks by adding appropriate terms to the equations for the circular cylinder discussed in Chapter 3.

العنوان:	STRESSES AT THE JUNCTION OF TWO NORMALLY INTERSECTING CIRCULAR CYLINDERS
المؤلف الرئيسي:	Khathlan, Abd Alrahman Abd Allah
مؤلفين آخرين:	Steele, Charles(Super)
التاريخ الميلادي:	1986
موقع:	ستانفورد
الصفحات:	1 - 156
رقم MD:	614792
نوع المحتوى:	رسائل جامعية
اللغة:	English
الدرجة العلمية:	رسالة دكتوراه
الجامعة:	Stanford University
الكلية:	College of Engineering
الدولة:	الولايات المتحدة الأمريكية
قواعد المعلومات:	Dissertations
مواضيع:	الهندسة المدنية، التصميمات الهندسية، الحاسب الآلي
رابط:	https://search.mandumah.com/Record/614792

ABSTRACT

Evaluation of stresses at the junction of two normally intersecting cylinders is an essential part of the design of pressure vessels and similar structures. In general, most of the previous analytical solutions of this problem have been limited to structures in which the ratio of the diameter of the intersecting pipe (nozzle) to the diameter of the intersected pipe (vessel) is less than one half. The objective of this work is the development of the computer code "FAST3" which can also handle larger diameter ratios.

The stress and strain distributions around the junction are expressed in the form of a Fourier series. An approach referred to as "the cut method" was developed and is utilized to generate stiffness coefficients for the low harmonics of the vessel solution. A circumferential cut in the vessel surface, inside the region covered by the nozzle, is used to prescribe discontinuities of forces and displacements. These discontinuities are used in conjunction with the solution of Sanders' equations for a circular cylinder to develop solutions at the boundary of the opening. For the higher harmonics, stiffness coefficients are computed using an asymptotic solution of the shallow shell equations. The combination of the cut method and the asymptotic method is shown to be useful for investigating cylindrical shells with a rigid inclusion or a hole.

Another approach is used to develop stiffness coefficients for the boundary of the nozzle. The vessel and nozzle solutions are incorporated in FAST3 with the appropriate continuity conditions between the two cylinders. Results indicate good agreement with the work of other investigators using experimental and numerical

techniques for several cylinder-to-cylinder models subjected to five different loading configurations. The code was used to develop tables of stress concentration factors to complement those published by the Welding Research Council.

العنوان:	STRESSES AT THE JUNCTION OF TWO NORMALLY INTERSECTING CIRCULAR CYLINDERS
المؤلف الرئيسي:	Khathlan, Abd Alrahman Abd Allah
مؤلفين آخرين:	Steele, Charles(Super)
التاريخ الميلادي:	1986
موقع:	ستانفورد
الصفحات:	1 - 156
رقم MD:	614792
نوع المحتوى:	رسائل جامعية
اللغة:	English
الدرجة العلمية:	رسالة دكتوراه
الجامعة:	Stanford University
الكلية:	College of Engineering
الدولة:	الولايات المتحدة الأمريكية
قواعد المعلومات:	Dissertations
مواضيع:	الهندسة المدنية، التصميمات الهندسية، الحاسب الآلي
رابط:	https://search.mandumah.com/Record/614792

STRESSES AT THE JUNCTION OF TWO NORMALLY INTERSECTING CIRCULAR CYLINDERS

A DISSERTATION SUBMITTED TO
THE DEPARTMENT OF CIVIL ENGINEERING
AND THE COMMITTEE ON GRADUATE STUDIES
OF STANFORD UNIVERSITY
IN PARTIAL FULFILLMENT OF THE REQUIREMENTS
FOR THE DEGREE OF
DOCTOR OF PHILOSOPHY

By

Abdulrahman Abdullah Khathlan

December 1986

I certify that I have read this thesis and that in my opinion it is fully adequate, in scope and quality, as a dissertation for the degree of Doctor of Philosophy.

Charles R Steele

(Principal Adviser)

I certify that I have read this thesis and that in my opinion it is fully adequate, in scope and quality, as a dissertation for the degree of Doctor of Philosophy.

Richard Krumhansl

I certify that I have read this thesis and that in my opinion it is fully adequate, in scope and quality, as a dissertation for the degree of Doctor of Philosophy.

James M. Gere

Approved for the University Committee on Graduate Studies:

Elizabeth Claus Traugott

Dean of Graduate Studies

ABSTRACT

Evaluation of stresses at the junction of two normally intersecting cylinders is an essential part of the design of pressure vessels and similar structures. In general, most of the previous analytical solutions of this problem have been limited to structures in which the ratio of the diameter of the intersecting pipe (nozzle) to the diameter of the intersected pipe (vessel) is less than one half. The objective of this work is the development of the computer code "FAST3" which can also handle larger diameter ratios.

The stress and strain distributions around the junction are expressed in the form of a Fourier series. An approach referred to as "the cut method" was developed and is utilized to generate stiffness coefficients for the low harmonics of the vessel solution. A circumferential cut in the vessel surface, inside the region covered by the nozzle, is used to prescribe discontinuities of forces and displacements. These discontinuities are used in conjunction with the solution of Sanders' equations for a circular cylinder to develop solutions at the boundary of the opening. For the higher harmonics, stiffness coefficients are computed using an asymptotic solution of the shallow shell equations. The combination of the cut method and the asymptotic method is shown to be useful for investigating cylindrical shells with a rigid inclusion or a hole.

Another approach is used to develop stiffness coefficients for the boundary of the nozzle. The vessel and nozzle solutions are incorporated in FAST3 with the appropriate continuity conditions between the two cylinders. Results indicate good agreement with the work of other investigators using experimental and numerical

techniques for several cylinder-to-cylinder models subjected to five different loading configurations. The code was used to develop tables of stress concentration factors to complement those published by the Welding Research Council.

Acknowledgments

I want to thank my adviser, Prof. Charles Steele, for his assistance and support. His knowledge and experience are the pillars on which this research was built. I also would like to thank Prof. James Gere and Prof. Helmut Krawinkler for participating in the reading committee.

I would like to thank my colleagues at the Applied Mechanics Division for their comments and discussions. I am grateful to Chad Balch for proofreading this manuscript.

This thesis is dedicated to my mother and my late father. Their love and compassion have been my guiding lights throughout my life. I will be indebted to them forever. May Allah reward both of them with the ultimate reward.

I am also grateful to all the members of Stanford Islamic Society. Their brotherhood and friendship have made my stay at Stanford very enjoyable.

Finally, I wish to express my gratitude to the University of Petroleum and Minerals in Dhahran, Saudi Arabia, for providing me with a scholarship.

Contents

List of Figures

Page

List of Tables

Page

Nomenclature

$\mathbf{a}$	vector of integration constants
$\vec{\mathbf{a}}_1, \vec{\mathbf{a}}_2, \vec{\mathbf{a}}_3$	unit vectors for the nozzle boundary
$\vec{\mathbf{A}}_1, \vec{\mathbf{A}}_2, \vec{\mathbf{A}}_3$	unit vectors for the opening boundary
$\mathbf{b}, \mathbf{B}$	vectors of integration constants
c	nozzle reduced thickness, Eq. (7.3.2)
$\mathbf{c}$	vector of integration constants
C	vessel reduced thickness, EQ. (3.2.4)
d	nozzle diameter
$\mathbf{d}$	displacement vector for the nozzle, Eq. (7.3.5)
D	vessel diameter
$\mathbf{D}$	displacement vector for the opening, Eq. (4.4.1)
$\mathbf{D}_x$	displacement vector for a cylinder, Eq. (3.3.12)
$\vec{\mathbf{e}}_\mathbf{x}, \vec{\mathbf{e}}_\mathbf{y}, \vec{\mathbf{e}}_\mathbf{z}$	unit vectors
E, E_n	modulus of elasticity for vessel and nozzle
$\mathbf{f}$	force vector for the nozzle, Eq. (7.3.4)
F_x	axial load on the vessel
$\mathbf{F}$	force vector for the opening, Eq. (4.4.1)
$\mathbf{F}_x$	force vector for a cylinder, Eq. (3.3.11)
$Iload$	load index, Table 2.1
$Isym$	symmetry index, Table 2.2
$\mathbf{k}$	nozzle stiffness matrix, Eq. (7.3.13)
$\mathbf{k}^*$	transformed nozzle stiffness matrix
$\mathbf{K}$	Vessel stiffness matrix, Eq. (7.2.8)
L	vessel length

M_C, M_L, M_T	circumferential, longitudinal and twisting moments applied to the nozzle
$M_r, M_\gamma, M_{r\gamma}$	bending moment resultants (moment per unit length)
$M_x, M_\phi, M_{x\phi}$	bending moment resultants (moment per unit length)
n	Fourier harmonic number
$N_r, N_\gamma, N_{r\gamma}$	in-plane stress resultants (force per unit length)
$N_x, N_\phi, N_{x\phi}$	in-plane stress resultants (force per unit length)
$N1$	number of mesh points along one fourth of the intersection curve
NHC	number of harmonics solved using the cut method
p	internal pressure
P	radial load on the nozzle
Q_x, Q_ϕ	transverse shear resultants (force per unit length)
r_0	nozzle radius
r_g	geodesic radius of curvature, Eq. (2.3.15)
r_s	arc length measure, Eq. (2.3.13)
R	vessel radius
S_1, S_2, S_3, S_4	edge distribution functions, Eq. (4.2.1)
t	nozzle thickness
T	vessel thickness
T_1, T_2, T_3, T_4	complex functions for cylinder, Eq. (3.3.7)
u	midsurface displacement in the x-direction
U_1, U_2, U_3, U_4, U_5	complex functions for the nozzle, Eq. (7.3.6)
v	midsurface displacement in the ϕ-direction
V_1, V_2, V_3, V_4, V_5	complex functions for the opening, Eq. (4.4.10)
V_x, V_n, V_r	effective transverse shear resultants (force per unit length)
w	midsurface displacement in the radial direction
x	coordinate along the vessel axis
y	coordinate normal to the plane of the structure
z	coordinate along the nozzle axis

Greek Symbols

α	nozzle end angle, Eq. (2.3.19)
β	angle measuring the cut size, Eq. (4.1.1)
γ	circumferential angle, Eq. (2.3.9)
Γ	intersection curve

δ	angle between the tangents to nozzle and vessel, Eq. (7.4.2)
δ_d	decay distance, Eq. (8.1.3)
$\epsilon_\gamma, \hat{\epsilon_\gamma}$	tangential strains in the vessel and nozzle
θ	circumferential angle for the nozzle
κ_x, κ_ϕ	curvature changes for a cylinder
κ_γ, κ_g	tangential and geodesic curvature changes for the boundary of the opening in the vessel
$\hat{\kappa}_\gamma, \hat{\kappa}_g$	tangential and geodesic curvature changes for the boundary of the nozzle
λ	nozzle size parameter, Eq. (8.1.2)
Λ	vessel length parameter, Eq. (8.4.1)
μ	normalized distance from the boundary
ν	Poisson's ratio
ξ	root of the shell equation, Eq. (3.3.6)
$\vec{\rho}_1, \vec{\rho}_2$	vectors defining the surfaces of the shells
σ_r, σ_γ	radial and tangential stresses in the vessel, Eqs. (8.2.5, 8.2.6)
$\tau, \hat{\tau}$	twist measures for the vessel and nozzle
ϕ	circumferential angle for the vessel
Φ	airy stress function
ψ, Ψ	complex stress-displacement functions, Eq. (3.2.7)

Other Symbols

$(\cdot)_p$	particular solution
$(\cdot)_c$	complementary solution
$(\cdot)^*$	quantity transfered to the vessel coordinates
$\bar{(\cdot)}$	normalized stress resultant

Chapter 1

Introduction

The cylindrical shell is a common structural component in nuclear, hydroelectric, and fossil fuel power plants, in offshore oil platforms, and in many other applications which require pipes and pressure vessels. It is frequently necessary to join one cylindrical shell to another, or to have openings and areas of reinforcement on the surface of the shell, which usually produce localized areas of high stress concentration (see Fig. 1.1). Due to the importance of such structures, there is a great need for a reliable, efficient analysis procedure in order to reduce the probabilities of failure. Despite that, reliable studies of the elastic stresses at the junction of two cylinders have been rare, even for the idealized problem of two cylinders with no fillet or reinforcement. Those methods that are available do not completely cover the wide range of geometrical parameters or the variety of loading configurations that exist in actual structures. Analytical solutions have generally been difficult to obtain because of the complicated geometry. Unlike perpendicular cylinder-to-sphere junctions, this problem does not possess rotational symmetry.

The Pressure Vessel Research Committee of the Welding Research Council and other organizations with interest in pressure vessels have embarked on an extensive experimental and analytical investigation program of the cylindrical shell intersection problem. Most of the theoretical work is related to idealized cylinder-to-cylinder junctions (see Fig. 1.2). In this case, the vessel (intersected cylinder)

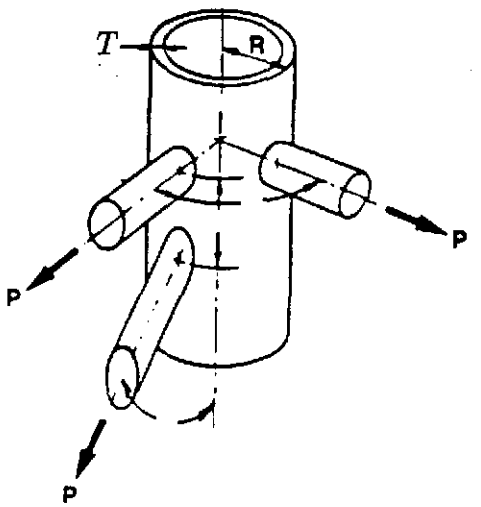

Figure 1.1

A cluster of pipes intersecting a larger pipe from different directions. This is a very common structural component in pressure vessels and offshore structures.

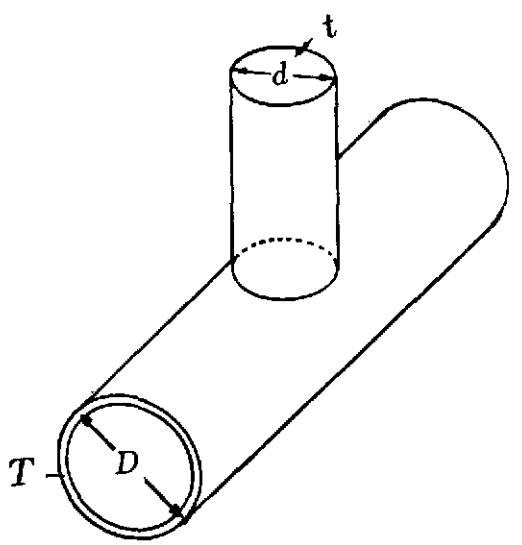

Figure 1.2

Idealized cylinder-to-cylinder junction frequently used in analytical investigations.

has a diameter D, and the nozzle (intersecting cylinder) has a diameter d. Unfortunately, the majority of the analytical solutions for this problem have been confined to cases where the nozzle is considered small relative to the vessel ($d/D \leq 0.5$). As a result, there is a demand for an analytical approach that is useful for handling cases with $d/D > 0.5$. The development of such a solution is the objective of this study.

§1.1 Literature Review

The early stages of research on the cylindrical shell intersection problem have been confined to cases in which the ratio of the diameter of the intersecting cylinder to the diameter of the intersected cylinder (d/D) is small. The reason is that for small values of d/D, it is possible to make certain approximations for the geometry of the intersection curve. In addition, because in the cases of small d/D the opening is located in a zone of the cylinder which is almost flat, referred to as the "shallow region", the use of *shallow shell theory* is justified.

1.1.1 Small Openings and Rigid Inclusions

One of the first to investigate this problem was Lufe (1947). He studied the stress field near a circular opening in a cylinder subject to uniform axial tension or internal pressure. Using perturbation techniques, Lufe expressed solutions in the form of power series in terms of a dimensionless hole size parameter that relates the size of the opening to the radius and thickness of the cylinder. The solution is valid for very small values of the hole size parameter. Following the same procedure, Van Dyke (1965) solved the same problem using an infinite series of Hankel functions of the first kind as a general solution. His approach was designed to be valid for slightly larger hole sizes. Boundary conditions at the opening were satisfied by using a collocation method, which led to a truncation of the series. In addition to the previous two loadings, his work also included the solution for torsion of the cylinder.

Solution for a rigid inclusion in a circular cylinder is important because it serves as a limiting case for a very thick nozzle intersecting a cylinder. Van Dyke (1967) solved the problem using an approach similar to his earlier work for the opening. Influence coefficients were used to satisfy the boundary conditions at the inclusion boundary. Bonde and Rao (1978) studied the problem of a pressurized cylinder with a rigid inclusion. Their solution was also in the form of Hankel functions. Unlike Van Dyke's solution which was written in terms of the displacements of the midsurface, Bonde and Rao used strain and curvature change measures to satisfy boundary conditions. Membrane and bending stresses were plotted versus the hole size parameter. The results exhibit an asymptotic behavior which is in contradiction to that obtained by Van Dyke.

Using an approximate estimate of the stresses in the vessel due to external loads applied to the nozzle, Wichman, et al. (1965) developed design curves for the Welding Research Council *Bulletin 107*. Their work is based on the analytical solution of Bijlaard (1955). He replaced the external loads by pressure distributions applied to rectangular patches on the cylinder face. A double Fourier series expansion was used to compute stresses at specific points in the vessel due to the applied loads. Although this approach is rather crude, and sometimes produces inaccurate results, it was one of the most commonly used design procedures because of its simplicity.

Wong, et al. (1985) used the same double Fourier series solution developed by Bijlaard to expand the range of problems that can be handled. Their work is supposed to be valid for large nozzles, interaction between neighboring nozzles, and rectangular nozzles. Instead of applying the surface pressure to a single rectangular area, the surface inside the intersection curve is divided into several rectangular and triangular elements. As the number of elements was increased, the solution converged to Bijlaard's solution.

1.1.2 Small-Nozzle Problems

Several investigators studied the problem of a small nozzle intersecting the main cylinder. Reidelbach (1961) attempted to solve the problem by providing a Fourier series expansion for the solution of the approximate Donnell thin shell equations. The harmonics of the Fourier series solution for the opening were assumed to be uncoupled. This assumption is essentially equivalent to the treatment of the intersected cylinder as a flat plate. Van Campen (1969) developed a triangular ring element to solve for stresses at nozzle-to-flat plate intersections. His solution was intended to serve as an approximation for cylinder-to-cylinder intersections with a diameter ratio $d/D \leq 1/4$.

Lekkerkerker (1965) used the assumption that the edge of the nozzle is flat to solve for stresses in problems with small diameter ratios. Instead of using Donnell's equations, the more accurate Flugge's equations for a flat-ended cylinder were used to evaluate influence coefficients for the nozzle edge. Similarly, influence coefficients for the opening in the vessel were developed using a combination of exponential and Bessel function solutions of the *shallow shell* equations.

During the same period, Eringen and Suhubi (1965) worked out a mathematical formulation for the problem of a cylinder-to-cylinder junction ($d/D \leq 0.3$) subjected to internal pressure. In their subsequent work (1969), numerical results for several models with a wide range of geometrical parameters were published.

Riley (1965) performed an experiment on a very thin model with diameter ratio of 0.5 subjected to internal pressure, radial load, in-plane and out-of-plane moments applied to the nozzle. Distribution of elastic stresses around the junction for all the loading cases were provided. Pan and Beckett (1970) used the same geometry to test their numerical approach to the solution using a collocation technique and the *Least Squares method.* Their solution was not stable numerically and was very sensitive to the position of the collocation points on the intersection curve. Reasonable agreement with the experimental results was obtained only by restricting all the

العنوان:	STRESSES AT THE JUNCTION OF TWO NORMALLY INTERSECTING CIRCULAR CYLINDERS
المؤلف الرئيسي:	Khathlan, Abd Alrahman Abd Allah
مؤلفين آخرين:	Steele, Charles(Super)
التاريخ الميلادي:	1986
موقع:	ستانفورد
الصفحات:	1 - 156
رقم MD:	614792
نوع المحتوى:	رسائل جامعية
اللغة:	English
الدرجة العلمية:	رسالة دكتوراه
الجامعة:	Stanford University
الكلية:	College of Engineering
الدولة:	الولايات المتحدة الأمريكية
قواعد المعلومات:	Dissertations
مواضيع:	الهندسة المدنية، التصميمات الهندسية، الحاسب الآلي
رابط:	https://search.mandumah.com/Record/614792

References

Bijlaard, P.P. (1955). "Stresses from Local Loadings in Cylindrical Pressure Vessels", *J. Appl. Mech. 22, Trans. ASME 77*, 805–816.

Bijlaard, P.P., Dohrmann, R.J. and Wang, I.C. (1967). "Stresses in Junction of Nozzle to Cylindrical Pressure Vessel for Equal Diameters of Vessel and Nozzle", *Nuclear Eng. and Design* 5", 349–365.

Bonde, D.H. and Rao, K.P. (1978). "Pressurized Cylindrical Shell With a Rigid Circular Inclusion", *Pressure Vessel Tech.* **100**, 158–163.

Brigham, E.O. (1974). *The Fast Fourier Transform.* (Englewood Cliffs, N.J., Prentice-Hall).

Donnell, L.H. (1933). "Stability of Thin Walled Tubes Under Torsion", NACA Report No. 479.

Eringen, A.C. and Suhubi, E.S. (1965). "Stress Distribution at Two Normally Intersecting Cylindrical Shells", *Nuclear Structural Eng.* **2**, 253–270.

Eringen, A.C., Naghdi, A.K., Mahmood, S.S., Thiel, C.C. and Airman, T (1969) "Stress Concentration in Two Normally Intersecting Cylindrical Shells Subject to Internal Pressure", *Welding Research Council Bulletin No. 139*, 1–34.

Flügge, W. and Conrad, D.A. (1958). "Thermal Singularities for Cylindrical Shells", *Proc. 3rd U.S. National Congress of Applied Mechanics.*

Flügge, W. (1960). *Stresses in Shells.* (Springer).

Goldenveizer A.L. (1961). *Theory of Elastic Thin Shells.* (Pergamon).

Gwaltney, R.C., Corum, J.M., Bolt, S.E. and Bryson, J.W. (1976). "Experimental stress Analysis of Cylinder-to-Cylinder Shell Models and Comparisons with Theoretical Predictions", Pressure Vessel Tech. **98**, 283–290.

Hoff, N.J. (1954). "Boundary Value Problem of the Thin Walled Circular Cylinder",

J. Appl. Math. **21**, 343-350.

Khan, A.S. and Woods, G. (1984). "A Comparative Study of the Stress Field around an Unreinforced Normally Intersecting Cylindrical Shells", *Int. J. Pressure Vessels Piping* **15**, 79–92.

Khathlan, A.A. and Steele C.R. (1986). "Analysis of Large Openings in Cylindrical Vessels, Including Nozzle Flexibility", *Proceedings of 1986 Pressure Vessels and Piping Conference Vol.***105**, Chicago, Illinois.

Lekkerkerker, J.G. (1972). "The Determination of elastic Stresses near Cylinder-to-Cylinder Intersections", *Nuclear Eng. and Design* **20**, 57–84.

Lufe, A.I. (1946). "Concentration of Stresses in the Vicinity of an Aperture in the Surface of a Circular Cylinder", *Prik. Mat. Mekh.* **10**, 397-496.

Mershon, J.L , Mokhtarian, K., Ranjan, G.V. and Rodabaugh, E.C. (1984). "Local Stresses in Cylindrical Shells Due to Loadings on Nozzles - Supplement to WRC Bulletin No. 107", *Welding Research Council Bulletin No. 297.*

Morley, L.S. (1959). "An Improvement on Donnell's Approximation for Thin Walled Circular Cylinders", *Quart. Jour. Mech. and Appl. Math.* **12**, 89–99.

Novozhilov, V.V. (1959). *The Theory of Thin Shells.* (Noordhoff).

Pan, K.C. and Beckett, R.C. (1970). "Stress and Displacement Analysis of a Shell Intersection", *Jour. Eng. for Industry 37, Trans. ASME* **92**, Series B, 303–308.

Reidelbach, W. (1961). *Der Spannungszustand in Ubergangsgebiet einer rechtwinkligen Rohrabzweigung.* Ing.-Archiv XXX, 293–316.

Riley, W.F. (1965). "Experimental Determination of Stress Distributions in Thin-Walled Cylindrical and Spherical Pressure Vessels with circular Nozzles", *Welding Research Council Bulletin No. 108*, 1–11.

Sanders, J.L. and Simmonds, J.G. (1970). "Concentrated Forces on Shallow Cylindrical shells", *J. Appl. Mech. 37, Trans. ASME* **92**, Series E, 367–373.

Simmonds, J.G. (1966). "A Set of Single, Accurate Equations for Circular Cylindrical Elastic Shells", *Int. J. Solids Structures* **2**, 525–541.

Steele, C.R. (1965). "Shells with Edge Loads of Rapid Variation-II", *J. Appl. Mech. 32, Trans. ASME* **87**, Series E, 87–98.

Steele, C.R. and Steele, M.L. (1983). "Stress Analysis of Nozzles in Cylindrical Vessels with External Load", *Pressure Vessel Tech.* **105**, 191–200.

Steele, C.R. and Steele, M.L. (1983). "Reinforced Openings in Large Steel Pressure Vessels: Effect of Nozzle Thickness", SHELLTECH Report No. 81-5, Stanford, California.

Steele, C.R. and Steele, M.L. (1985). "Comparison of FAST2 Calculations and Experimental results for Cylinder-to-Cylinder Shell Models ORNL-1, ORNL-3,

and ORNL-4", SHELLTECH Report No. 85-1, Stanford, California.

Taylor, C.E. and Lind, N.C. (1966). "Photoelastic Study of the Stresses near Openings in Pressure Vessels", *Welding Research Council Bulletin No. 113.*

Timoshenko, S. and Woinowsky-Krieger, S. (1959). *Theory of Plates and Shells.* (McGraw-Hill, Inc.).

Ugural, A.C. and Fenster, S.K. (1975). *Advanced Strength and Applied Elasticity.* (Elsevier North-Holland, Inc., New York, N.Y.).

Ugural, A.C. (1981). *Stresses in Plates and Shells.* (McGraw-Hill Inc., New York, N.Y.).

Van Campen, D.H. (1970). "On the Stress Distribution in an Arbitrarily Loaded Nozzle-to-Flat Plate Connection", *Nuclear Eng. and Design* **11**, 495–516.

Van Dyke, P. (1965) "Stresses about a Circular Hole in a Cylindrical Shell", *AIAA J.* **3**, 1733–1742

Van Dyke, P. (1967). "Stresses in a Cylindrical Shell with a Rigid Inclusion", *AIAA J.* **5**, 125–137.

Wong, F.M., Craft, W.J. and East, G.H. (1985). "Stresses and Displacements in Vessels due to Loads Imposed by Single and Multiple Piping Attachments", *Pressure Vessel Tech.* **107**, 51–59.

Wichman, K.R., Hopper, A.G. and Mershon, J.L. (1965). "Local Stresses in Spherical and Cylindrical Shells Due to External Loadings", *Welding Research Council Bulletin No. 107* (Revised 1979).

العنوان:	STRESSES AT THE JUNCTION OF TWO NORMALLY INTERSECTING CIRCULAR CYLINDERS
المؤلف الرئيسي:	Khathlan, Abd Alrahman Abd Allah
مؤلفين آخرين:	Steele, Charles(Super)
التاريخ الميلادي:	1986
موقع:	ستانفورد
الصفحات:	1 - 156
رقم MD:	614792
نوع المحتوى:	رسائل جامعية
اللغة:	English
الدرجة العلمية:	رسالة دكتوراه
الجامعة:	Stanford University
الكلية:	College of Engineering
الدولة:	الولايات المتحدة الأمريكية
قواعد المعلومات:	Dissertations
مواضيع:	الهندسة المدنية، التصميمات الهندسية، الحاسب الآلي
رابط:	https://search.mandumah.com/Record/614792

Appendix A

Table A-1

Normalized stress resultants in the vessel due to an external radial load P on the nozzle (maximum stress is on the transverse axis).

$Iload = 1$, $d/t = 20$, $T/t = 0.5$

λ	d/D	M_r	N_r	M_θ	N_θ
4.5	506	.082	.038	.025	.039
5.0	625	.068	.041	.021	.043
5.5	756	.059	.050	.019	057
6.0	.900	.056	.072	.021	.079

$Iload = 1$, $d/t = 20$, $T/t = 1.0$

λ	d/D	M_r	N_r	M_θ	N_θ
3.0	.450	.077	.057	.029	.068
3.5	.612	.058	.064	.022	091
4.0	.800	.046	.108	.020	188

$Iload = 1$, $d/t = 30$, $T/t = 0.5$

λ	d/D	M_r	N_r	M_θ	N_θ
5.5	.504	.076	029	.023	.036
6.0	.600	.066	.030	.020	.038
6.5	.704	.057	.032	.018	.044
7.0	.817	.054	.037	.017	.053

$Iload = 1 \quad , d/t = 30 \quad , T/t = 1.0$

λ	d/D	M_r	N_r	M_θ	N_θ
4.0	.533	.063	.042	.023	.051
4.5	.675	.049	.048	.018	.075
5.0	.833	.042	.079	.018	.135

$Iload = 1 \quad , d/t = 30 \quad , T/t = 2.0$

λ	d/D	M_r	N_r	M_θ	N_θ
2.5	.417	.044	.057	.036	.145
3.0	.600	.032	.067	.024	.186

$Iload = 1 \quad , d/t = 50 \quad , T/t = 0.5$

λ	d/D	M_r	N_r	M_θ	N_θ
7.0	.490	.070	.021	.021	.040
7.5	.563	.064	.021	.019	.047
8.0	.640	.056	.021	.017	.050
8.5	.722	.047	.024	.014	.053

$Iload = 1 \quad , d/t = 50 \quad , T/t = 1.0$

λ	d/D	M_r	N_r	M_θ	N_θ
5.0	.500	.062	.028	.022	.040
5.5	.605	.051	.029	.018	.050
6.0	.720	.043	.033	.016	068
6.5	.845	.038	.046	.106	.086

$Iload = 1$, $d/t = 50$, $T/t = 2.0$

λ	d/D	M_r	N_r	M_θ	N_θ
3.5	.490	.038	.039	.028	.097
4.0	.640	.028	.044	.020	.117
4.5	.810	.022	.069	.015	.207

$Iload = 1$, $d/t = 100$, $T/t = 1.0$

λ	d/D	M_r	N_r	M_θ	N_θ
7.0	.490	.058	.018	.020	.059
7.5	.563	.053	.019	.018	.074
8.0	.640	.050	.019	.018	.096
8.5	.722	.047	.017	.018	.165

$Iload = 1$, $d/t = 100$, $T/t = 2.0$

λ	d/D	M_r	N_r	M_θ	N_θ
5.0	.500	.035	.023	.022	.063
5.5	.605	.028	.024	.017	.076
6.0	.720	.023	.026	.014	.091
6.5	.845	.019	.034	.010	.110

$Iload = 1$, $d/t = 100$, $T/t = 5.0$

λ	d/D	M_r	N_r	M_θ	N_θ
3.0	.450	.0091	.026	.037	.200
3.5	.612	.0074	.034	.028	.206
4.0	.800	.0052	.046	.014	.308

$Iload = 1$, $d/t = 200$, $T/t = 2.0$

λ	d/D	M_r	N_r	M_θ	N_θ
7.0	.490	.035	.015	.018	.086
7.5	.563	.031	.015	.016	096
8.0	.640	.029	.015	.016	.124

$Iload = 1$, $d/t = 200$, $T/t = 5.0$

λ	d/D	M_r	N_r	M_θ	N_θ
4.5	.506	.0077	.015	.028	.096
5.0	.625	.0056	.014	.019	.076
5.5	.756	.0043	.015	.012	.104
6.0	.900	.0052	.036	.034	.185

$Iload = 1$, $d/t = 200$, $T/t = 10.0$

λ	d/D	M_r	N_r	M_θ	N_θ
3.0	.450	.0021	.017	.035	.230
3.5	.612	.0016	.019	.030	.204
4.0	.800	.0011	.026	.018	.311

Table A-2

Normalized stress resultants in the vessel due to an external longitudinal moment M_L on the nozzle (maximum stress is off-axis).

$Iload = 2$, $d/t = 20$, $T/t = 0.5$

λ	d/D	M_r	N_r	M_θ	N_θ
4.5	506	055	.032	.017	.070
5.0	.625	048	.043	.016	.062
5.5	.756	.046	.090	.015	.095
6.0	.900	.064	.266	.014	.260

$Iload = 2$, $d/t = 20$, T/t =1.0

λ	d/D	M_r	N_r	M_θ	N_θ
3.0	.450	.067	.049	.025	.118
3.5	.612	.053	.047	.020	.116
4.0	.800	.039	.075	.018	.157

$Iload = 2$, $d/t = 30$, $T/t = 0.5$

λ	d/D	M_r	N_r	M_θ	N_θ
5.5	504	.047	.031	.015	.062
6.0	600	.045	.048	.014	.062
6.5	.704	.048	.073	.013	.095
7.0	.817	.056	.117	.011	.137

$Iload = 2$, $d/t = 30$, $T/t = 1.0$

λ	d/D	M_r	N_r	M_θ	N_θ
4.0	.533	052	.034	.019	.105
4.5	.675	042	.042	.017	.103
5.0	.833	035	.090	.017	.160

$Iload = 2$, $d/t = 30$, $T/t = 2.0$

λ	d/D	M_r	N_r	M_θ	N_θ
2.5	.417	.056	.053	.044	.251
3.0	.600	.039	.049	.030	.208

$Iload = 2$, $d/t = 50$, $T/t = 0.5$

λ	d/D	M_r	N_r	M_θ	N_θ
7.0	.490	.043	.024	.012	.054
7.5	.563	.043	.034	.011	.061
8.0	.640	.045	.046	.011	.066
8.5	.722	.050	.053	.022	.057

$Iload = 2$, $d/t = 50$, $T/t = 1.0$

λ	d/D	M_r	N_r	M_θ	N_θ
5.0	.500	.046	.024	.016	.095
5.5	.605	.039	.031	.014	.086
6.0	.720	.034	.046	.013	.107
6.5	.845	.032	.058	.010	.144

$Iload = 2$, $d/t = 50$, $T/t = 2.0$

λ	d/D	M_r	N_r	M_θ	N_θ
3.5	.490	.038	.034	.024	.202
4.0	.640	.029	.034	.018	.181
4.5	.810	.019	.073	.017	.204

$Iload = 2$, $d/t = 100$, $T/t = 1.0$

λ	d/D	M_r	N_r	M_θ	N_θ
7.0	.490	.037	.017	.012	.073
7.5	.563	.034	.017	.012	.070
8.0	.640	.032	.017	.011	.067
8.5	.722	.035	.020	.031	.073

$Iload = 2$, $d/t = 100$, $T/t = 2.0$

λ	d/D	M_r	N_r	M_θ	N_θ
5.0	.500	.029	.020	.016	.167
5.5	.605	.024	.031	.014	.151
6.0	.720	.019	.052	.013	166
6.5	.845	.013	.082	.010	.245

$Iload = 2$, $d/t = 100$, $T/t = 5.0$

λ	d/D	M_r	N_r	M_θ	N_θ
3.0	.450	.013	.024	.046	.454
3.5	.612	.010	.024	.032	.351
4.0	.800	.007	.049	.021	.283

$Iload = 2$, $d/t = 200$, $T/t = 2.0$

λ	d/D	M_r	N_r	M_θ	N_θ
7.0	.490	.023	.018	.012	.132
7.5	.563	.022	.021	.011	.113
8.0	.640	.020	.023	.011	.128
8.5	.722	.018	.023	.019	.120

$Iload = 2$, $d/t = 200$, $T/t = 5.0$

λ	d/D	M_r	N_r	M_θ	N_θ
4.5	.506	.008	.015	.020	.316
5.0	.625	.006	.032	.016	.271
5.5	.756	.005	.070	.014	.284
6.0	.900	.004	.133	.013	.535

$Iload = 2$, $d/t = 200$, $T/t = 10.$

λ	d/D	M_r	N_r	M_θ	N_θ
3.0	.450	004	.016	.054	.549
3.5	.612	003	.018	.040	.426
4.0	.800	.002	.032	.032	312

Table A-3

Normalized stress resultants in the vessel due to an external circumferential moment M_C on the nozzle (maximum stress is along the transverse axis).

$Iload = 3$, $d/t = 20$, $T/t = 0.5$

λ	d/D	M_r	N_r	M_θ	N_θ
4.5	.506	.218	.089	.067	.076
5.0	.625	203	.099	.063	.080
5.5	.756	183	.119	.058	.089
6.0	.900	158	.176	.053	.125

$Iload = 3$, $d/t = 20$, $T/t = 1.0$

λ	d/D	M_r	N_r	M_θ	N_θ
3.0	.450	.197	.120	.075	.061
3.5	.612	.168	.134	.061	.065
4.0	.800	.124	.163	.042	.075

$Iload = 3$, $d/t = 30$, $T/t = 0.5$

λ	d/D	M_r	N_r	M_θ	N_θ
5.5	.504	.206	.073	.063	.087
6.0	.600	.198	.078	.061	.077
6.5	.704	.188	.086	.058	.065
7.0	.817	.177	.115	.055	.088

$Iload = 3$, $d/t = 30$, $T/t = 1.0$

λ	d/D	M_r	N_r	M_θ	N_θ
4.0	.533	.179	.102	.065	.063
4.5	.675	.152	.114	.054	.070
5.0	.833	.116	.153	.040	.114

$Iload = 3$, $d/t = 30$, $T/t = 2.0$

λ	d/D	M_r	N_r	M_θ	N_θ
2.5	.417	.124	.134	.105	.142
3.0	.600	.103	.149	.072	.138

$Iload = 3$, $d/t = 50$, $T/t = 0.5$

λ	d/D	M_r	N_r	M_θ	N_θ
7.0	.490	198	.048	.060	.069
7.5	.563	186	.053	.057	.066
8.0	.640	179	.050	.055	.043
8.5	.722	.176	.059	.054	.035

$Iload = 3$, $d/t = 50$, $T/t = 1.0$

λ	d/D	M_r	N_r	M_θ	N_θ
5.0	.500	.177	.072	.062	.069
5.5	.605	.161	.080	.056	.075
6.0	.720	.142	094	.049	.102
6.5	.845	.123	.133	.043	.161

$Iload = 3$, $d/t = 50$, $T/t = 2.0$

λ	d/D	M_r	N_r	M_θ	N_θ
3.5	.490	.118	.103	081	.141
4.0	.640	.100	.115	061	.129
4.5	.810	.073	.136	.036	.128

$Iload = 3 \quad , d/t = 100 \quad , T/t = 1.0$

λ	d/D	M_r	N_r	M_θ	N_θ
7.0	.490	.169	.048	.057	.091
7.5	.563	.163	.051	.055	.082
8.0	.640	.160	056	.053	.071
8.5	.722	.167	063	.055	.038

$Iload = 3 \quad , d/t = 100 \quad , T/t = 2.0$

λ	d/D	M_r	N_r	M_θ	N_θ
5.0	.500	.116	.069	.068	.151
5.5	.605	.104	.075	.057	.129
6.0	.720	.091	.085	.046	.175
6.5	.845	.079	.119	.036	.262

$Iload = 3 \quad , d/t = 100 \quad , T/t = 5.0$

λ	d/D	M_r	N_r	M_θ	N_θ
3.0	.450	.031	.072	.135	.428
3.5	.612	.029	.091	.099	.382
4.0	.800	.027	.125	.072	.385

$Iload = 3 \quad , d/t = 200 \quad , T/t = 2.0$

λ	d/D	M_r	N_r	M_θ	N_θ
7.0	490	.115	.046	.059	.176
7.5	563	.115	.050	.088	.203
8.0	.640	.113	.057	.055	.178
8.5	.722	.122	.066	.059	.058

$Iload = 3$, $d/t = 200$, $T/t = 5.0$

λ	d/D	M_r	N_r	M_θ	N_θ
4.5	506	.032	.051	.101	.422
5.0	.625	.030	.059	.084	.313
5.5	756	.028	.064	.059	.163
6.0	.900	.026	.085	.041	.158

$Iload = 3$, $d/t = 200$, $T/t = 10.0$

λ	d/D	M_r	N_r	M_θ	N_θ
3.0	.450	.007	.047	.142	.540
3.5	.612	.007	.064	.121	.489
4.0	.800	.008	.077	.102	.568

Table A-4

Normalized stress resultants in the vessel due to internal pressure p (maximum stress is along the longitudinal axis).

$Iload = 0$, $d/t = 20$, $T/t = 0.5$

λ	d/D	M_r	N_r	M_θ	N_θ
4.5	506	.609	.622	.162	2.19
5.0	625	.606	.560	.164	2.00
5.5	.756	.446	.463	.119	1.72

$Iload = 0$, $d/t = 20$, $T/t = 1.0$

λ	d/D	M_r	N_r	M_θ	N_θ
3.0	.450	.531	.519	.138	2.73
3.5	.612	.644	.526	.192	2.60
4.0	.800	.614	.390	.210	1.84

$Iload = 0$, $d/t = 30$, $T/t = 0.5$

λ	d/D	M_r	N_r	M_θ	N_θ
5.5	.504	.674	.586	180	2.46
6.0	.600	.512	.530	.130	2.34
6.5	.704	.397	.496	.098	2.19

$Iload = 0$, $d/t = 30$, $T/t = 1.0$

λ	d/D	M_r	N_r	M_θ	N_θ
4.0	.533	.714	.497	209	2.86
4.5	.675	.715	.430	224	2.41
5.0	.833	.467	.258	149	1.72

$Iload = 0$, $d/t = 30$, $T/t = 2.0$

λ	d/D	M_r	N_r	M_θ	N_θ
2.5	.417	.295	.359	131	3.67
3.0	.600	.384	.411	.227	3.86

$Iload = 0$, $d/t = 50$, $T/t = 1.0$

λ	d/D	M_r	N_r	M_θ	N_θ
5.0	500	.812	.439	.235	3.19
5.5	605	.768	.403	.225	2.97
6.0	.720	.609	.333	.173	2.59

$Iload = 0$, $d/t = 50$, $T/t = 2.0$

λ	d/D	M_r	N_r	M_θ	N_θ
3.5	.490	.449	381	.218	4.28
4.0	.640	.521	389	.309	3.92
4.5	.810	.342	228	.222	2.72

$Iload = 0$, $d/t = 100$, $T/t = 2.0$

λ	d/D	M_r	N_r	M_θ	N_θ
5.0	.500	.595	.335	.281	4.71
5.5	.605	548	.298	.267	4.28
6.0	.720	.328	.201	.131	3.69

$Iload = 0$, $d/t = 100$, $T/t = 5.0$

λ	d/D	M_r	N_r	M_θ	N_θ
3.0	.450	.089	.137	.299	6.06
3.5	.612	.124	.171	.495	6.75
4.0	.800	.038	.071	.585	5.21

$Iload = 0$, $d/t = 200$, $T/t = 5.0$

λ	d/D	M_r	N_r	M_θ	N_θ
4.5	506	.145	145	.308	7.63
5.0	625	.079	085	.191	6.62

$Iload = 0$, $d/t = 200$, $T/t = 10.0$

λ	d/D	M_r	N_r	M_θ	N_θ
3.0	.450	.014	.033	466	6.58
3.5	.612	.010	.056	.705	7.16
4.0	.800	-.024	.281	.958	5.72

Table A-5

Normalized stress resultants in the vessel due to an axial force F_x on the vessel (maximum stress is along the transverse axis).

$Iload = 5$, $d/t = 20$, $T/t = 0.5$

λ	d/D	M_r	N_r	M_θ	N_θ
4.5	.506	.435	.895	.127	2.62
5.0	.625	.580	1.08	.192	2.85
5.5	.756	.794	1.49	.301	3.10
6.0	.900	1.07	2.38	.506	3.72

$Iload = 5$, $d/t = 20$, $T/t = 1.0$

λ	d/D	M_r	N_r	M_θ	N_θ
3.0	.450	.297	.589	.073	2.80
3.5	.612	.374	.873	.121	3.47
4.0	.800	.591	1.83	.277	4.90

$Iload = 5$, $d/t = 30$, $T/t = 0.5$

λ	d/D	M_r	N_r	M_θ	N_θ
5 5	.504	.595	.889	.175	3.02
6 0	.600	.753	1.04	.240	3.05
6.5	.704	889	1.34	.305	3.21
7.0	.817	1.12	2.09	.408	3.79

$Iload = 5$, $d/t = 30$, $T/t = 1.0$

λ	d/D	M_r	N_r	M_θ	N_θ
4.0	.533	.437	.693	.123	3.49
4.5	.675	581	1.05	.199	4.17
5.0	.833	804	2.10	.369	5.42

$Iload = 5$, $d/t = 30$, $T/t = 2.0$

λ	d/D	M_r	N_r	M_θ	N_θ
2.5	.417	.162	.372	.033	3.17
3.0	.600	.174	.563	.048	4.01

$Iload = 5$, $d/t = 50$, $T/t = 0.5$

λ	d/D	M_r	N_r	M_θ	N_θ
7.0	.490	.853	.775	.258	3.10
7.5	.563	1.07	.869	345	3.03
8.0	.640	1 18	1.03	.385	2.82

$Iload = 5$, $d/t = 50$, $T/t = 1.0$

λ	d/D	M_r	N_r	M_θ	N_θ
5.0	.500	.565	.606	.159	3.86
5.5	.605	.701	.792	.222	4.17
6.0	.720	.844	1.13	.296	4.50
6.5	.845	1.04	2.12	.432	5.81

$Iload = 5$, $d/t = 50$, $T/t = 2.0$

λ	d/D	M_r	N_r	M_θ	N_θ
3.5	.490	.228	.398	.074	3 89
4.0	.640	.271	.617	.098	4 93
4.5	.810	.353	1.30	.166	6 87

$Iload = 5$, $d/t = 100$, $T/t = 1.0$

λ	d/D	M_r	N_r	M_θ	N_θ
7.0	.490	.901	.526	.283	3.76
7.5	.563	.985	.605	.322	3.35
8.0	.640	1.09	.756	.378	2.83

$Iload = 5$, $d/t = 100$, $T/t = 2.0$

λ	d/D	M_r	N_r	M_θ	N_θ
5.0	.500	.356	.381	.133	4.76
5.5	.605	.433	.527	.183	5.49
6.0	.720	.502	.774	.249	6.17
6.5	.845	.616	1.51	.402	7.96

$Iload = 5$, $d/t = 100$, $T/t = 5.0$

λ	d/D	M_r	N_r	M_θ	N_θ
3.0	.450	.050	.164	.028	4.21
3.5	.612	.054	.254	-.024	5.39
4.0	.800	.074	.624	-.178	8.36

$Iload = 5$, $d/t = 200$, $T/t = 2.0$

λ	d/D	M_r	N_r	M_θ	N_θ
7.0	.490	.610	.377	279	4.68
7 5	.563	.632	.455	.302	4.08
8 0	.640	.651	.608	.343	3.13

$Iload = 5$, $d/t = 200$, $T/t = 5.0$

λ	d/D	M_r	N_r	M_θ	N_θ
4.5	.506	.078	.172	.070	5 64
5.0	.625	.096	.277	.089	6 98
5.5	.756	.113	.506	.083	8.61

$Iload = 5$, $d/t = 200$, $T/t = 10.0$

λ	d/D	M_r	N_r	M_θ	N_θ
3.0	.450	.013	.080	-.036	4.50
3.5	.612	.015	.138	-.149	5.86
4.0	.800	.028	.141	-.747	8.61

العنوان:	STRESSES AT THE JUNCTION OF TWO NORMALLY INTERSECTING CIRCULAR CYLINDERS
المؤلف الرئيسي:	Khathlan, Abd Alrahman Abd Allah
مؤلفين آخرين:	Steele, Charles(Super)
التاريخ الميلادي:	1986
موقع:	ستانفورد
الصفحات:	1 - 156
رقم MD:	614792
نوع المحتوى:	رسائل جامعية
اللغة:	English
الدرجة العلمية:	رسالة دكتوراه
الجامعة:	Stanford University
الكلية:	College of Engineering
الدولة:	الولايات المتحدة الأمريكية
قواعد المعلومات:	Dissertations
مواضيع:	الهندسة المدنية، التصميمات الهندسية، الحاسب الآلي
رابط:	https://search.mandumah.com/Record/614792

STRESSES AT THE JUNCTION OF TWO NORMALLY INTERSECTING CIRCULAR CYLINDERS

A DISSERTATION SUBMITTED TO
THE DEPARTMENT OF CIVIL ENGINEERING
AND THE COMMITTEE ON GRADUATE STUDIES
OF STANFORD UNIVERSITY
IN PARTIAL FULFILLMENT OF THE REQUIREMENTS
FOR THE DEGREE OF
DOCTOR OF PHILOSOPHY

By

Abdulrahman Abdullah Khathlan

December 1986